Summer 8-13-2021

FGFR4 glycosylation and processing in cholangiocarcinoma promote cancer signaling

Andrew J. Phillips
University of Nebraska Medical Center

FGFR4 glycosylation and processing in cholangiocarcinoma promote cancer signaling

by:

Andrew Phillips

A DISSERTATION

Presented to the Faculty of the University of Nebraska Medical Center Graduate College in Partial Fulfillment of the Requirements for the Degree of Doctor of Philosophy

Cancer Research Doctoral Program

Under the Supervision of Professor Justin L. Mott, M.D., Ph.D.

University of Nebraska Medical Center

Omaha, Nebraska

June 2021

Supervisory Committee:

Jennifer Black, Ph.D.

Keith Johnson, Ph.D.

Lois Starr, M.D., Ph.D.

ACKNOWLEDGEMENTS

The work presented here is representative of my time in the Mott lab and speaks to the challenges, difficulties, growth and accomplishments of the lab as a whole. Justin, your lab is an amazing place of opportunity for those fortunate enough to set foot in it. I am forever grateful to have had the opportunity to work under your guidance and supervision, learn from your wisdom and experiences, and be a part of this tight-knit and supportive lab environment. You taught me so much about science and research, but you also taught me about leadership, running a lab effectively, working with others and navigating one's way through life. The work you do to spread good to your lab and UNMC, as a whole, does not go unnoticed. You work so incredibly hard to make UNMC a place of learning and growth for its students in more ways than I can ever know. I am so fortunate to have you as a mentor.

I would like to give a huge thank you to my supervisory committee members: Dr. Jenny Black, Dr. Keith Johnson and Dr. Lois Starr. During my time in graduate school, they challenged me to become a better scientist through their broad knowledge base and thoughtful questions. It is clear how much my committee cared about my growth and progress as a scientist. They never stopped challenging me or asking me questions regarding my projects. Their excitement and curiosity towards my projects made each committee meeting a unique opportunity for me to grow. I am very grateful for their tireless devotion to my growth as a researcher, communicator and scientist.

The MD-PhD Scholars program at UNMC is an absolutely amazing community of students, faculty, mentors and educators. Drs. Romberger, Smith and Mott have fearlessly strived to make this program a supportive and caring environment for its student members. Sonja, thank you for all of your years of hard work for this program.

Your dedication to helping the students was a huge reason I became so passionate about UNMC's MD-PhD Scholar's program. Jen, you're amazing. You stepped in and quickly became a vital piece of the program and play a huge role in its continued success.

As a wise man once said (and continues to say), "Teamwork makes the dreamwork." That wise man is Cody Wehrkamp. Cody, it was a genuine pleasure getting to learn from. You are, through and through, a good person who leads quietly, but undeniably leads.

Matt, you have been a great friend. From Mountain Dew Mondays to our quote board to countless Office references to just being around when I need someone to double check my math, I so much appreciate you being a source of humor, fun and reassurance for me in the lab.

Yamnah, your perseverance and determination through both good times and challenging times is admirable. Your sense of humor and dependability make you a pleasure to work with. I so much appreciate our friendship and how we can be goofy while still working. The lab is very lucky to have you.

Marissa, while your time in lab was brief, you accomplished so much! Your determination and ambition are truly incredible, and I appreciate your contributions to the lab and my research.

Hannah, thank you for being such a hardworking and dedicated summer student. You ran more caspase assays in one summer than I ran during my graduate school career. You are a very quick learner and an excellent scientist. Somehow, you could always tell when my advice to you was legitimate and when it was… less legitimate. I

know I didn't always have a good answer for you or even an answer, but you still stuck around and did such an amazing job!

Andy, you are a quick learner and so intelligent. Thank you for being so excited to learn new techniques and for asking such good questions. I know the future of the Mott lab is in good hands with you.

Ashley, thank you for being such a great role model and scientist. I know that there were often times that I did things different from how you might have, but I so much appreciate your continued help and support. In addition, you helped me to better design experiments and went through lots of my writing to make it better. Thank you for all of your help!

Mary Anne, I honestly am struggling with where to begin. Since starting in the Mott lab, you have been an ever-present source of comfort, kindness, support, humor, and discomfort. You are intuitive when it comes to people and are an amazing friend to those you care about. And you care about so many people. And cats. And rubber chickens/ducks.. With or without you in lab, you remained present. Your funny pictures all over lab, random texts to lab members and surprise visits/birthday celebrations were the best parts of my day!

To Tim, Danae, Mallory and Ramona, from the very beginning, you have welcomed me in as part of your family. Between family dinners, walks to the park, trips to the zoo, and just hanging out, you have made me a part of your lives, and for that, I am so grateful. I cannot thank you enough for all that you have done for me.

To my amazing parents and sister, words cannot describe what the three of you mean to me. Although we're far away from each other, I feel so much a part of your lives and feel how much you want to be a part of mine. Your support, love and care

throughout this process has been invaluable to me. Thank you from the bottom of my heart. Mom, I so much appreciate your advice and ability to problem solve with me. Dad, you are an incredible source of knowledge, and I am so fortunate that you choose to share it with me. Stephanie, you are an ever-present source of happiness and support. You are so encouraging, protective and intuitive.

To Skylar, you are my everything and make me feel like nothing is impossible. Your energy and excitement drive me, and I cannot imagine my life without you.

And finally, to the patients, families, friends and loved ones affected by cholangiocarcinoma, I ask you to endure. It is a rare, but terrible disease. Stay strong, and continue to fight. The community of those affected by cholangiocarcinoma is strong, determined and supportive. And the path to new treatments is long, but it is so very worth it. I encourage you to please share your stories with others, look out for each other, and know that you are not alone. Research can be slow, but finding new treatments and ultimately a cure is a top priority for researchers. It is coming.

ROLE OF FGFR4 GLYCOSYLATION AND PROCESSING IN CHOLANGIOCARCINOMA SIGNALING AND PROGRESSION

Andrew J. Phillips, Ph.D.

University of Nebraska, 2021

Supervisor: Justin Mott, M.D., Ph.D.

Cholangiocarcinoma is a cancer of cholangiocytes, or epithelial cells lining the biliary tract. It is associated with a poor prognosis and additional therapeutic treatments are needed to help patients affected by this disease. Fibroblast growth factor receptor 4 (FGFR4) is receptor tyrosine kinase that is involved in various physiologic and pathologic processes. TCGA analysis of thirty different tumor types showed the highest FGFR4 mRNA levels in cholangiocarcinoma. At the protein level, FGFR4 was observed in the majority of cholangiocarcinomas screened and, higher levels were associated with a poorer prognosis. FGFR4 is an N-linked glycosylated receptor tyrosine kinase that we show here is modified through a cleavage process called regulated intramembrane proteolysis, where the intracellular kinase domain is released from the plasma membrane. Both glycosylation status and regulated intramembrane proteolysis have been shown to be involved in modifying cancer phenotypes. As such, a multifaceted approach to FGFR4 signaling was taken to look at the role of glycosylation on FGFR4 signaling and processing. Additionally, the regulated intramembrane proteolysis process was studied, and we identified a new form of FGFR4, R4-ICD, with a signaling role in cholangiocarcinoma cells.

CONTENTS

LIST OF FIGURES

LIST OF TABLES

LIST OF ABBREVIATIONS

ADAM	A disintegrin and metalloprotease
APH-1	Anterior pharynx defective
Arg, R	Arginine
Asn, N	Asparagine
ATP	Adenosine triphosphate
Beta APP	Beta amyloid precursor protein
cDNA	Complementary deoxyribonucleic acid
CYP7A1	Cytochrome P450, family 7, subfamily A, member 1; Cholesterol 7 alpha-hydroxylase
Cys, C	Cysteine
DAPI	4′,6-diamidino-2-phenylindole
DEPC	Diethyl pyrocarbonate
DNA	Deoxyribonucleic acid
DTT	Dithiothreitol
EDTA	Ethylenediaminetetraacetic acid
EGF	Epidermal growth factor
EGTA	Ethylene glycol-bis(β-aminoethyl ether)-N,N,N′,N′-tetraacetic acid
FBS	Fetal bovine serum
FGF	Fibroblast growth factor

FGFR	Fibroblast growth factor receptor
GFP	Green fluorescent protein
Gln, Q	Glutamine
Gly, G	Glycine
GSI IX	Gamma secretase inhibitor nine
hFGF19	Human fibroblast growth factor 19
ICD	Intracellular domain
Ig	Immunoglobulin
kDa	Kilodalton
KLA	Alpha-klotho
KLB	Beta-klotho
LFNG	Lunatic fringe
MFNG	Manic fringe
MMP	Matrix metalloprotease
NaCl	Sodium chloride
NaF	Sodium fluoride
Na_3VO_4	Sodium orthovanadate
NCT	Nicastrin
NGI-1	N-linked glycosylation inhibitor 1
NICD	Notch intracellular domain

NP-40	Nonidet P40
NT	Nucleotide
OST	Oligosaccharyltransferase
PEN2	Presenilin enhancer 2
PMA	Phorbol myristate acetate
PNGase F	Peptide:N-glycosidase F
PKC	Protein kinase C
Pro, P	Proline
PSEN	Presenilin
PTM	Post-translational modification
pY	Phosphotyrosine
R4-ICD	FGFR4 intracellular domain
RIP	Regulated intramembrane proteolysis
RFNG	Radical fringe
RNA	Ribonucleic acid
RTK	Receptor tyrosine kinase
SDS-PAGE	Sodium dodecyl sulfate polyacrylamide gel electrophoresis
siRNA	Small interfering ribonucleic acid
SH2	Src-homology 2
shRNA	Small hairpin ribonucleic acid

TM	Transmembrane
UTR	Untranslated region

CHAPTER 1: INTRODUCTION

The focus of this dissertation is the receptor tyrosine kinase, FGFR4. Studies here report on glycosylation and proteolytic processing events that affect FGFR4 function, and how this information can be used to help patients with cholangiocarcinoma, a rare liver cancer with a dismal prognosis. The following sections introduce relevant aspects of cholangiocarcinoma, receptor signaling, and post-translational processing.

Cholangiocarcinoma

Cholangiocarcinoma is a cancer of the cholangiocytes, or the epithelial cells that line the biliary tree [1]. The biliary tree is a branching system of bile ducts within and outside of the liver that carries bile produced in the liver to the gallbladder or duodenum. Cholangiocarcinoma can be either intrahepatic or extrahepatic, depending on where the tumor originates. A common form of extrahepatic cholangiocarcinoma, called the Klatskin tumor, occurs at the branching point of the left and right hepatic ducts or the hilum, and, if detected early enough, can be treated through orthotopic liver transplant in addition to adjuvant and neoadjuvant therapies [2]. Highly selected patients who receive a transplant for cholangiocarcinoma treatment have a 5-year survival similar to that of an individual receiving a liver transplant for other reasons: roughly 65% (vs 75% for all liver transplants) [2]. However, the majority of cholangiocarcinoma patients are not transplant candidates and have a poor prognosis, with 5-year survival rates at or below 10% [1]. In part, this is due to the silent nature of the tumor when it is in its early stages. Individuals seldom present with symptoms until the tumor has grown and metastasized, and even then, symptoms can be nonspecific, for example: abdominal pain, weight loss, fatigue, and loss of appetite. At later stages, patients may show signs and symptoms of biliary obstruction, such as jaundice, scleral icterus, and severe itching.

Several known risk factors exist for cholangiocarcinoma, including primary sclerosing cholangitis, hepatolithiasis, bile duct cysts, toxic agents (e.g., Thorotrast), and liver fluke infections [3]. Due to cultural and risk factor-associated differences, the incidence of cholangiocarcinoma varies greatly by geographic region. For example, the consumption of raw or semi cooked seafood in Southeast Asia leads to liver fluke infections resulting in a much higher prevalence of cholangiocarcinoma in that part of the world; approximately 33.4/100,00 in Thai men and 12.3/100,000 in Thai women [3]. In the United States, however, liver fluke infestation is not endemic, and the prevalence of cholangiocarcinoma is estimated at 0.5-2.0/100,000 [4, 5]. The majority of cases in the US occur sporadically or as a result of primary sclerosing cholangitis. Still, it is the second most common primary malignant liver cancer.

Medical treatment options for patients with cholangiocarcinoma are quite limited. The current typical treatment is gemcitabine plus cisplatin [6]. Compared with gemcitabine alone, patients on the dual therapy showed a small but measurable 3.6 month increase in survival on average. Because the clinical benefit of current therapeutic options is so limited in patients with cholangiocarcinoma, patients are encouraged to take advantage of clinical trials whenever possible. In the meantime, finding new therapeutic targets in cholangiocarcinoma remains a top priority.

Receptor tyrosine kinases

Receptor tyrosine kinases, or RTKs, are a large group of type 1 transmembrane proteins that contain an N-terminal extracellular ligand binding domain, a helical single pass transmembrane domain, and a C-terminal intracellular kinase domain. In humans, there are 58 known RTKs, however, these proteins are very well-conserved across species. They play a variety of different physiologic roles, but importantly can also

contribute to disease states, including diabetes, inflammation, vascular changes and cancer [7-9].

Mechanistically, canonical RTK signaling occurs first through ligand binding. Upon ligand binding to the extracellular domain of the receptor, conformational changes occur which allow for protein dimerization. It should be noted that some RTKs oligomerize even in the absence of ligand, for example the insulin receptor and IGF1 receptor which are expressed as disulfide-linked dimers. In either case, conformational changes follow ligand binding, leading to receptor tyrosine kinase domain activation via transphosphorylation, in which the tyrosine kinase domains of dimerized RTKs phosphorylate one another [7, 10]. Prior to ligand binding, an individual tyrosine kinase domain of an RTK has an autoinhibitory conformation to prevent tyrosine phosphorylation and subsequent downstream signaling from occurring. The structural determinant of this inhibitory conformation varies greatly among RTKs. For example, in FGFR1, residues in the activation loop do not specifically interfere with ATP binding, but rather seem to stabilize the inactive form. This is contrary to the insulin receptor, where ATP binding is directly (sterically) blocked in the inactive form of the receptor [11]. When ligand binding and dimerization occur, changes in the tyrosine kinase domain lead to destabilization of the autoinhibitory region and in some cases, the inhibitory portion of the juxtamembrane region [8, 12].

Dimerization of ligand-bound receptors has been hypothesized to occur through one of several different mechanisms: bivalent ligands pulling or crosslinking two receptors together, ligand-ligand interactions (where the two receptors do not touch), receptor-receptor interactions (where the two ligands do not touch) or some variation of the two extremes. In the case of fibroblast growth factor receptors (FGFRs), several models have been proposed. In one case, x-ray crystallography demonstrated the

dimerization of two FGFR1c receptors through interaction with two FGF2 molecules and two cofactor molecules (heparin) in a 2:2:2 fashion. In this model, the receptors were in direct contact with one another. Each FGF molecule interacted with both receptors but each formed a major interaction with one and a minor interaction with the other such that each receptor had one FGF tightly bound and one FGF more weakly bound. Heparin was in direct contact with both ligands and both receptors at the second immunoglobulin-like loop (IgII) [13]. An alternate crystal structure showed heparin serving as the bridge in connecting two separate FGF1/FGFR2 complexes. In this situation, the 2:2:2 ratio was disrupted [14]. Variations seen between experiments may simply be due to the variations among FGFRs and FGFs (i.e., FGF1 versus FGF2), availability of cofactors, or environmental conditions (temperature, salt concentration, pH, etc.). Notably, FGFR4 binds ligand in cooperation with Klotho coreceptors and is not heparan sulfate-dependent. Indeed, FGF19, which preferentially activates FGFR4, is an endocrine FGF due to its lack of affinity for heparan sulfate. While ligand binding to the extracellular domains promotes dimerization, the transmembrane and intracellular domains also have the ability to form dimeric contacts. In either case, dimerization ultimately leads to receptor activation.

Once transphosphorylation is complete, specific phosphotyrosine (pY) residues in the kinase domain can directly bind proteins containing Src-homology 2 (SH2) domains or phosphotyrosine binding domains. Alternatively, docking proteins (FRS2, IRS1, Gab1) may directly bind the phosphotyrosine residues in the activated tyrosine kinase domain and subsequently recruit proteins containing SH2 or phosphotyrosine binding domains to trigger the activation of a signal cascade [7, 9, 10, 15-17]. RTK signaling also leads to receptor ubiquitination and subsequent internalization and redistribution or lysosomal degradation of the receptor, creating a process for negative

feedback and means for regulating signaling [18]. FGFR4 has been shown to undergo less ubiquitination and is primarily endocytosed and recycled, whereas FGFR1-3 tend to have higher levels of ubiquitination and primarily undergo lysosomal degradation [19]. Perhaps this is not surprising, but of the RTK FGFR proteins, FGFR4 contains the fewest number of lysine residues intracellularly (FGFR1: 29, FGFR2: 30, FGFR3: 26, FGFR4: 16). Lysine residues are targeted by E3 ubiquitin ligases for ubiquitination. Accumulation of ubiquitin molecules can modify protein function and signaling but can also serve as a tag for protein degradation. Lysine to arginine mutations within the intracellular domain of FGFR1 prevented FGFR1 from entering the lysosome and promoted its recycling [19].

More recent studies have shown that RTKs can signal through a process called regulated intramembrane proteolysis (RIP). In RIP, a majority of the ectodomain—the extracellular portion of the protein—of an integral membrane protein is cleaved by a sheddase, a generic term for a group of proteases (typically a disintegrin and metalloprotease protein, ADAM) that cleave integral membrane proteins at the juxtamembrane region of the ectodomain. The remaining portion of the ectodomain is typically 12-35 amino acids in length, although this number may vary from source to source [20]. This shedding event alters the conformation of the remaining receptor which allows γ-secretase to cleave the receptor within its transmembrane domain (**Figure 1**). From there, the released intracellular portion of the protein can serve a variety of different functions. The intracellular fragment can translocate to the nucleus, as seen with Notch, ERBB4, FGFR3, PTK7, and RYK [21-24]. Additionally, the intracellular domain (ICD) can localize to the mitochondria, as seen with ERBB4 ICD, where it serves as a pro-apoptotic signal [25, 26]. EPHB2 ICD has been shown to phosphorylate and

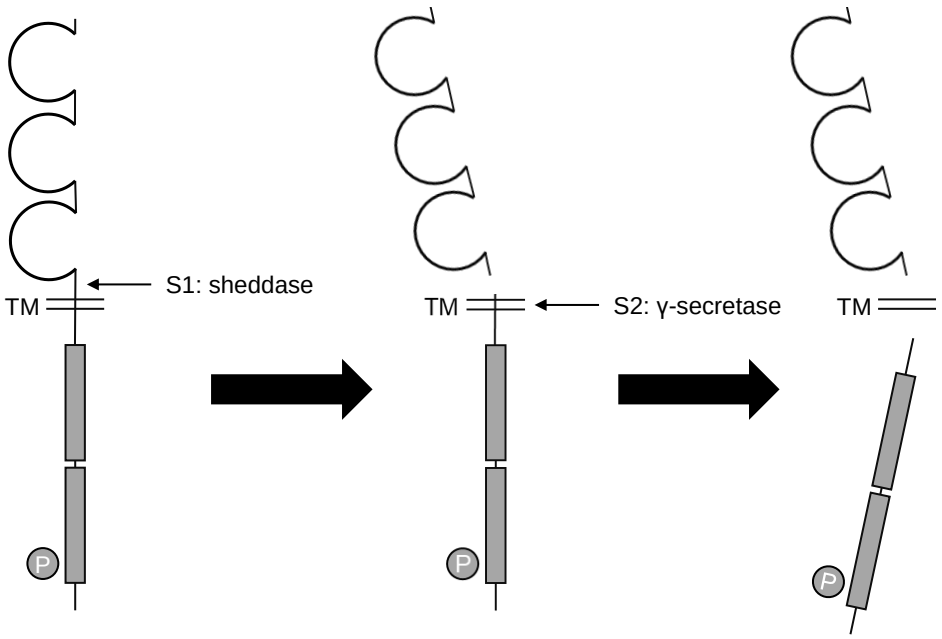

Figure 1. Regulated intramembrane proteolysis of receptor tyrosine kinases.

A receptor tyrosine kinase is shown with three extracellular Immunoglobulin-like loops, a transmembrane (TM) domain, and an intracellular kinase domain. In regulated intramembrane proteolysis (RIP), an initial cleavage event, S1, is proceeded by a secondary cleavage event, S2. S1 cleavage is frequently catalyzed by sheddase proteases like ADAM proteins, and S2 cleavage is catalyzed by γ-secretase.

modulate the localization of other membrane receptors [27]. In cancer, ligand-induced cleavage of EPHB2 by MMP proteins was shown to initiate cell repulsion, allowing for cell migration or metastasis [28]. Alternatively, preventing AXL cleavage promoted resistance of lung adenocarcinoma cells to treatment by Erlotinib [29]. MET ICD appears to simply undergo rapid degradation [30]. With these examples in mind, it becomes quite clear that there is a high degree of variability regarding the role/function of the released intracellular domain following RIP, including relocalization to activate new signaling or transcription, or alternatively the ICD is degraded to halt signaling.

In cancer, several different alterations to RTK pathways and signaling can promote malignancy. These alterations include genomic amplifications, gain of function mutations, autocrine activation, or chromosomal rearrangements leading to fusion proteins [31]. As such, a number of targeted therapeutics are designed to inhibit RTKs. RTK inhibitors prevent phosphorylation of downstream targets by directly inhibiting RTK phosphorylation or by preventing RTKs from interacting with their binding partners. Both forms of inhibition can occur competitively or allosterically. Commonly, drugs have targeted the ATP binding site; however, this binding site is conserved in RTKs and frequently results in drugs having off target interactions. While there are situations where a drug interacting with more than just its intended target can increase its efficacy (a notable example being the multi-kinase inhibitor sorafenib with efficacy in hepatocellular carcinoma), targeting multiple kinases can potentially increase the toxicity associated with a drug [32]. As such, the development of drugs targeting allosteric sites has become increasingly more common, as these sites can produce conformational changes in the ATP binding pocket, but are less highly conserved between receptors and therefore, have higher variability in structure. Allosteric targeting of low conserved sites ultimately allows for general higher selectivity in these drugs. Selectivity has been achieved

through other approaches as well. In the case of FGFR4, a unique cysteine residue at position Cys-552 was noted and an inhibitor that binds the ATP binding pocket was modified to have an accessible ‘warhead’ domain for covalent Cys modification (Hagel et al., 2015, Cancer Discovery). This led to the development of Fisogatinib (BLU554), which binds FGFR4 with affinity 100-fold higher than FGFR1 and 1000-fold higher than FGFR2 and FGFR3 [33].

FGFR family of proteins and cancer

FGFRs are a subfamily of receptor tyrosine kinases that interact with fibroblast growth factors. These receptors/ligands have been shown to play a role in embryonic development, tissue repair, proliferation, migration and cell survival. Structurally, these proteins consist of three extracellular Ig-like domains at their N-terminus, a single pass transmembrane domain, and an intracellular protein kinase domain (C-terminus). Alternative splicing can occur in FGFRs 1-3 and is often tissue-specific to alter affinity for different FGFs [34]. Ligand-receptor binding among FGFs and FGFRs can occur with a good deal of cross-activation. Cofactors required for receptor activation help to promote tissue-specific receptor activation and reduce promiscuity. Most FGFs use heparan sulfate proteoglycans as their cofactors, whereas FGF19/15, FGF21 and FGF23 use klotho proteins as their coreceptors [35, 36]. Beta klotho (KLB) serves as a coreceptor for FGF19/15 and 21, while alpha klotho (KLA) serves as a coreceptor for FGF23 [37, 38]. In addition to requiring different cofactors, the FGF19/15 subfamily of proteins (FGF19/15, FGF21 and FGF23) participate in hormonal- paracrine- and autocrine-signaling.

FGFR1 and FGFR3 have previously been demonstrated to undergo proteolytic cleavage in which the intracellular kinase domain is cleaved from the full-length receptor.

In 1996, Levi et al. demonstrated selective activity of MMP2 on FGFR1 (in the presence or absence of FGF), which prompted the release of an extracellular domain capable of binding FGFs. Cleavage was shown to take place between Val-368 and Met-369 on the extracellular side of the receptor near the transmembrane region [39]. Ten years later, Loeb et al. demonstrated that granzyme B cleaved FGFR1 intracellularly between residues Asp-432 and Ser-433 [40]. Granzyme B-mediated cleavage of FGFR1 resulted in nuclear localization of FGFR1's intracellular kinase domain [41]. FGFR3 undergoes ligand-induced RIP following receptor endocytosis. This S1 cleavage event is metalloproteinase-independent for FGFR3. A second cleavage event, S2, occurs via γ-secretase activity and releases the intracellular kinase domain, which then translocates to the nucleus, like the FGFR1 intracellular domain [22, 42].

Germline mutations in FGFRs can lead to congenital conditions such as Pfeiffer syndrome (FGFR1 or FGFR2), Crouzon syndrome (FGFR2 or FGFR3), and achondroplasia (FGFR3) to name a few [43] [44, 45]. These conditions are associated with increased kinase activity and unregulated signaling, resulting in recognizable clinical developmental syndromes. Somatic mutations and changes in expression of FGFRs have been observed to play a role in the development and progression of numerous types of cancer. A screening study that looked at 4,853 tumor samples showed FGFR alterations in 7.1% of samples. Of the samples that showed alterations, 66% were amplifications, 26% were mutations and 8% were rearrangements. FGFR1 was most commonly altered, and FGFR4 was least commonly altered, with roughly a seven-fold difference between the two [46]. FGFR1 has been shown to promote tumorigenesis and progression in various cancers including: gastric, prostate, breast, lung, and colon cancer [47-50]. FGFR1 gene amplification is more common in cancers than are mutational changes to the protein. FGFR1 gene amplification is observed in

approximately 20% of squamous-type non-small cell lung carcinomas, 5-7% of small cell carcinomas, and is very rarely observed in lung adenocarcinomas [46, 51, 52]. FGFR1 fusions are quite rare in solid tumors; however, they have been observed sporadically in gastrointestinal stromal tumors, breast cancer, glioma and glioblastoma, with various fusion partners involved. FGFR2 is the FGFR most commonly involved in fusion mutations. Numerous fusion partners exist for FGFR2, and these mutations are commonly observed in cholangiocarcinoma (8-13%) [53]. FGFR2 fusions have also been observed infrequently in colorectal cancer and hepatocellular carcinoma. Point mutations that result in constitutive activation of FGFR3 are common in bladder cancer (66.6% have an S249C mutation in the extracellular domain, which promotes ligand-independent receptor dimerization) [54]. FGFR3 fusion mutations are common in glioblastoma and bladder and lung cancer. In contrast to FGFR1 and FGFR2, most fusions with FGFR3 occur with a common fusion partner, transforming acidic coiled coil 3 protein (TACC3), and consist of the FGFR3 N-terminal, transmembrane, kinase and kinase insert domains fused to the TACC3 coiled coil domain to produce constitutively active signaling through the FGFR3 kinase domain [50, 55, 56]. In addition to the cancers described previously, FGFR mutations have been observed in a number of other tumors, including gliomas, head and neck squamous cancer, lung squamous cell carcinoma, and cervical cancer. FGFR4 activating mutations are rarely seen, but can occasionally be identified in rhabdomyosarcomas and other pediatric cancers. FGFR4 fusion mutations have only recently been discovered in non-small cell lung cancers [50].

FGFR inhibitors have been and are currently being tested in clinical trials. Several of these inhibitors target FGFR1-4 with little selectivity (Pozopanib HCL, Erdafitinib, Futibatinib, Derazantinib, LY2874455) or target FGFR1-3 with much less affinity for FGFR4 (Infigratinib, Pemigatinib, Rogaratinib, AZD4547, Debio 1347).

Fisogatinib is an FGFR4-selective inhibitor. Currently, anti-FGFR drugs are primarily being used to treat urothelial cancer or cholangiocarcinomas which harbor FGFR2 fusions [57].

FGFR4

Like the other FGFRs, FGFR4 is composed of three extracellular Ig-like domains, a helical transmembrane domain, a juxta-membrane region, and a protein tyrosine kinase domain. Unlike other FGFRs, the extracellular domain of FGFR4 is not alternatively spliced [58, 59]. FGFR4 undergoes N-linked glycosylation, but glycosylation does not appear to be necessary for proper folding of the extracellular domain or for ligand binding [60, 61]. Sequence analysis of human full length FGFR4 shows five possible sites for N-linked glycosylation, that can exhibit high-mannose or complex-type (mature) glycosylation [62]. Potential glycosylation sites are identified as an asparagine (Asn) residue followed by any amino acid except proline, and then a serine or threonine. Previous studies have identified terminally glycosylated FGFR4 (complex-type) as the form primarily involved in signaling [62]. It is likely the complex-type glycoform of FGFR4 is the primary signaling form, because it has been fully processed through the Golgi and delivered to the plasma membrane where ligand-receptor interactions occur. Glycosylation plays an essential role in Notch function and ligand binding [63] and may play a role in FGFR4 function and ligand binding as well.

Under physiologic conditions, FGFR4 serves as a regulator of bile acid synthesis. Bile acids are produced and secreted by hepatocytes into the biliary tree and small intestine, then reabsorbed in the ileum and recycled back to the liver via enterohepatic circulation [64]. The ileum also secretes the hormone, FGF19, in response to bile acid reabsorption. Bile acids enter the epithelial cells of the ileum and activate the nuclear

bile acid receptor, FXR, increasing FGF19 production and secretion. FGF15 is the mouse ortholog of human FGF19, so sometimes this protein is referred to collectively as FGF19/15. FGF19 secreted from intestinal epithelial cells circulates via the portal circulation to the liver, serving as a negative regulator of bile acid production by binding FGFR4 expressed on hepatocytes. Thus, FGFR4 is strongly expressed in the liver. We have observed FGFR4 protein present in hepatocytes but not in normal bile duct epithelial cells (cholangiocytes) in the liver (Mohr et al., unpublished observations).

In malignancy, FGFR4 signaling has been shown to promote cell proliferation and inhibit apoptosis through the MAPK/ERK, AKT and STAT3 pathways, among others. In breast cancer, FGFR4 activation of the MAPK/ERK pathway inhibited apoptosis by increasing the expression of Bcl-x_L [65, 66]. In cholangiocarcinoma, we found that FGFR4 increases XIAP protein expression to inhibit apoptosis (Mohr et al., unpublished). Increased FGFR4 expression and/or mutation in cancer has been linked to poorer overall prognosis [67-74]. Mutations in FGFR4 are not known drivers of cholangiocarcinoma, but we have observed elevated FGFR4 mRNA and protein expression in the majority of human cholangiocarcinoma samples when compared to normal cholangiocytes.

FGFR4 is the primary receptor for FGF19, itself a tumor driver [75, 76]. Over 3% of intrahepatic cholangiocarcinoma patients show FGF19 genomic amplification [77]. Alternatively, FGFR4 expression has been observed in a majority of cholangiocarcinoma tumors, and its expression correlated with a poor prognosis [68].

FGFR4-selective inhibitors, BLU9931 (and analog, Fisogatinib/BLU-554), and H3B-6527 irreversibly bind a unique cysteine residue located at position 552, adjacent to the ATP-binding pocket, and inhibit FGFR4. Upon testing, BLU9931 was found to be potent and showed preferential inhibition of FGFR4 in cell free experiments: FGFR4

IC_{50}: 3 nM, FGFR1 IC_{50}: 591 nM, FGFR2 IC_{50}: 493 nM, FGFR3 IC_{50}: 150 nM [78]. Fisogatinib, a structural analog of BLU9931, is currently in phase II clinical trials for the treatment of hepatocellular carcinoma. Because of FGFR4's rapid turnover in hepatocellular carcinoma, a reversible, FGFR4-selective inhibitor approach was proposed, leading to the development of FGF401/Roblitinib. The covalent irreversible inhibitor was not available for newly synthesized FGFR4 while a reversible inhibitor should not be consumed and can act on newly made FGFR4. In short, FGFR4 is being rapidly synthesized and degraded, and each molecule of the irreversible inhibitor only functions for as long as the receptor exists. With a reversible inhibitor, the drug can have a prolonged effect by avoiding degradation with the receptor. FGF401/Roblitinib has an IC50 of 1.1 nM for FGFR4 and demonstrated a 1000-fold selectivity over a panel of 65 other kinases [79].

Similar to what was observed with FGFR1 [39, 40] and FGFR3 [22], recent data has shown that FGFR4 is proteolytically cleaved through regulated intramembrane proteolysis [60, 80] (see also our results in Chapter 4), leading to the release of the intracellular domain. Merilahti *et al.* demonstrated that γ-secretase inhibition altered FGFR4 processing, and indirectly showed that an ADAM protein may be involved in proteolysis. Those studies did not characterize the regulated proteolysis or function of the released intracellular domain. Here, we provide additional experimental evidence that the intracellular domain is produced via proteolysis, we characterize the sheddase involved, and we determine the regulated production and functions of the FGFR4 intracellular domain (R4-ICD).

FGF19

There are 18 human FGF proteins that fall into 6 different subclasses. An additional group of homologous factors, called FGF11-14, serve as nuclear factors and are unable to activate any of the FGFRs [50]. The majority of receptor-dependent FGF proteins signal through FGFRs in a paracrine or autocrine manner; however, one subclass functions hormonally, sending soluble blood-borne signals throughout the body. This is the FGF19 subclass and is made up of FGF19/15, FGF21 and FGF23. These three proteins lack a heparan sulfate binding domain, allowing them to avoid being limited to autocrine or paracrine signaling. As discussed previously, the FGF19 subclass utilizes cofactors alpha klotho (KLA) or beta klotho (KLB) as a cofactor or coreceptor when signaling through FGFRs. FGF19 utilizes beta klotho.

FGF19 has known functions within the liver and the gallbladder. In the liver, it negatively regulates bile acid synthesis by reducing CYP7A1 expression in hepatocytes, reduces gluconeogenesis, and promotes protein and glycogen synthesis. FGF19 also causes relaxation of the gallbladder muscle tissue [81].

In mice with genetic depletion of FGF15, the mouse FGF19 homolog, administration of human FGF19 was able to effectively lower blood glucose in a hyperglycemia model by promoting liver glycogen synthesis [81]. Transgenic mice overexpressing FGF19 developed hepatocellular carcinoma by ten months of age, showing an oncogenic effect beyond the metabolic effect. These mice showed hepatocyte proliferation and differentiation prior to ten months [82]. Since hepatocytes endogenously express FGFR4, and since FGF19 has a higher affinity for FGFR4 than the other FGFRs, robust activation of this signaling axis within hepatocytes was expected. While data show that FGFR4 expression correlates with a poorer prognosis in cholangiocarcinoma patients [68], our data also suggest that normal human

cholangiocytes lack expression of FGFR4. As such, an abundance of FGF19 is unlikely to promote the development of cholangiocarcinoma in an otherwise healthy animal. FGFR4 activation in hepatocytes leads to signaling through the Ras/Raf/MEK/ERK and PI3K/AKT pathways [83]. Activating mutations in Ras are frequently seen as major drivers in tumorigenesis and approximately 20% of all human tumors have activating mutations in *Ras* genes [84]. As such, high dose FGF19 can functionally mimic an activating mutation in *Ras* and lead to tumorigenesis in FGFR4-expressing cells.

Notch signaling

The Notch family is made up of four transmembrane glycoprotein receptors, Notch1-4. This group of proteins is highly conserved across species. The glycosyltransferases that modify Notch proteins, such as Lunatic Fringe and Protein O-Fucosyltransferase-1, have been tied to cancers. Lunatic Fringe, thought to be a tumor suppressor, was shown to be deficient in basal-like breast cancer and prostate cancer [85, 86]. Additionally, Protein O-Fucosyltransferase-1 (along with FGF19) gene amplification has been observed in hepatocellular carcinoma, among other cancers [87, 88].

Functionally, Notch signaling can promote or suppress cell proliferation, cell death, or differentiation and plays fundamental roles in developmental body patterning as well as in adult tissue repair and regrowth. As such, abnormal Notch signaling (increased or decreased) can lead to disease states including tetralogy of Fallot, syndactyly, Alagille syndrome, and others [89, 90]. Alagille syndrome demonstrates the relationship of Notch signaling to the biliary tree, where partial loss of Notch ligand (Jagged-1) expression prevents the complete development of intrahepatic bile ducts. Patients generally have a loss of one of the two Jagged-1 alleles (hemizygous), leading to reduced Notch signaling. The portal vein endothelial cells normally express Jagged-1

and signal to neighboring bipotential liver cells to induce differentiation into biliary epithelial cells. When there is reduced Notch signaling, there is reduced intrahepatic bile duct development and a congenital cholestatic disease can result. We note that Notch signaling is also identified in malignant cholangiocarcinoma [91] and that hepatocytes transduced with an oncogene plus Notch activation form cholangiocarcinomas [92].

Notch influences other cancers, too, where over 50% of T-cell acute lymphoblastic leukemias have activating mutations in the Notch receptor. These mutations are observed within the extracellular heterodimerization domain and/or the intracellular PEST domain [93]. Structurally, Notch proteins are type 1 transmembrane receptor hetero-oligomers, consisting of a large extracellular domain that contains tandem EGF-like repeats (29-36) which participate in ligand binding [94]. Additionally, they have a negative regulatory region that, as the name would suggest, autoinhibits Notch activity in the absence of ligand, a single pass transmembrane region and an intracellular portion. The Notch intracellular domain, NICD, contains an RBPJ-associated module (RAM) domain, six ankyrin repeats (ANK, involved in protein interactions) and a PEST domain that reduces Notch stability by promoting proteasomal degradation [95, 96]. Following Notch protein synthesis but prior to its integration into the plasma membrane, the Notch receptor is cleaved at its S1 site while in the trans Golgi network. This site is approximately 70 amino acids N-terminal from the transmembrane domain. The two protein products from this cleavage event remain associated through calcium-dependent ionic bonds. This ultimately results in a large entirely extracellular portion of Notch bound to a smaller membrane-spanning portion (known as the TMF or transmembrane fragment) [97]. Upon ligand binding the Notch receptor, the cell expressing the transmembrane ligand on its plasma membrane attempts to endocytose the ligand (and bound receptor). This traction force on the Notch receptor is

hypothesized to cause conformational changes in the negative regulatory region, which ultimately leads to deprotection and ADAM-mediated cleavage of the S2 site (on the extracellular portion of the transmembrane fragment, 12 amino acids from the membrane), leaving behind the Notch extracellular truncation (NEXT). Following S2 cleavage, endocytosis of ligand and a portion of the Notch receptor can occur on the cell expressing ligand. S2 cleavage is the rate limiting step in Notch activation for the receptor-expressing cell. At this point, γ-secretase accesses the S3 cleavage site located in the intramembrane region near the outer leaflet of the plasma membrane on NEXT. This is followed by a second γ-secretase-mediated cleavage, S4, which occurs near the middle of the transmembrane region, resulting in release of the NICD [98]. NICD then mediates Notch signaling via its action in the nucleus [96, 97]. Once released from the plasma membrane, the NICD interacts with DNA binding proteins in the CSL family and regulates transcription of selected genes.

Notch canonical signaling in humans and mice occurs through activation by ligands of the Delta like (DLL1, DLL3, DLL4) and Jagged (Jagged-1, Jagged-2) protein families. Data suggest that signaling is dictated primarily by which receptor (Notch1-4) is activated, and not which ligand is used to activate the receptor [96]. Notch cleavage and signaling has also been shown to occur in a ligand-independent manner, utilizing CD28 and the T-cell receptor of nearby T-cells [99-101]. Data suggest that ADAM17 was the protease necessary for ligand-independent S2 cleavage of Notch, whereas ADAM10 was the protease in ligand-induced S2 cleavage [102].

Notch proteins contain a large number of EGF repeats which can be O-glycosylated (O-fucose or O-glucose) to modify ligand-receptor signaling and allow for subsequent receptor modification to occur. Fringe-family proteins are glycosyltransferase enzymes involved in Notch modification that recognize O-fucose

molecules. Fringe is able to add additional sugar moieties to the Notch receptor to regulate ligand binding specificity. For example, the addition of a single N-acetyl glucosamine molecule on EGF repeat 12 by Fringe can promote Notch binding and activation by ligand, Delta, and reduce binding and receptor activation by an alternate ligand, Serrate (a Jagged analog), in *Drosophila.* In mammals, multiple Fringe proteins (Lunatic Fringe, LNFG; Manic Fringe, MNFG; and Radical Fringe, RNFG) add N-acetyl glucosamine to EGF-like repeats 8 and 12 on Notch-1 [96, 103] and promote binding to Delta-like ligand 1 (DLL1) [104-106]. LFNG- and MFNG-mediated glycosylation (addition of N-acetyl glucosamine at EGF repeats 6 and 36) reduced Notch1-Jagged-1 signaling [107].

Presenilin and γ-secretase

The Notch S3 and S4 cleavage events are both performed by γ-secretase, an aspartyl protease that is made up of four subunits: nicastrin (Nct), anterior pharynx defective 1 (APH-1), presenilin enhancer 2 (PEN2), and presenilin 1 or 2 (PSEN1 or 2). Nicastrin, APH-1 and PEN2 promote proper maturation and assembly of γ-secretase and allow the correct post-translational modifications to occur. PSEN1 or 2 is the catalytically active subunit with aspartyl protease activity [108]. There is evidence to suggest that PSEN can cleave single pass transmembrane proteins (within or outside of the TM region), regardless of sequence, so long as the extracellular portion of the protein is fewer than 200-300 amino acids in length. Additionally, there appears to be a correlation between length of the ectodomain and efficiency with which γ-secretase cleavage occurs; a protein with a larger ectodomain appeared to be cleaved less efficiently than one with a smaller ectodomain [109]. As such, for proteins like Notch or

β-APP, the initial ectodomain shedding event is necessary to shorten the extracellular domain allowing for subsequent γ-secretase cleavage.

Merilahti and colleagues conducted a screening experiment to look for receptor tyrosine kinases that could be proteolytically cleaved by γ-secretase [80]. In this screen, 45 human receptor tyrosine kinases were tested for their ability to undergo RIP via γ-secretase in controlled conditions in transfected cells. They reasoned that activation of a sheddase, combined with inhibition of γ-secretase, would lead to stabilization of a partially cleaved intermediate, and detection of that intermediate was taken as evidence that a receptor was a γ-secretase substrate. Phorbol 12-myristate13-acetate (PMA) was used to activate Protein kinase C which in turn activates some sheddases. PMA is a small molecule activator of Protein kinase C (PKC) with a structure similar to that of diacylglycerol, an endogenous PKC activator. PKC promotes sheddase activity, leading to RIP. Another tool used in their study was γ-secretase inhibitor IX (GSI IX, also known as DAPT). GSI IX works through targeting the C-terminal domain (primarily transmembrane domain seven) of presenilin [110]. Promotion of sheddase activity (through PMA) and inhibition of γ-secretase activity (GSI IX), led to the accumulation of membrane-anchored C-terminal fragments of RTKs that are normally cleaved by γ-secretase. Nine RTKs that had previously been shown to undergo RIP were confirmed, and 12 additional RTKs, including FGFR4, were newly shown to undergo RIP [80]. Their data were only shown with tagged exogenous FGFR4 under the described experimental conditions and they did not assess for a function of the proteolytic product. Thus, FGFR4 can undergo RIP, and our studies demonstrate the relevance of this processing in signaling and in human tumors.

Extracellular proteases

Most extracellular proteases fall into one of three main groups: metalloproteases (MMPs, Adamalysins, and others), serine proteases, and cysteine proteases. Extracellular proteases have been widely targeted pharmacologically due to their important roles in both physiologic and pathologic processes. MMPs, or matrix metalloproteinases, are a family of 24 human zinc-dependent endopeptidases able to cleave and degrade extracellular matrix protein components [111-113]. Many MMPs are soluble enzymes; however, MT-MMPs, or membrane-type MMPs are a group of six membrane-associated matrix metalloproteases. Under physiologic conditions, they contribute to tissue homeostasis and remodeling. In cancer, increased expression or activation of MMPs can promote tumor cell growth, invasion and metastasis into surrounding tissue, in addition to increasing angiogenesis [113]. Early MMP inhibitors worked primarily through zinc chelation, which led to a lack of drug specificity, reducing clinical applicability.

ADAM (a disintegrin and metalloproteinase) proteases are membrane-anchored proteins whose catalytic domains share structural similarity with MMP catalytic domains. As a result, ADAMs also require zinc for protease activity. Unlike MMPs, however, ADAM proteins lack a hemopexin-like domain and have a cysteine-rich domain, EGF-like domain and a disintegrin domain (their namesake) [111]. Functionally, ADAMs primarily regulate tumor cell adhesion and growth signaling [113]. Some MMPs, including MMP7 and MMP14, can act as sheddases which proteolytically release the extracellular portion of transmembrane proteins [114, 115]. Just over half of known ADAM proteins (18/33) are predicted to have protease activity, with ADAMs 9, 10, 12 and 17 having demonstrated sheddase activity [113, 114]. These proteins play a crucial role in initiating regulated intramembrane proteolysis by carrying out the initial cleavage event.

Proposed effects of glycosylation on FGFR4 signaling and processing

Thus far, several examples of proteolytic processing of integral membrane proteins have been discussed, including various RTKs and Notch. In each of these examples, an extracellular sheddase-mediated cleavage event is necessary for subsequent proteolysis and release of the ICD. Receptor activation may be necessary for this cleavage cascade to occur, as seen with FGFR3. In other cases (Notch, in particular), glycosylation and other post-translational modifications are essential for receptor function and affected signaling. In the case of Notch, O-linked glycosylation of the EGF-like repeats was able to modify receptor ligand interactions. These specific sites of glycosylation varied from species to species, but they were at least 300 amino acids away from the TM region (*Homo sapiens*, *Drosophila melanogaster*), suggesting that their major role was to modify receptor-ligand interactions.

In FGFR4, five extracellular N-linked glycosylation sites exist, with the most C-terminal site (Asn-322) located less than 50 amino acids from the transmembrane region. The three most C-terminal sites (Asn-290, -311, and -322) fall within the IgIII loop, and the two other sites (Asn-112, -258) are located between the IgI and IgII and the IgII and IgIII loops, respectively. FGFR4 ligand binding occurs between the N-terminal portion of IgII and the C-terminal portion of IgIII. With this in mind, it would be reasonable to hypothesize that glycosylation of FGFR4 could modify its ability to be cleaved through altering receptor-ligand interactions and/or by directly altering the interaction with sheddase(s) (**Figure 2**). In Chapter 3 of this dissertation, I show that the cleavage product of FGFR4, R4-ICD, was increased by removing N-linked glycans from the ectodomains of cell surface proteins or by reducing a cell's intrinsic ability to glycosylate proteins at Asn residues. This led to our subsequent experiments to further

test the role of glycosylation in regulating FGFR4 cleavage, where we employed site-directed mutagenesis to prevent glycosylation of the predicted five Asn that could be modified. Each of these Asn residues was individually mutated to a glutamine residue and expressed as a single mutant. In addition, a combined 4Q mutant, in which 4 of the 5 asparagine residues were mutated to glutamine, was generated.

In addition to looking at the effects of glycosylation on FGFR4 signaling and processing, I investigated how FGFR4 proteolysis to R4-ICD occurs. In cholangiocarcinoma cells, inhibiting FGFR4 signaling has been shown to reduce cell

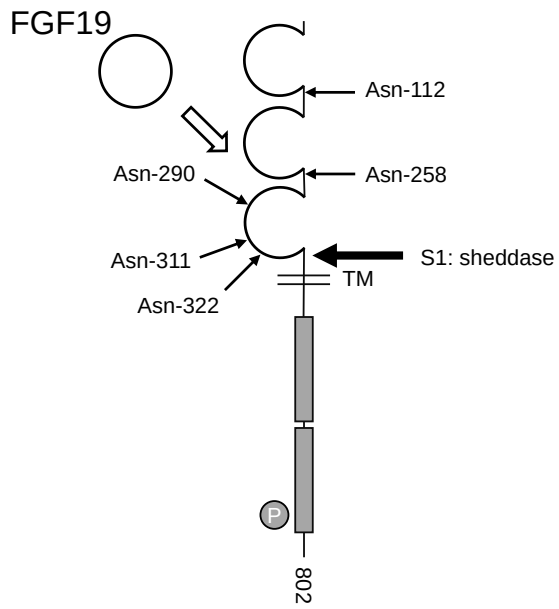

Figure 2. Schematic of FGFR4 with possible sheddase cleave site.

Structurally, FGFR4 contains three extracellular immunglobulin-like loops, and five asparagine (Asn) residues capable of undergoing N-linked glycosylation. FGF19, a ligand for FGFR4, has been shown to bind at the receptor between immunoglobulin-like loops two and three. Here, the ligand binding site and putative S1 cleavage area are highlighted and the proximity of these two areas to N-linked glycosylation sites is emphasized.

proliferation and increase cell susceptibility to apoptosis. As such, inhibiting FGFR4 may be a reasonable approach to treating patients with FGFR4-positive cholangiocarcinoma. Initial screening experiments by others have shown that FGFR4 can be proteolytically processed by γ-secretase, but γ-secretase activity typically requires that the substrate has undergone an initial shedding event. Further, those studies did not functionally characterize the R4-ICD.

We reasoned that in the absence of the extracellular domain, R4-ICD would be freed from the inhibitory effect of the receptor and freed from reliance on ligand, thus having constitutive activity. Experiments in this dissertation demonstrated that R4-ICD is the predominant form of FGFR4 observed in human cholangiocarcinoma tissue samples and glycosylation regulates R4-ICD production. Importantly, glycosylation of FGFR4 itself decreased proteolytic processing, contrary to the effects of non-selective deglycosylation that increased proteolytic processing of FGFR4, suggesting that glycosylation of other cellular factor(s) regulates R4-ICD production (Chapter 3). Further, ADAM10 acted as the sheddase necessary for FGFR4 processing to R4-ICD and PSEN2 contributed to R4-ICD production as well. In addition, inhibition of the FGFR4 kinase reduced processing of FGFR4. Finally, we demonstrated that R4-ICD, in the absence of full-length FGFR4, could activate tumor cell signaling.

CHAPTER 2: METHODS

Cell culture:

Human malignant cholangiocarcinoma cells, KMCH and HuCCT1, were kindly provided by Dr. Gregory Gores. Cells were cultured in high-glucose DMEM supplemented with 10% fetal bovine serum (FBS), G418 (50 µg/mL), and insulin (0.5 µg/mL). FGFR4 plasmids were generously provided by Dr. Javed Khan (National Cancer Institute) and have been described previously [74]. HuCCT1 cells were transfected and selected with puromycin (2-10 µg/mL). Single-cell colonies were isolated.

Immunoblotting:

Cells were lysed by the addition of 50 mM Tris-HCl, 150 mM NaCl, 1 mM EDTA, 1 mM dithiothreitol, 1 mM α-phenylmethylsulfonyl fluoride, 1 mM Na_3VO_4, 100 mM NaF, and 1% Triton X-100, pH 7.4. Following SDS-PAGE and transfer to nitrocellulose membrane, FGFR4 signal was detected via immunoblotting: FGFR4 monoclonal rabbit (Cell Signaling Technology: #8562) or Actin monoclonal mouse (Sigma Aldrich: A2228). Antibody specificity was verified via the molecular weight of FGFR4, a decrease in signal upon use of an shRNA against FGFR4 (see chapter 4), and restored signal with transfection of an FGFR4 expression plasmid.

Post-translational modifications:

Glycosylation was altered by enzyme-mediated deglycosylation, inhibition of glycosyltransferase, or site-directed mutagenesis. PNGase F and Endoglycosidase H were from New England Biolabs (PNGase F: P0704S, Endoglycosidase H: P0702S). NGI-1 (Selleckchem: S8750) was added to cells at 0-100 µM, overnight. Kifunensine (Cayman Chemical: 10009437), 5 µM, was added to cells for 0-16 hours.

Enzyme-mediated deglycosylation, lysate: Cells were lysed in the manufacturer-supplied lysis buffer at a final concentration of 1% NP-40. Lysates were vortexed briefly

three times and placed on ice between each. Lysates were centrifuged (13,000*g*, 5 min) and the supernatant saved. The supernatant (5 µL) was incubated under native or denaturing conditions (denaturing buffer, 100°C incubation), per the manufacturer and the reaction started by addition of 500 units of enzyme. The reaction was terminated with one volume of 2X Laemmli buffer, and the samples were heated to 95°C for 5 min.

Enzyme-mediated deglycosylation, live cells: Cells were plated at 70-80% confluency in a 12-well plate. Medium was replaced with Opti-MEM medium (ThermoFisher Scientific: 22600050) containing 5,000 units of PNGase F per mL for 1-4 hours. Protein isolation was performed on ice to prepare samples for immunoblotting, as above.

Phosphatase: The manufacturer's protocol was used (New England Biolabs, Lambda Protein Phosphatase: P0753S), with modification. Protein isolation and denaturation steps were identical to those performed in the PNGase F denatured lysate protocol. Following deglycosylation, 2 µL of protein metallophosphatase (PMP) buffer (50 mM HEPES, 100 mM NaCl, 2 mM DTT, 0.01% Brij 35, pH 7.5), 2 µL of 10 mM $MnCl_2$ and 6 µL of water were added to the 10 µL sample to give a total reaction volume of 20 µL.

Site-directed mutagenesis:

Agilent QuikChange Lightning, 210519, or New England Biolabs Q5 Site-Directed Mutagenesis, E0554, were used to replace each of the five predicted glycosylation residues (Asn-112, -258, -290, -311, -322) to convert asparagine to glutamine. All mutations were confirmed through sequencing.

Site-directed mutagenesis (in depth):

NEB (E0554S): primer sets were of various lengths (10-20 NTs), and the six most 3' NTs had only one site of binding in the plasmid sequence to reduce off-target binding. Forward and reverse primers were designed to be directly adjacent, but non-overlapping, with the mutation incorporated into only one of them (near the 5' end of the forward primer). Prior to ordering, primers were checked for self-annealing sites, hairpin loops, or complementarity [116]. Annealing was typically performed at 60°C. This method was successfully used to mutate sites N112 and N258.

Agilent (210519): primers were designed, in part, using Agilent's online program. Sequences were entered in, and specific mutation(s) were selected. Agilent then provided a set of completely overlapping complementary primer pairs which both contained the mutation(s). The seven most 3' NTs had only one site of binding in the plasmid sequence to reduce off-target binding. Prior to ordering, primers were checked for self-annealing sites, hairpin loops, or complementarity [116]. An annealing temperature of 60°C was used with a general elongation rule of 30 seconds/kb. The Agilent protocol was followed precisely, aside from using SOC broth instead of NZY^{+} broth. This method was successfully used to mutate sites N290, N311, and N322.

Active lysate isolation:

We measured receptor cleavage of FGFR4 full-length protein to R4-ICD, in the absence of protein synthesis and glycosylation, in crude lysate, based on reports using crude cell lysate to measure endogenous enzyme activity [117, 118]. Cells were mechanically lysed in hypotonic non-denaturing lysis buffer (30 mM NaCl, 20 mM Tris, pH 7.4), either by Dounce homogenization (larger volumes) or needle shearing (small

samples). Initial experiments on the same sample demonstrated no difference between these methods. Dounce homogenization (glass/ground glass) was done with 20 passes per sample and needle shearing with 20 passes through a 29-gauge needle. Lysates were either frozen immediately or incubated at 37°C. Processing was arrested by adding Laemmli buffer and heating to 95°C for 5-minutes.

Protein isolation from frozen tissue:

This process can be time sensitive. As such, all necessary supplies were gathered and select supplies were cooled with liquid nitrogen before removing samples from the -80°C freezer. In the fume hood, gather the following supplies: weigh boats, lysis buffer (the same buffer used for normal protein isolation), pipette/tips, syringe/needle, mortar and pestle, sharps container, liquid nitrogen, gloves, formalin cups with cassettes and Eppendorf tubes.

Liquid nitrogen was poured into the mortar to cool it down. Once cooled, additional liquid nitrogen was added to the mortar along with the tissue sample. Liquid nitrogen was added as needed to keep tissue frozen. Covering the mortar with one hand and holding the pestle in the other, the tissue was crushed with a single blow. This served to break the tissue into several pieces, so that a portion could be saved for RNA isolation, frozen back down, or placed into the tissue cassette (and formalin) for sectioning and slide creation.

The portion remaining in the mortar was used for protein isolation and was crushed into a fine powder, while maintaining cold temperature. Liquid nitrogen (swirling) was used to collect the powder back to the bottom of the mortar. Highly desmoplastic tissue is very challenging to grind. The ground up tissue was collected into a weigh boat containing lysis buffer and passed through a syringe and needle until the solution was

homogenized. The homogenate was then transferred to a 1.5 mL tube, and protein (or RNA) isolation was performed using the protocol described above.

Migration:

Cells were plated into transwell inserts at 5,000 cells/well in serum-free medium (Sigma, CLS3422-48EA). Medium in the lower chamber contained 10% fetal bovine serum (FBS). At 24 hours, non-migrated cells were removed and the insert processed [119]. Cells from five non-overlapping images (field of view was 1 mm x 1.4 mm) per insert were counted using CellProfiler (CellProfiler pipeline has been included below).

CellProfiler pipeline used:

Pipeline name	Setting items
Metadata	Extract meta data? No
NamesAndTypes	Asign a name to: All images
	Process in 3D? No
	Select the image type: Grayscale image
	Name to assign these images: Nuclei
	Set intensity range from: Manual
	Maximum intensity: 255
Groups	Do you want to group your images? No
IdentifyPrimaryObjects	Use advanced settings? Yes
	Select the input image: Nuclei
	Primary objects to be identified: Nuclei
	Typical diameter of objects, in pixel units (Min, Max): 3, 9
	Discard objects outside the diameter range? Yes
	Discard objects touching the border of the image? Yes
	Threshold strategy: Adaptive
	Thresholding method: Otsu
	Two-class of three-class thresholding? Three classes
	Assign pixels in the middle intensity class to the foreground or the background? Foreground
	Threshold smoothing scale: 1.3488
	Threshold correction factor: 1
	Lower and upper bounds on threshold: 0, 1
	Size of adaptive window: 10
	Method to distinguish clumped objects: Shape
	Method to draw dividing lines between clumped objects: Shape
	Automatically calculate size of smoothing filter for declumping? Yes

	Automatically calculate minimum allowed distance between local maxima? Yes
	Speed up by using lower-resolution image to find local maxima? Yes
	Display accepted local maxima? No
	Full hole in identified objects? After declumping only
	Handling of objects if excessive number of objects identified: Continue
MeasureObjectSizeShape	Select object sets to measure: Nuclei
	Calculate the Zernike features? No
	Calculate the advanced features? No
MeasureObjectIntensity	Select images to measure: Nuclei

Caspase activity:

Caspase 3/7 activity was measured by quantifying the release of Rhodamine-110 from the peptide DEVD (Promega: G7792) according to the manufacturer's instructions, with quadruplicates of each group. Cells were treated as described in the figure legends. The following day, apoptosis was stimulated with 10 ng/mL TNF-related apoptosis-inducing ligand (R&D Systems, 375-TL-010) for 6 hours. Alternatively, apoptosis was stimulated with Cisplatin (Fresenius Kabi: 63323-103-51) and gemcitabine (Zydus Hospira Oncology: 0409-0185-01) at 50 and 5 μM respectively, or staurosporine (Fisher Scientific: BP2541-100) at 2 ng/mL for 24 hours.

FGFR4 localization:

Cells plated on collagen-coated coverslips were fixed in 3% paraformaldehyde in dPBS with 100 mM PIPES, 3 mM $MgSO_4$ & 1 mM EGTA then permeabilized in 0.1% Triton X-100 in dPBS. Primary antibodies (Protein-Tech anti-FGFR4: 11098-1-AP or Abcam anti-Giantin: ab37266) were used at 1:50. Secondary antibody (Thermo Fisher, donkey anti-rabbit, 594 nm: A21207, donkey anti-mouse, 488 nm: A21202) was added (1:2,000, FGFR4 or 1:200, Giantin) for 45 minutes at room temperature. Samples were

mounted in ProLong Gold with DAPI. A Zeiss LSM 800 with Airyscan was used for confocal imaging.

Differential centrifugation

A differential-fractionation protocol modified from Bitler, et al., 2010 and Ramsby et al., 1994 was performed and is described below [120, 121]. Cells at confluency were washed with 1X PBS, trypsinized and pelleted through centrifugation (200 x g for two minutes). The supernatant was discarded, and the pellet was resuspended in 200 µL of digitonin lysis buffer (0.01% digitonin, 100 mM NaCl, 300 mM sucrose, 10 mM PIPES (pH 6.8), 3 mM $MgCl_2$, 5 mM EDTA, 2 mM Na_3VO_4, 50 µM ammonium molybdate, 10 mM NaF and complete protease inhibitors (Roche) and incubated on ice for five minutes. Sample was then centrifuged for 10 minutes at 400 x g. The supernatant (cytosolic fraction) was collected and saved. The pellet was resuspended in 200 µL Triton X-100 lysis buffer (0.5% Triton X-100, 100 mM NaCl, 300 mM sucrose, 10 mM PIPES (pH 7.4), 3 mM $MgCl_2$, 3 mM EDTA, 2 mM Na_3VO_4, 50 µM ammonium molybdate, 10 mM NaF and complete protease inhibitors (Roche)) and incubated on ice for five minutes. Sample was then centrifuged at 5,000 x g for 10 minutes, and the supernatant was collected as the membrane fraction. The remaining pellet was resuspended in 300 µL Tween 20/DOC lysis buffer (1% Tween 20, 10 mMNaCl, 0.5% deoxycholate, 10 mM PIPES (pH 7.4), 1 mM $MgCl_2$, 2 mM Na_3VO_4, 50 µM ammonium molybdate, 10 mM NaF and complete protease inhibitor (Roche)). Pellet homogenization was performed 20 times using a dounce homogenizer followed by ten cycles of sonication (30 seconds on, followed by 30 seconds off. The sample was then centrifuged for 10 minutes at 7,000 x g, and the supernatant was collected as the nuclear fraction.

Protease inhibition screening

Active cell lysates were collected via Dounce homogenization. Inhibitors were individually added to the lysate or the lysate was subjected to heat denaturation at 95°C for 1 or 5 minutes. A list of inhibitors used, the concentration at which they were used and their known molecular targets is provided below:

GW280264x	2 μM	ADAM10 and ADAM17	
GI254023x	2 μM	ADAM10	
Ilomastat	20 μM	multiple MMPs	
Ortho-phenanthroline	100 μM	multiple MMPs	
Granzyme B inhibitor	10 μM	granzyme B	

Lysates were then incubated for an hour at 37°C. Processing was arrested by adding Laemmli buffer and heating to 95°C for 5-minutes.

RNA isolation

The following steps were performed in a chemical fume hood to minimize exposure to harmful chemicals. Medium was removed from each well of a six-well plate. To each well, 500 μL of Trizol reagent was added. Cell homogenization was performed by pipetting the Trizol reagent up and down several times. The Plates with Trizol reagent were incubated for 5 minutes at room temperature and the homogenates were then collected in microcentrifuge tubes. To each tube, 100 μL of chloroform was added. Tubes were then vortexed for 15-30 seconds and then incubated for 15-20 minutes at

room temperature. Samples were centrifuged for 15 minutes at 12,000 x G, 4°C. This separated samples into an RNA phase layer (top, clear) and an organic layer (bottom, red). Being very careful not to remove any of the phenol, the top clear layer was removed and placed into clean microfuge tubes. To the clear layer, 250 µL of isopropanol was added, and the samples were gently mixed by inversion. Samples were incubated at room temperature for 10 minutes and then centrifuged for 10 minutes at 12,000 x G, 4°C. The supernatant was removed without disrupting the RNA pellet. The pellet was then washed with 1 mL of 70% ethanol and centrifuged again for 5 minutes at 7,500 x G, 4°C. Ethanol was carefully removed and the pellet was allowed to air dry for 5-10 minutes. The pellet was resuspended in 100 µL of DEPC-containing water and incubated at 55°C for 10 minutes. Samples were then immediately quantified and stored at -80°C to prevent degradation.

Knockdown using siRNA

HuCCT-FGFR4 cells were grown to ~60% confluency in a six-well plate. A modified RNAiMAX protocol optimized for our cells was used. Negative control or siRNA was added to 250 µL of OptiMEM medium at a concentration 200 nM. In a separate tube, 5 µL of RNAiMAX solution was added to 250 µL of OptiMEM medium. The two mixtures were combined and allowed to sit at room temperature for ~15 minutes. The full volume (~500 µL) was then added to one well of a six-well plate. Cells were incubated with negative control or siRNA for 36-72 hours at 37°C in CO_2-controlled incubator. Once cells reached confluency, protein or RNA isolation was performed using standard protocols.

Reverse transcription polymerase chain reaction (cDNA synthesis)

Two µg of RNA were added to a solution containing 10 µM random hexamers and 1 mM dNTPs. The samples were heated at 65°C for 5 minutes and then cooled on ice. To each sample volume, an equal volume of the following solution was added: 2x first strand buffer, 25 mM DTT, 2 unit/µL RNase inhibitor (ThermoFisher: N8080119), 20 units/µL M-MuLV reverse transcriptase (New England Biolabs: M0253S). This reaction was allowed to incubate for 20 minutes at 42°C followed by 10 minutes at 95°C.

Quantitative polymerase chain reaction

SYBR green reagent was used for detection. In a 20 µL reaction volume, 10 µL of SYBR green, 6 µL of DEPC H_2O, Primer mix (final concentration of 0.5 µM) and 3 µL of cDNA were mixed together in a 96 well plate. Optimization of primer and cDNA concentrations were performed prior to starting the experiment.

The thermocycler was run using the following setup:

1. Activation: 95°C for 2 minutes
2. Denaturation: 95°C for 5 seconds
3. Annealing/extension: 60°C for 30 seconds
    a. Steps 2 and 3 repeated 40 times
4. Melt curve: 65-95°C with 0.5°C increments, 5 seconds/increment

Enrichment for FGFR4

Cell lysate was collected using Pierce lysis buffer (25 mM Tris HCl pH 7.4, 150 mM NaCl, 1% NP-40, 1 mM EDTA, 5% glycerol). Cells were scraped off the plate into buffer and vortexed three times with a five-minute incubation on ice between each vortex. Between 120 and 200 µg of protein was aliquoted into each tube. Primary

antibody (FGFR4: Thermofisher MA5-18084, p-ELK-1: Cell Signaling 9186S), 1:100 (v/v), was added to each aliquot and was allowed to incubate with rotation at 4°C for an hour. Protein G magnetic beads were then added to each sample at a 1:5 dilution. Samples were then incubated with rotation at 4°C for one hour. Magnetic separation of the beads was performed, and the remaining solution was discarded. Beads were washed six times with 30 mM NaCl, 20 mM Tris, pH 7.4. Beads were then resuspended in 2 μM $ZnCl_2$, and human recombinant ADAM10 (R&D systems 936-AD) was added at a final concentration of 22 ng/μL, 44 ng/μL or 66 ng/μL. Samples were incubated for one hour at 37°C. The reaction was terminated and protein was eluted from the beads by the addition of 5x Laemmli buffer followed by a five-minute incubation at 70°C. Beads were removed (magnetically) and samples were saved and analyzed via immunoblot.

Recombinant human ADAM10 activity and active cell lysate activity were tested using a peptide substrate containing a fluorophore on one end and quenching molecule on the other end (R&D systems: ES010). Stock solution of substrate 10 mg/mL in DMSO, and substrate is used at a final concentration of 0.22 g/mL. Excitation wavelength used was 320 nm, and absorption wavelength measured was 405 nm.

Transient transfection of mammalian cells:

Cells at 70-90% confluency in a well of a 6-well plate were used for transfection. Lipofectamine 3000 reagent, 3.75 μL was added to 125 μL of Opti-MEM medium. In a separate tube, 5 μg of uncut plasmid DNA and 10 μL of P3000 reagent were added to 125 μL of Opti-MEM media. Their contents were combined and incubated for 10-15 minutes at room temperature. The total volume (~250 μL) was added to one well of a 6 well plate, and the cells were allowed to incubate and grow for 2-4 days at 37°C.

Stable transfection of mammalian cells:

This protocol is nearly identical to the transient transfection protocol, except that linearized plasmid DNA was used in the transfection process. The linearization protocol was as follows:

1x BSA, 1x buffer (appropriate for restriction enzyme), restriction enzyme, plasmid (variable amount), water to volume were added to a PCR tube. Samples were digested for 1 hour at required temperature. To stop the reaction, samples were heated to the specified “kill” temperature for the required duration. The transfection was then continued as normal.

Production of clonal cell lines:

Transfected cells were allowed to grow in regular medium for 24 hours. At this point, the medium was removed and puromycin-containing (3 μg/mL) medium was added to the cells. Medium was changed every 2-4 days, more often if necessary, to remove dead cells. This was done until >80% of the cells had been removed. At this point, medium change occurred infrequently, as needed. The cell population in the dish was very low, and single cells were allowed to grow in selection medium. Once a majority of single cell colonies had proliferated into colonies of 200+ cells, colonies were isolated/picked. Medium was removed and trypsin was briefly added to the plate. Using the inverted microscope for colony visualization, the P10 pipette (with 10 μL of medium in the tip) was slowly and carefully scraped across a single colony, using the medium in the tip to pull up cells. Cells were then transferred to a single well of a 24 well plate. This process was repeated until most/all of the colonies had been picked. Cells in each well in the 24 well plate were allowed to grow to near confluency before being expanded to

two wells of a 12 well plate (one well for protein isolation and screening, one well for maintenance).

HuCCT R4-ICD PB1 cells were produced through stable transfection of HuCCT cells with pCDNA 3.1 containing cDNA coding for FGFR4 residues 391-802 with a C-terminal HA tag. No selection gene was present in the plasmid, so colonies were grown and individually screened for expression of R4-ICD by immunoblot.

HuCCT R4-ICD C3 and C6 cells were produced through stable transfection of HuCCT cells with pBABEzeo containing cDNA coding for FGFR4 residues 391-802. This plasmid contains a zeocin-resistance gene. As such, cells were grown in medium containing zeocin, 800 μg/mL. Clonal growth, colony selection and screening via immunoblot followed.

Statistical analysis:

For quantitative comparisons between two conditions, the Student's t-test was used. When comparing more than two conditions, ANOVA test with post-hoc correction (Bonferroni) was used.

CHAPTER 3: Glycosylation of FGFR4 in cholangiocarcinoma regulates processing and cancer signaling

Andrew J. Phillips
Marissa B. Lobl
Yamnah A. Hafeji
Hannah R. Safranek
Ashley M. Mohr
Justin L. Mott

Abstract

Recent advances in targeted treatment for cholangiocarcinoma have focused on fibroblast growth factor (FGF) signaling. There are four receptor tyrosine kinases that respond to FGFs, and posttranslational processing has been demonstrated for each FGF receptor. Here, we investigated the role of N-linked glycosylation on processing and function of FGFR4. We altered glycosylation through enzymatic deglycosylation, small molecule inhibition of glycosyltransferases, or through site-directed mutagenesis of selected asparagine residues in FGFR4. Signaling was tested through caspase activation, migration, and subcellular localization of FGFR4. Our data demonstrate that FGFR4 has multiple glycoforms, with predominant bands relating to the full-length receptor that has a high-mannose and hybrid-type glycan form and a complex-type or mature glycan form. We further identified a set of faster migrating FGFR4 bands that correspond to the intracellular kinase domain, termed R4-ICD. These glycoforms and R4-ICD were detected in human cholangiocarcinoma tumor samples, where R4-ICD was predominant. Removal of glycans in intact cells by enzymatic deglycosylation resulted in increased processing to R4-ICD. Inhibition of glycosylation using NGI-1, an oligosaccharyltransferase inhibitor, reduced glycosylation of FGFR4, increased processing, and sensitized cells to apoptosis. Mutation of Asn-112, Asn-258, Asn-290, or Asn-311 to glutamine modestly reduced apoptosis resistance, while mutation of Asn-322 or simultaneous mutation of the other four asparagine residues caused a loss of FGFR4-dependent cytoprotection. None of the glycomutants altered the migration of cancer cells. Finally, mutation of Asn-112 caused a partial localization of FGFR4 to the Golgi. Overall, preventing glycosylation at individual residues reduced the cell survival function of FGFR4 and receptor glycosylation may regulate access to an extracellular protease or proteolytic susceptibility of FGFR4.

Introduction

Cholangiocarcinoma is a primary liver cancer of the epithelial cells lining the biliary tract. Cholangiocarcinoma commonly presents late in disease and patients have a very poor prognosis; less than 10% 5-year survival [1]. Treatment options include newly approved small molecule inhibitors targeting FGFRs, IDH1, and ROS1 [122, 123]. However, many of these treatment options are only approved for a select group of patients. As such, gemcitabine plus cisplatin remains a common first-line therapy [6]. In the meantime, finding new therapeutic targets in cholangiocarcinoma remains a top priority.

One such group of therapeutic targets includes receptor tyrosine kinases (RTK), such as fibroblast growth factor receptors (FGFR). FGFR4 signaling has a role in healthy liver function through regulation of bile acid synthesis. In cancer biology, FGFR4 has been shown to play a role in malignant signaling through its overexpression. This has been observed in various tumors including breast, lung, gastric cancers, rhabdomyosarcoma, nasopharyngeal carcinoma, and cholangiocarcinoma [67, 68, 71, 74].

There are five FGFRs (only four with functional kinase domains) and twenty-three FGF ligands [37]. FGF19 is expressed in biliary tissue and is amplified in 4-6% of cholangiocarcinomas [77, 124-126]. FGF19's receptor, FGFR4, is also expressed in cholangiocarcinoma. Ligand binding occurs between the second and third immunoglobulin loop structures. In the presence of the coreceptor, beta klotho (KLB), receptor dimerization can occur and autophosphorylation of the FGFR kinase domain follows [127, 128]. N-linked glycosylation of FGFR4 plays a role in FGFR4 localization and signaling [61, 62].

Some similarities exist between Notch and the FGFR family protein, FGFR3. Dysregulation of Notch signaling has been implicated in cancer. Notch3 overexpression was observed in approximately 40% of non-small cell lung cancers (NSCLC). Often, this was observed with reduced manic fringe expression. Manic fringe is one of the three human glycosyltransferases that modify Notch proteins [103, 129]. When manic fringe expression was restored, Notch3 was destabilized, and tumor growth was reduced [130]. FGFR3 has been shown to undergo regulated intramembrane proteolysis. After ligand binds to the extracellular portion of FGFR3 and the kinase domain is phosphorylated, S1 cleavage occurs, releasing the extracellular domain. The membrane-anchored remaining portion of FGFR3 undergoes a second cleavage event, S2, which effectively releases the intracellular domain from the plasma membrane, allowing nuclear translocation. As is observed in Notch signaling, FGFR3 activation (receptor phosphorylation) is required for proteolysis to occur [22]. FGFR4 has five extracellular asparagine residues which match the Asn-X-Ser/Thr sequon (where X is any amino acid except proline) required for N-linked glycosylation to occur. These asparagine residues are located at positions 112, 258, 290, 311, and 322. The current study investigated the functional role of FGFR4 glycosylation in cholangiocarcinoma and the effects of glycosylation on processing to R4-ICD.

Results

FGFR4 glycosylation in cholangiocarcinoma

N-linked glycosylation is predicted to occur at five residues in FGFR4 (**Figure 3A**). Cholangiocarcinoma cell lines, HuCCT1-FGFR4 and KMCH, demonstrated two predominant full length FGFR4 forms running at roughly 90 and 110 kDa on

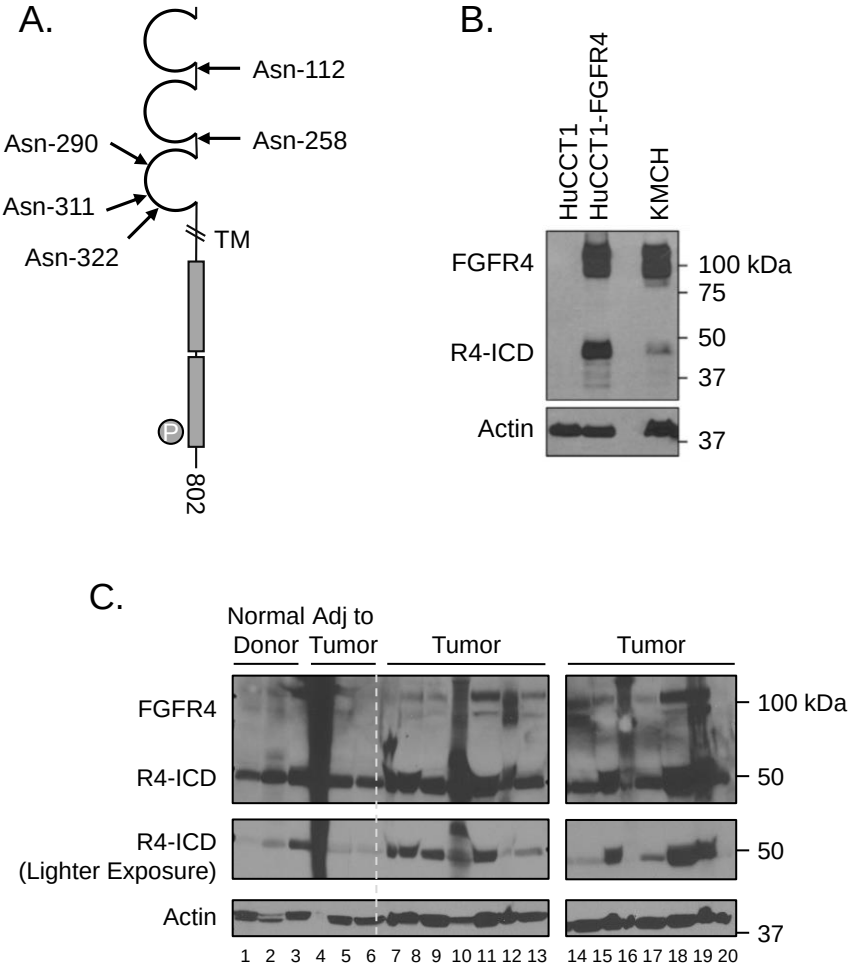

Figure 3. FGFR4 glycosylation in cholangiocarcinoma.

A. Schematic of FGFR4 showing three Ig-like loops, five predicted N-linked glycosylation sites, the transmembrane (TM) domain and the intracellular C-terminal kinase domain. B. HuCCT1, HuCCT1-FGFR4, and KMCH cells were immunoblotted for FGFR4. Full-length receptor is visualized at 90-110 kDa and R4-ICD is observed as signal around 45-50 kDa; representative of n=3. C. FGFR4/R4-ICD protein expression in three healthy (donor) liver samples, three non-tumor samples adjacent to liver cancer (Adj to tumor), and fourteen human cholangiocarcinoma tumor samples.

immunoblots, plus signals at 45-50 kDa, consistent with the predicted size of the intracellular domain (amino acids 391-802). The faster migrating forms (45-50 kDa) were collectively termed R4-intracellular domain (R4-ICD) based on size and immunoreactivity to the C-terminal anti-FGFR4 antibody. R4-ICD was absent in cells lacking full-length FGFR4 (HuCCT1 parental) and was present in cells transfected with FGFR4 (HuCCT1-FGFR4; **Figure 3B**). Because we observed R4-ICD in HuCCT1 cells transfected with cDNA for FGFR4, and cDNA is not a substrate for splicing, we reasoned that R4-ICD is not an alternative splice variant. Similar 45-50 kDa forms of FGFR4 have been reported, although their function has not been studied [60, 80]. In summary, FGFR4 protein showed multiple forms with the 90-110 kDa forms potentially representing glycosylated receptor and the faster migrating R4-ICD forms likely representing proteolytically processed FGFR4. The level of R4-ICD signal relative to full-length showed variability, suggestive of regulation.

FGFR4 in human liver tissue and cholangiocarcinoma

FGFR4 in human cholangiocarcinoma was investigated from archived, frozen tumor samples. Samples were from 3 normal livers adjacent to tumor, 3 non-tumor livers, and 14 tumors, including 6 male and 8 female patients. One cancer patient was 32 years old, the rest were in the range of 50-72 years, with an average age of 60 (**Table 1**). R4-ICD signal was stronger than full-length FGFR4 in human samples and R4-ICD was observed in all 14 of the tumor samples. The lighter exposure blot demonstrated substantially higher levels of R4-ICD in tumor samples compared to non-tumor. Robust signal from full-length FGFR4 was observed in 12 of 14 tumor samples, but only 3 out of 6 normal tissues. Note that one tumor-adjacent sample (lane 4) was likely poorly preserved and exhibited a strong signal without distinct banding for FGFR4

Lane	Tumor	Age	Sex	Anatomic site	Notes	Histologic grade (differentiated)	AJCC stage
7	T6#	72	F	liver	intrahepatic		pT2a, pN0, pMX
8	T5*	64	M	liver		moderately	pT3, pN0, pMX
9	T1	59	F	liver	intrahepatic	moderately to poorly	T2, N0, MX
10	T2	55	M	liver	intrahepatic	well	pT2, pN0, pMX
11	T3	52	F	liver		moderately	pT1, NX, MX
12	T4	50	F	liver	multiple tumors within the hepatic parenchyma	moderately	T3, N0, MX
13	T7	63	F	liver	intrahepatic		
14	T8	66	M	liver	intrahepatic	poorly	pT1, NX, MX
15	T9	50	M	gallbladder	gallbladder (met)	moderately	pT3, pN1
16	T10	32	M	liver		moderately	pT2a, pN0, pMX
17	T11	65	F	pancreas	pancreas (met)	moderately	pT3, pN1
18	T12	69	M	liver	intrahepatic	well	pT1a, NX, MX
19	T13	72	F	liver	intrahepatic	poorly	pT2, NX, MX
20	T14	72	F	liver	Intrahepatic	moderately	pT2, pN0, pMX
	Normal donor liver						
1	ND1			liver	transplant (donor)		
2	ND2			liver	transplant (donor)		
3	ND3			liver	transplant (donor)		
	Adjacent normal tissue			**Anatomic site**			
4	N1			liver	adjacent to HCC		
5	N2#			liver	adjacent to cholangiocarcinoma		
6	N3*			liver	adjacent to cholangiocarcinoma		

Table 1.
Patient characteristics for 14 tumor samples and 6 non-tumor livers were utilized in this study. *Indicates that tumor T5 and liver sample N3 were from different regions of the same liver. # Indicates that tumor T6 and liver sample N2 were from different regions of the same liver.

and very weak actin levels. Overall, tumor samples showed high levels of FGFR4 and R4-ICD (**Figure 3C**).

FGFR4 glycosylation was examined by treatment with Endoglycosidase H to remove high-mannose and hybrid-type glycans. Endoglycosidase H caused a shift of the 90 kDa band to two faster migrating bands at approximately 80-85 kDa. The 90 kDa band was fully susceptible to Endoglycosidase H processing, indicating that this band represents the high-mannose and hybrid-type glycan form of FGFR4 while the 110 kDa band was not susceptible. Both denatured and native preparations were similarly susceptible to Endoglycosidase H (**Figure 4A**).

PNGase F cleaves glycans between the innermost N-acetylglucosamine and the protein, removing both high-mannose and complex-type glycans. Treatment of cell lysates with PNGase F altered the migration of both the 90 kDa and 110 kDa FGFR4 bands, providing further evidence that they represent FGFR4 glycoforms (**Figure 4B**). Collectively, these data confirm that FGFR4 is N-glycosylated, identify the 90 kDa band as the immature high-mannose/hybrid-type glycan form, and identify the 110 kDa band as the terminally-modified complex-type glycan form. We speculate that the doublet seen after deglycosylase treatment represents a non-glycan posttranslational modification to FGFR4. To determine whether the FGFR4 or R4-ICD bands observed following enzymatic deglycosylation represented different phosphorylation states of FGFR4, lysates were treated with lambda phosphatase. No obvious shifts of 80-110 kDa forms were seen, suggesting that phosphorylation of full length FGFR4 does not play a major role in FGFR4 migration. However, no positive control was included in this experiment. R4-ICD was largely converted to the faster of 2-3 forms at 45-50 kDa upon phosphatase treatment. Shifting seen for R4-ICD indicates the multiple bands of R4-ICD

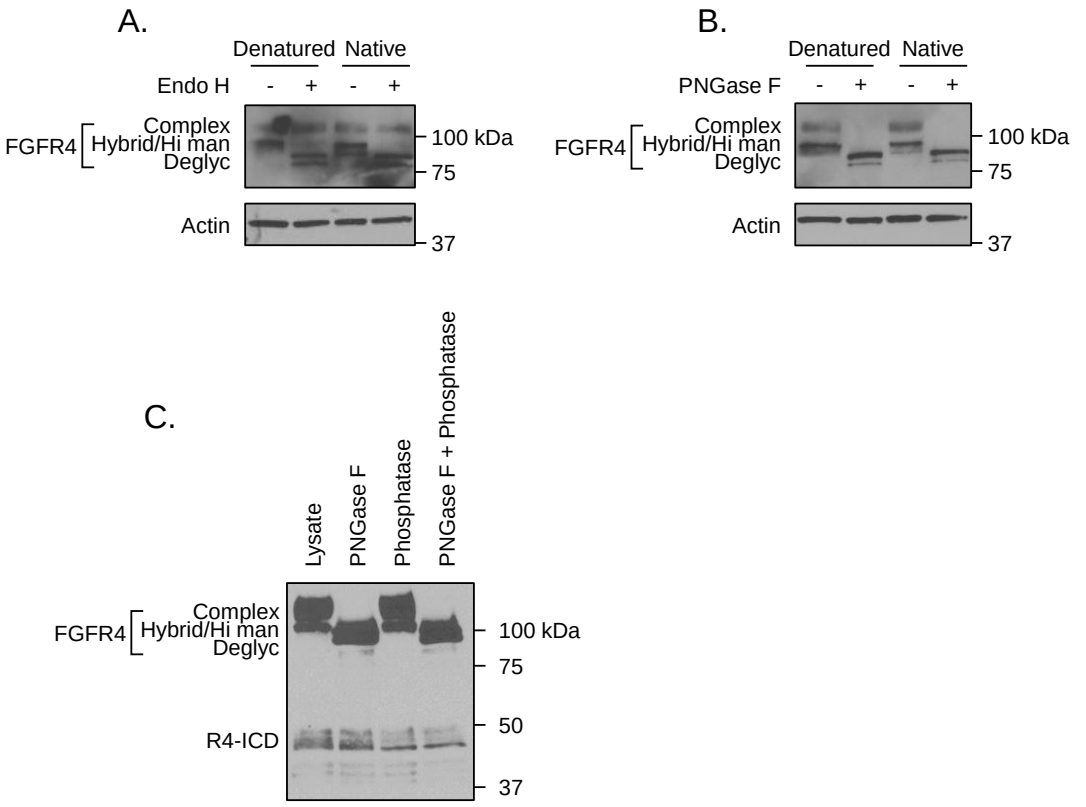

Figure 4. FGFR4 deglycosylation increased R4-ICD production.

A. Endoglycosidase H treatment of HuCCT1-FGFR4 cell lysates. The band labeled "Deglyc" represents the deglycosylated form of FGFR4, and the band labeled "Hybrid/Hi man" represents the hybrid or high mannose form of FGFR4. B. PNGase F treatment of HuCCT1-FGFR4 cell lysate. C. Treatment of HuCCT1-FGFR4 cell lysates with both PNGase F and Lambda phosphatase. Each experiment was performed one time.

may represent different phosphorylation states of the protein (**Figure 4C**). The stability of the different phospho-forms of R4-ICD was not determined.

Next, live cells in culture were incubated with PNGase F in the media to enzymatically deglycosylate FGFR4 at the cell surface. Western blot analysis demonstrated that complex glycosylated FGFR4 (110 kDa) shifted to an 85 kDa band, similar to deglycosylated FGFR4, while the hybrid/high mannose 90 kDa form persisted (**Figure 5A**). PNGase F enzyme is presumably excluded from the cell interior, thus deglycosylation is restricted to FGFR4 that is present on the cell surface, presumably explaining the difference in the migration compared to Figure 2B. PNGase F digestion for 1-2 hours resulted in increased R4-ICD signal, especially at ~50 kDa (**Figure 5A**). PNGase F treatment of live cells led to an approximately 3-fold increase in R4-ICD levels, particularly in HuCCT FGFR4 cells (**Figure 5B**). These data suggested that FGFR4 processing to R4-ICD was enhanced when N-linked glycans were removed.

HuCCT1-FGFR4 cells treated with NGI-1 (an inhibitor of oligosaccharyltransferase) showed a concentration-dependent loss of glycosylation (**Figure 6A**). When cells were treated with 10 μM NGI-1, there was a partial reduction of glycosylated FGFR4, and R4-ICD levels increased (**Figure 6A**). At 100 μM NGI-1, glycosylation of FGFR4 was blocked completely, R4-ICD was not increased, and cells were sensitized to TRAIL-induced apoptosis (**Figure 6A, B**). Control cells (those not treated with TRAIL) also showed increased cell death with 100 μM of NGI-1, suggesting some drug toxicity. HuCCT-FGFR4 cells were next treated with kifunensine, an inhibitor of mannosidase I (**Figure 6C**). This inhibitor will prevent trimming of mannose residues and prevents subsequent maturation of N-linked glycans. At 8 hours of kifunensine treatment, there was a partial reduction of the complex-type glycoform of FGFR4 and increased R4-ICD levels, reminiscent of the effects of 10 μM NGI-1. By 16 hours of

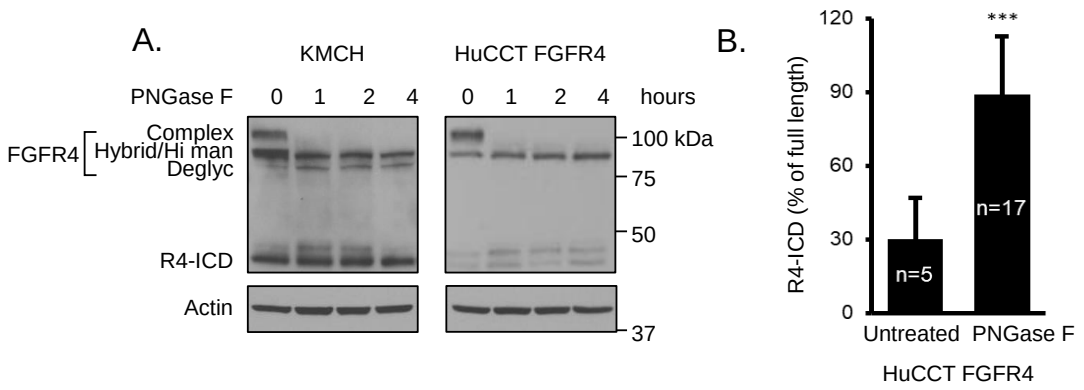

Figure 5. PNGase F increases R4-ICD levels in cells

A. KMCH and HuCCT1-FGFR4 cells were treated with PNGase F in the culture medium. B. R4-ICD-to-full-length FGFR4 (percent) was averaged from untreated and PNGase F-treated HuCCT1-FGFR4 cells. Banding between 30 and 50 kDa was considered R4-ICD and banding between 85 and 115 kDa was considered full length FGFR4. Total sample number quantified is indicated on graph. n=5. *** indicates $p < 0.001$.

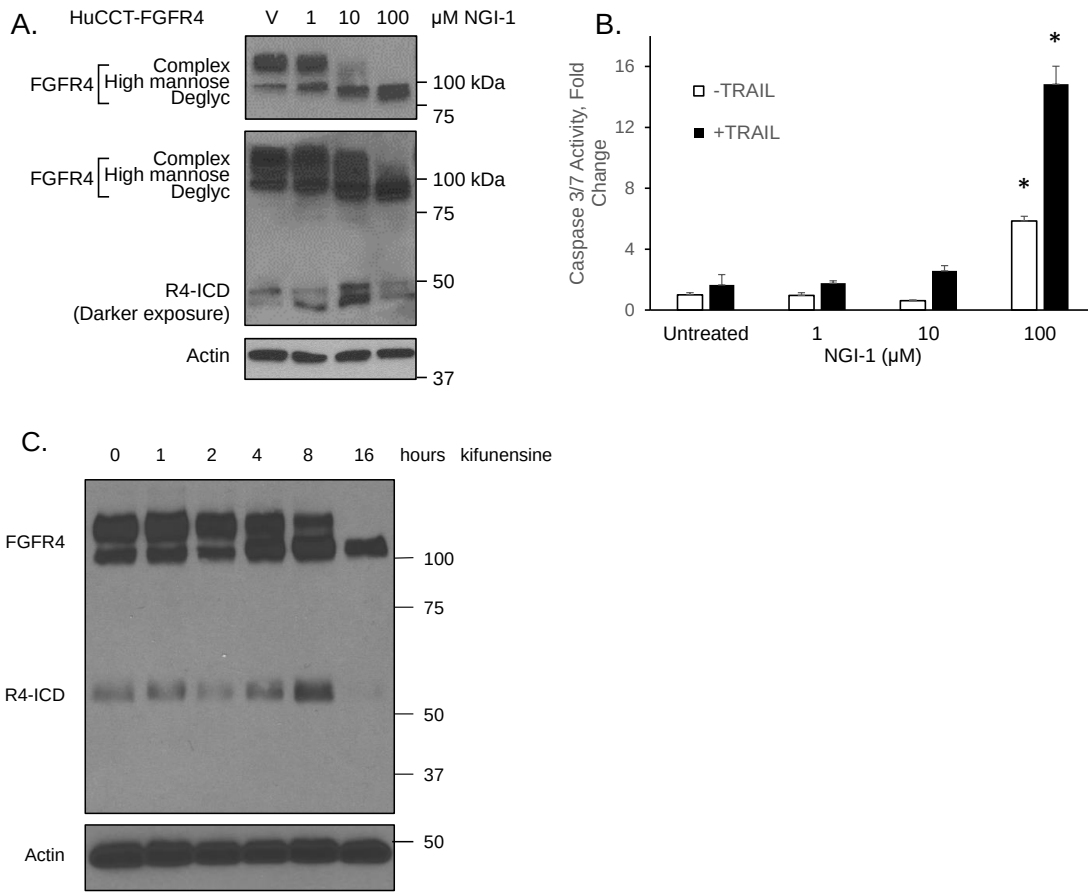

Figure 6. NGI-1 and kifunensine treatments reduced FGFR4 glycosylation and cytoprotection.

A. HuCCT1-FGFR4 cells were treated with vehicle ("V") or NGI-1 overnight, at the indicated concentrations. n=3. B. Caspase activity was measured on HuCCT1-FGFR4 cells treated overnight with NGI-1 followed by a 6-hour treatment with 10 ng/mL TRAIL. Quadruplicate samples measured, repeated twice; representative data shown. * indicates $p<0.05$. C. HuCCT-FGFR4 cells were treated with kifunensine, 5 μM, for 0-16 hours. R4-ICD levels increased at 8 hours, and 110 kDa FGFR4 was absent at 16 hours. A and B were performed twice and C was performed three times.

kifunensine treatment, the 110 kDa FGFR4 band disappeared, and R4-ICD levels were low. Both these data are reminiscent of the effects observed with PNGase F (Figure 3), where reduced FGFR4 glycosylation increased levels of R4-ICD, suggesting that the process of FGFR4 deglycosylation or partial glycosylation promoted processing, but that completely deglycosylated FGFR4 did not promote processing.

To promote FGFR4 processing to R4-ICD in the absence of protein synthesis and glycosylation changes, crude lysate was obtained (termed active lysate) and either frozen immediately or incubated at 37°C to allow endogenous proteases to act. Processing of FGFR4 to R4-ICD occurred with incubation, and at least twice as much R4-ICD was seen in cells expressing wild type FGFR4 after a 1 hour incubation of active lysates (**Figure 7A, B**). Initial experiments using HuCCT1-FGFR4 cells were performed to determine if 20- or 60-minute incubation was required, and both were adequate. We tested processing to R4-ICD in active lysates of cells expressing mutant forms of FGFR4 to understand the role of each of the five glycosylation sites on proteolysis. This approach, in part, would allow us to determine if increased processing upon deglycosylation was due to glycosylation of FGFR4 or of another protein. Cell lines expressing the following forms of mutant FGFR4 were used: N112Q, N258Q, N290Q, N311Q, N322Q, and quadruple mutant 4Q (only 322 remained an asparagine). Two or three clones per FGFR4 mutant were used to account for clonal variation. Results were quantified and graphed as the ratio of R4-ICD to FGFR4 (**Figure 7B**). Blots used for quantification are shown in **Figure 7C-H**. Note the shift in molecular weight for FGFR4 mutants N258Q and N290Q compared to wild-type (**Figure 7D, E**). Wild type FGFR4 showed the highest amount of processing, and the N290Q mutant showed limited additional processing to R4-ICD. Mutant 4Q also showed no additional processing. Most glycomutants showed only a subtle decrease in processing (**Figure 7B**). In addition, it

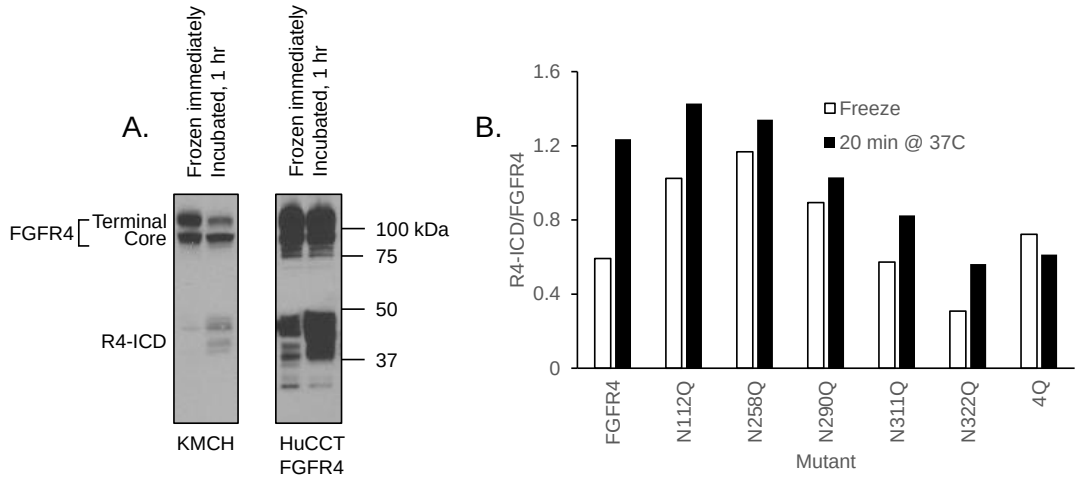

Figure 7, continued on next page.

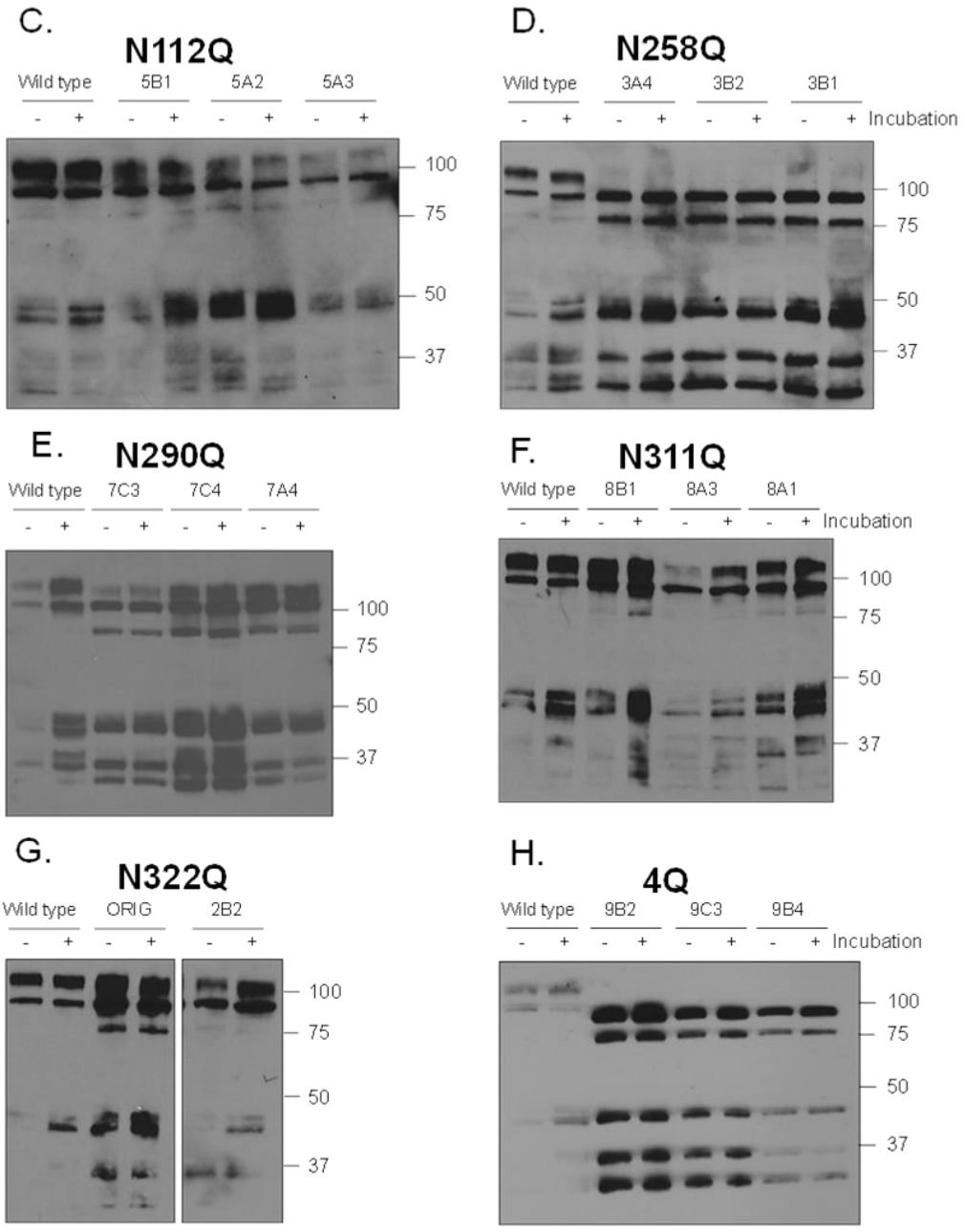

Figure 7, continued on next page.

Figure 7. Mutation of selected glycosylation sites reduced processing of FGFR4 to R4-ICD.

A. Active cell lysates for KMCH and HuCCT1-FGFR4 cells were either frozen immediately or incubated at 37°C for 1 hour. n=5. B. Active lysates of cells expressing glycosylation mutants of FGFR4 were incubated at 37°C to measure processing to R4-ICD. Three selected clones for each mutant (except N322Q where we had two clones) were averaged. R4-ICD/FGFR4 ratio is graphed. C-H. Active lysates from the mutant-expressing clones are shown. Samples were either frozen immediately after lysis (-), or they were incubated for 20 minutes at 37°C (+). Descriptions of cell lines containing mutant FGFR4 follow: N112Q-expressing cell lines were 5B1, 5A2 and 5A3. N258Q-expressing cell lines were 3A4, 3B2 and 3B1. N290Q-expressing cell lines were 7C3, 7C4 and 7A4. N311Q-expressing cell lines were 8B1, 8A3 and 8A1. N322Q-expressing cell lines were ORIG and 2B2. 4Q-expressing cell lines were 9B2, 9C3 and 9B4.

appeared as though basal R4-ICD levels were somewhat elevated in the cells expressing mutant FGFR4 compared to wild-type. This could be due to reduced steric hindrance, allowing for easier initial S1 cleavage and may ultimately help to explain why the relative change in processing between frozen samples and those incubated for 20 minutes was reduced in the cells expressing mutant FGFR4 compared to wild-type. Thus, while deglycosylation in the whole cell increased R4-ICD formation, we could not replicate this effect with FGFR4 glycomutants.

We considered that glycomutants may not be trafficked properly. **Figure 8A** shows a representative anti-FGFR4 immunofluorescence image of several control cell lines: cells expressing FGFR4 through stable transfection with cDNA (top two panels; HuCCT-FGFR4) or two separate cell lines with endogenous expression of FGFR4 (bottom two panels; KMCH and Mx-ChA-1). In both exogenously (cDNA transfection) and endogenously expressing cells, we observe positive cytoplasmic staining for FGFR4. The top two images in **Figure 8A** represent two different layers of imaging in the z plane for a single cell (0.6 μM difference between two images) and allow for better visualization of FGFR4 localization at the plasma membrane in the upper right image (see arrows). Images collected from cells expressing mutant FGFR4 are shown in **Figure 8B**. In cells expressing wild-type FGFR4, staining appeared not only at the plasma membrane but also distributed intracellularly. Cells expressing N258Q, N290Q, N311Q, or N322Q resembled the wild-type FGFR4 distribution. In cells expressing the N112Q mutant, intracellular FGFR4 showed a region of concentrated staining adjacent to the nucleus (**Figure 8B**). In the 4Q cells, intracellular, irregular staining was more intense than wild-type FGFR4 (but not concentrated in a single region). We performed dual immunofluorescence on N112Q and 4Q mutant cell lines for FGFR4 and a Golgi marker, giantin. **Figure 8C** shows a representative image of each cell line in addition to KMCH and Mz-ChA-1 cells, which both have endogenous expression of FGFR4. In cells

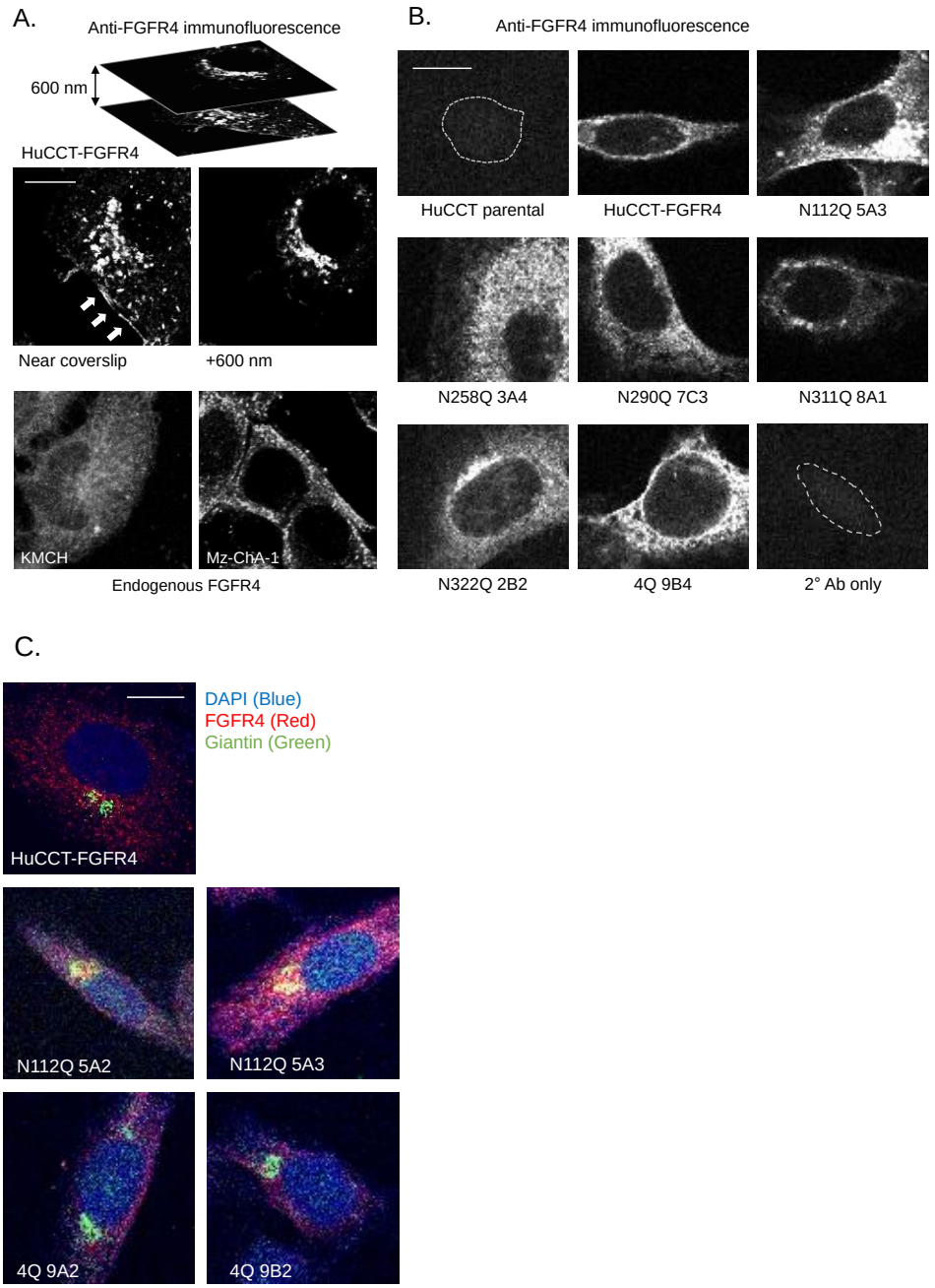

Figure 8. Cellular localization of FGFR4

A. Cells expressing exogenous FGFR4 (HuCCT FGFR4) and cells expressing endogenous FGFR4 (KMCH, Mz-ChA-1) were stained for FGFR4 (white). The top two panels of HuCCT FGFR4 cells demonstrate FGFR4 staining at the plasma membrane (near coverslip) and in the cytoplasm (+600 nm). B. Immunofluorescence of cells expressing mutant forms of FGFR4 were stained to look for FGFR4 localization. C. Immunofluorescence for both FGFR4 (red) and giantin (green), with nuclei visualized by DAPI (blue), was performed on cells expressing wild type FGFR4 and mutants N112Q and 4Q. Bar = 10 µm.

expressing N112Q-FGFR4 only, FGFR4 appeared to co localize with giantin (yellow). In these images, FGFR4 is largely observed in the cytoplasm. However, it can be observed at the plasma membrane, particularly when performing a z-stack and looking at different layers of the cell (**Figure 8A**)

We next tested if any of the cells expressing FGFR4 glycomutants showed altered cell migration or resistance to cell death. All of the clones supported migration similar to wild type FGFR4. A single clone of the N112Q mutant (5A3) showed significantly reduced migration compared to a single clone each of N258Q (3B3) and N311Q (8A3). No additional statistical differences were observed. Thus, each mutant was capable of promoting a similar migratory effect as wild type (**Figure 9**).

Next, we tested the ability of FGFR4 to protect cells from apoptosis. Caspase activity was measured after challenge with chemotherapeutics or staurosporine. Parental HuCCT1 cells lacking endogenous FGFR4 were sensitive to apoptosis (**Figure 10A, B**). Wild type FGFR4 efficiently protected cancer cells from chemotherapy-induced apoptosis. Cell lines expressing mutant FGFR4 were mostly protected from chemotherapy-induced cell death compared to HuCCT1 parental cells, but to a lesser extent than wild type FGFR4. The N322Q mutation showed the least protection, with the 4Q mutant also providing less cytoprotection (**Figure 10A**). In staurosporine-treated cells, mutant cell lines expressing FGFR4 N322 or 4Q did not provide any statistical survival benefit to cells compared to parental HuCCT1 cells. Overall, most of the glycomutants offered at least partial cytoprotection. A summary of the results is shown in **Table 2**.

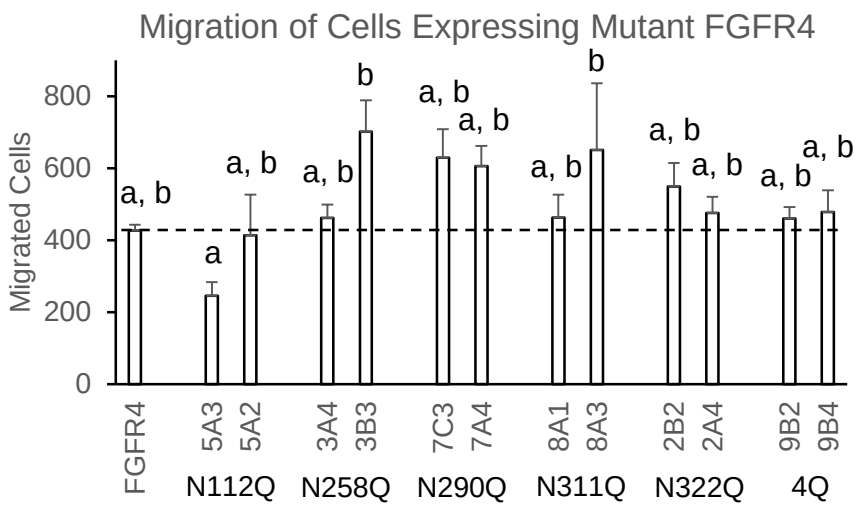

Figure 9. Migration and apoptosis of cells expressing FGFR4 glycomutants.

A. Two clones for each mutant were tested for migration over 24 h by transwell assay. n=3, mean ± SEM. No clones showed a statistically significant difference from wild type; however there were several statistically significant differences between clones. These differences are highlighted by letters above each bar. Any bars that share a letter are not statistically different from one another (ANOVA with Bonferroni *post hoc*).

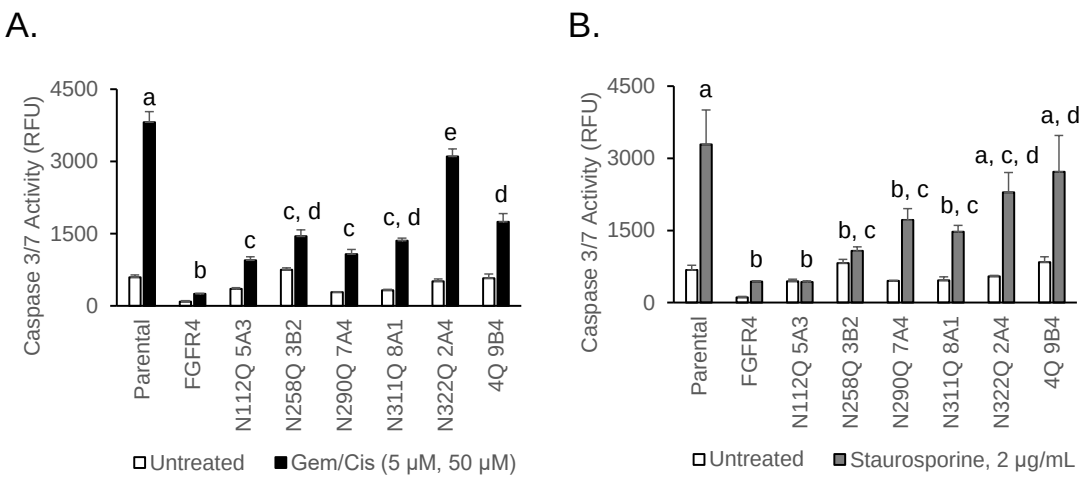

Figure 10. Mutant FGFR4 protection against cell death.

A, B. One clone for each mutant was treated with gemcitabine and cisplatin (5 μM and 50 μM, respectively, panel A), or staurosporine (2 μg/mL, panel B) for 24 hours. HuCCT1 cells lacking FGFR4 are labeled parental. n=4, mean ± SEM. Only treated (filled) samples were compared statistically and bars that share a letter are not significantly different from each other (ANOVA with Bonferroni *post hoc*).

	FGFR4	N112Q	N258Q	N290Q	N311Q	N322Q	4Q
Cleavage to R4-ICD	+++	++	+	0	++	++	0
Migration	++	+	++	+++	++	++	++
Cytoprotection Against Gem/Cis	+++	++	++	++	++	+	++
Cytoprotection Against Staurosporine	+++	+++	++	++	++	+	+

Table 2.

Summary of the glycomutants and their effects on R4-ICD production, cell migration, and resistance to apoptosis. The degree of each activity observed is indicated on a relative scale from zero to 3+.

Discussion

FGFR signaling has received increased attention in cholangiocarcinoma with the identification of FGFR2 fusion mutations that are more common in this tumor type. Other FGF receptors have the potential to promote malignant signaling, and this study examined FGFR4. Data in this manuscript primarily relate to how glycosylation regulates the processing, function, and localization of FGFR4. We demonstrate that non-specific deglycosylation or blocking of glycosylation increased processing of FGFR4 to a proteolytic fragment, R4-ICD. Individual and combined glycomutants of FGFR4 did not recapitulate this increased processing, suggesting the effect is not due to deglycosylation of FGFR4 itself. All mutants supported cell migration while selected mutants were less efficient at protecting from apoptosis. Overall, these data show that glycosylation helps to regulate the processing, signaling, and localization of FGFR4 in cholangiocarcinoma cells. Each of these roles will be discussed here.

Understanding N-linked glycosylation of proteins requires defining several terms. Core/high mannose-type N-glycans are added to an asparagine residue in the endoplasmic reticulum and contain only terminal mannose sugars attached the N-acetylglucosamine (GlcNAc) core. Hybrid-type N-glycans are produced in the Golgi and are made up of unsubstituted mannose chains and GlcNAc linkages off of the GlcNAc core. Terminal/complex-type glycans are mature glycosylation patterns that are generated in the Golgi through trimming high-mannose glycan structures followed by subsequent addition of other sugar residues, often with sialic acid residues at the termini. The complex-type glycans are the most common form seen on secreted and cell surface proteins [131, 132].

Processing of FGFR4 to R4-ICD has only recently been recognized, and the product corresponds to the kinase domain, separated from the regulation of the ligand-

binding region. We showed R4-ICD production from endogenous (KMCH) and transgenic FGFR4 and that R4-ICD is the predominant form of FGFR4 in human cholangiocarcinoma tumor samples. The rationale for studying the role of glycosylation in FGFR4 processing is two-fold. First, Notch signaling (a proteolysis-driven event) is regulated by receptor glycosylation [63]. Complex-type glycosylated FGFR4 was identified as the functional form for regulating cholesterol biosynthesis [62]. Second, activation of FGFR3 was necessary for its cleavage [22]. From here, we reasoned that FGFR4 glycosylation may influence receptor activation and subsequently R4-ICD production. Indeed, we observed increased R4-ICD with deglycosylation.

Removal of N-linked sugars or inhibition of N-linked glycosylation promoted processing of FGFR4 to R4-ICD. This increased processing was seen in conditions of indiscriminate deglycosylation (PNGase F treatment of cells or incubation with inhibitors of glycosylation). Targeted genetic inhibition at individual sites on FGFR4 did not show this increase. FGFR4 with each predicted Asn mutated was tested for processing to R4-ICD. R4-ICD was observed in cells expressing mutant forms of FGFR4, at some level. However, additional processing in the incubated samples was not strong (N290) or was absent (4Q) in two mutants. These data indicated that processing was slower in the N290Q and 4Q mutant cells (and somewhat slower in N112Q, N258Q, N311Q, and N322Q). It still occurs, as R4-ICD is seen in cell lysates from all mutant cell lines at time zero, but loss of glycosylation may reduce the sensitivity to protein cleavage. This reduced processing efficiency was revealed in the active lysate assay when we imposed a time constraint. Importantly, we did not find that a specific glycosylation site was responsible for processing, despite seeing more R4-ICD after deglycosylation of proteins in the cell. Still, with five potential glycosylation sites, there are 32 potential glycosylation mutant combinations; our experiments included seven of these. It remains plausible that

a particular pattern of glycomutants could demonstrate increased processing. Additionally, it should be noted that we attempted to produce cells expressing a 5Q mutant form of FGFR4 multiple times, but each time we were unsuccessful.

Regarding signaling, FGFR4 promoted cancer cell survival. In general, glycosylation mutants of FGFR4 were less cytoprotective than wild type FGFR4. However, cells expressing mutant FGFR4 were still more protected than cells lacking FGFR4. The two mutants that provided the least protection were N322Q and 4Q. These two mutants have mirror image effects on glycosylation—N322Q can be glycosylated at all sites except Asn-322, while 4Q can only be glycosylated at position 322. The observation that these two mutants had the least protection from cell death suggests that position 322 dominated the survival signaling and to match the defect in cytoprotection it required that all other glycosylation sites be changed. Glycosylation at position Asn-322 may be a strong determinant of survival function. One possible explanation for this high dependence upon glycosylation at position 322 relates to its proximity to FGFR4's transmembrane domain, amino acids 370-390, affecting conformational signaling to the intracellular domain. Alternatively, it is possible that glycosylation at Asn-322 facilitates ligand binding.

Our studies on apoptosis relied on caspase activation as a marker and compared the amount of caspase activation upon induction of apoptosis between cell lines. An alternative interpretation might consider the magnitude of caspase activation from untreated to treated conditions, determining fold-change in caspase signal. This alternate approach still indicated that the N322Q mutant was least protective. Examining fold of caspase activation indicated that N290Q, N311Q, and 4Q mutants all had similar protective effects that were impaired compared to wild type. Thus, there were no

dramatic differences in interpretation of the results when using fold change versus total magnitude of caspase signal in treated cells, so we relied on the latter.

Modifying the glycosylation of FGFR4 had some effect on localization in the N112Q and 4Q mutant cell lines. In cells expressing N112Q FGFR4, we observed some staining for FGFR4 that colocalized at or near the Golgi. Notably, in all cells, FGFR4 immunofluorescent signal was not confined to the plasma membrane. This distribution may reflect insufficient immunofluorescence signal from the membrane-bound full-length receptor as well as the processed R4-ICD (potentially freed from the membrane fraction), or may indicate FGFR4 present on the network of membrane vesicles within the cell. Previously published FGFR4 immunofluorescent images in cultured cells also showed that FGFR4 staining did not predominantly localize to the limiting plasma membrane [133].

Despite initial data that showed that reduced glycosylation of FGFR4 might enhance processing to R4-ICD, our glycomutants did not support such direct regulation. Our subsequent studies on proteolytic regulation and regulation of apoptotic signaling (see Chapter 4) help define the mechanisms of R4-ICD production and its significance in cancer signaling in cholangiocarcinoma.

CHAPTER 4: FGFR4 cleavage by ADAM10 and γ-secretase produces R4-ICD, a functional intracellular kinase.

Andrew J. Phillips
Yamnah A. Hafeji
Matthieu R. Spriet
Hannah R. Safranek
Joseph M. Pachunka
Ashley M. Mohr
Justin L. Mott

Abstract

Fibroblast growth factor receptors make up a family of four receptor tyrosine kinases that respond to signaling through fibroblast growth factors. One of these receptors, fibroblast growth factor receptor 4 (FGFR4), has been shown to be overexpressed in cholangiocarcinoma and linked with a poorer overall prognosis among patients. We also found that a smaller-than-predicted form of FGFR4 predominated in human cholangiocarcinoma samples. In the current chapter, we determined whether FGFR4 was able to undergo regulated intramebrane proteolysis, an event in which the intracellular domain is cleaved away from the remaining portion of the receptor. We demonstrated through shRNA knockdown of FGFR4 and stable transfection that FGFR4 intracellular domain (R4-ICD) was a product of FGFR4 cleavage. R4-ICD was more stable than full-length FGFR4. Production of R4-ICD was reduced through inhibition of FGFR4, suggesting responsiveness to signaling. Cells transfected to express just R4-ICD retained signaling and apoptosis resistance seen with full length FGFR. We used small molecule inhibitors and genetic inhibition of proteases to determine the proteases involved in R4-ICD production and showed that FGFR4 could be cleaved to R4-ICD by ADAM10 and γ-secretase.

Introduction

Cholangiocarcinoma is a primary cancer of the epithelial cells lining the biliary tract (cholangiocytes). This cancer is associated with a poor prognosis and approximately a 10% five-year survival rate [1]. Typical cholangiocarcinoma diagnoses occur somewhat late in tumor development and progression, since early stages of the disease often have few or no symptoms. Even with an early diagnosis, patient prognosis is still quite poor. While new treatments are being developed, many of them target specific mutations or can only be used in a subset of patients. As such, the best first line systemic treatment has not been established by clinical trials, though a platinum-containing chemotherapeutic plus gemcitabine outperformed gemcitabine alone [6].

One field of recent expansion is in the area of drugs targeting receptor tyrosine kinases (RTKs). This class of medication has been tested in numerous clinical trials and is currently FDA-approved for cancer therapy. Receptor tyrosine kinases are a group of 58 different proteins that contribute to diverse physiologic and disease processes. Structurally, these proteins are type I transmembrane proteins, consisting of an extracellular N-terminal ligand-binding domain, a single pass transmembrane domain and a C-terminal kinase domain (for example, see **Figure 3A**). Briefly, signaling usually occurs first by receptor-ligand interaction. Once ligand has bound, receptor dimerization can occur, which facilitates kinase domain transphosphorylation and subsequent downstream signaling [7, 10]. Recent studies have also shown that RTKs can signal through a process called regulated intramembrane proteolysis (RIP). In RIP, a sheddase, or protease with the ability to cleave the extracellular domain of the receptor, removes most of the ectodomain of an RTK, leaving a short extracellular stub. This initial cleavage event, S1, is followed by γ-secretase-mediated cleavage in the transmembrane-spanning domain, which releases the intracellular domain (ICD) from the plasma membrane. From here, there are several fates for the ICD, including

translocation to the nucleus (in the case of ERBB4, FGFR3, PTK7 and RYK) [21-24], localization to mitochondria (ERBB4) [25, 26], phosphorylation of membrane receptors (EPHB2) [27], initiation of cancer cell repulsion (EPHB2) [28], or simply degradation [30]. Screening of 45 human RTKs as potential γ-secretase substrates confirmed nine previously known γ-secretase substrates and discovered 12 previously unknown substrates, including FGFR4 [80]. Specifically, the cleaved ICD for FGFR4 was determined to be approximately 45 kDa (see supplemental data from the reference).

FGFR4 kinase inhibition has been considered as a therapeutic approach in cancer with recent clinical trials for the treatment of hepatocellular carcinoma. The discovery of FGFR4 signaling in other cancers, like breast, lung, gastric cancers, rhabdomyosarcoma, nasopharyngeal carcinoma, and cholangiocarcinoma, may lead to additional clinical trials [67, 68, 71, 74]. In the context of cholangiocarcinoma, FGFR4 has been shown to be overexpressed in most patients (Phillips et al., 2021, in review; see chapter 3). In addition, findings by Xu *et al.* showed that FGFR4 protein expression correlated with poorer prognosis in patients with cholangiocarcinoma [68]. Like FGFR1 and 3, there is limited data supporting FGFR4 as a substrate for RIP. Our studies showed that this proteolytically processed form of FGFR4, termed R4-ICD, is abundant in human cholangiocarcinoma tumor samples and was the predominant form detected (Phillips et al., in review; see chapter 3). At this point, however, no studies have determined the function of the FGFR4 intracellular domain (R4-ICD). Here, we demonstrate that R4-ICD maintains signaling capacity in cholangiocarcinoma cells. Further, we identified ADAM10 and γ-secretase as likely candidates to be the proteases that act on FGFR4 to produce the constitutively active R4-ICD.

Results

On separation via polyacrylamide gels, full length FGFR4 migrated as two dominant bands; one at 110 kDa and one at 90 kDa. We have previously demonstrated both are glycosylated proteins (see Chapter 3). In addition, faster migrating forms were observed around the 45-50 kDa mark, collectively termed R4-ICD (**Figure 11**, see also **Figure 4B,** Chapter 3, KMCH and HuCCT-FGFR4). To confirm that the 45-50 kDa polypeptides reflect authentic FGFR4 forms, we used an shRNA approach to deplete FGFR4. In cells stably transfected to express one of two shRNAs against FGFR4 (419 and 510), full length FGFR4 protein was reduced 43-97%. The 45-50 kDa FGFR4 signal decreased by 86-96% in the same samples. This demonstrated that both full length and R4-ICD forms of FGFR4 were sensitive to shRNA targeting *FGFR4* mRNA, though we note a limitation in that the actin signal was also lower in the knock down cells. In addition, phosphorylated AKT levels were reduced when FGFR4 was knocked down (**Figure 11**), demonstrating that FGFR4 signaling was a principal means by which AKT was activated in KMCH cells.

Conversely, HuCCT cells normally lack FGFR4 protein and showed both full length and R4-ICD forms upon transfection with an expression plasmid containing the *FGFR4* cDNA sequence (**Figure 3B,** chapter 3). The R4-ICD protein from endogenous expression (in KMCH cells) matched the migration of R4-ICD in FGFR4 transfected cells (HuCCT-FGFR4). Thus, based on immunoreactivity, reduced signal on knockdown, increased signal on enforced expression, and apparent migration, we identify these faster migrating 45-50 kDa bands as forms of FGFR4, termed R4-ICD. Because cDNA is not a substrate for splicing, we reasoned that our observation of R4-ICD in HuCCT-FGFR4 cells (transfected with *FGFR4* cDNA) does not represent a splice form and may be due to proteolytic processing of FGFR4 protein.

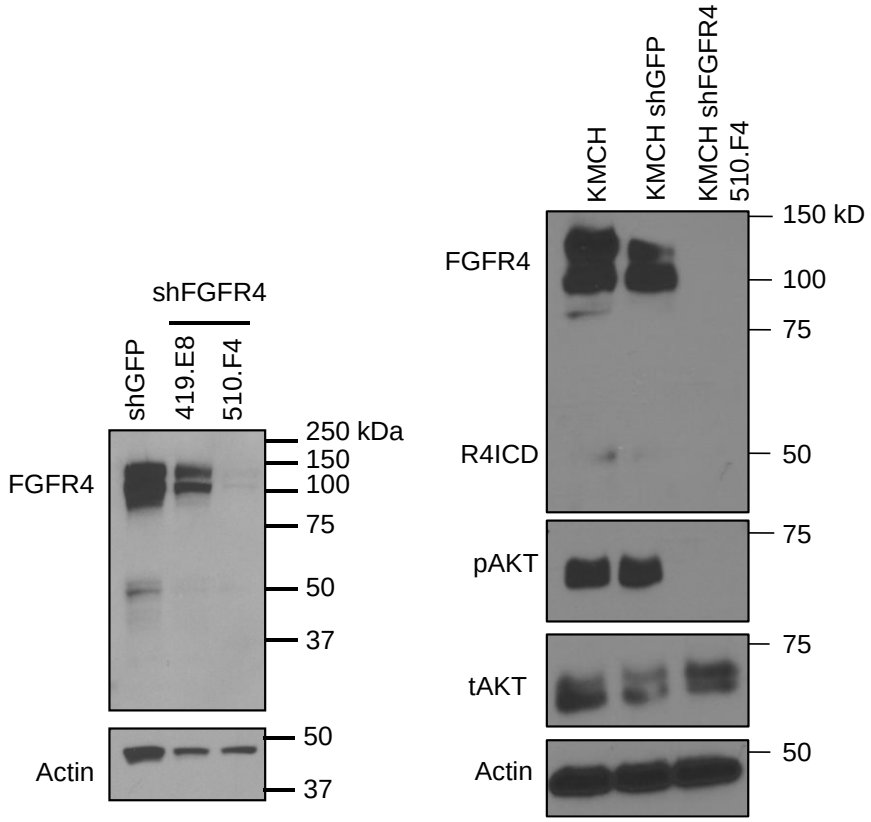

Figure 11. Stable knockdown of FGFR4 in KMCH cells.

KMCH cells were stably transfected to express either of two shRNAs targeting *FGFR4* mRNA (419.E8 and 510.F4). Knockdown was achieved in both clones with the 510.F4 shRNA able to knock down FGFR4 expression by more than 90% (left panel). Control cells in the left panel were stably transfected with an shRNA to green fluorescent protein (GFP). Parental KMCH were additionally included in the right panel. Phosphorylated AKT (Thr-308) is abbreviated pAKT and total AKT as tAKT. This experiment was performed three times.

To assess the function of R4-ICD, we generated clones of HuCCT cells that stably express a pCDNA 3.1-Flag-HA plasmid encoding amino acids 391-802 of FGFR4 (numbering based on the RefSeq NM_002011.5) after an N-terminal Flag/HA tag. From HuCCT cells that lack FGFR4, we generated empty-vector transfected cells (EV), cells expressing wild type FGFR4 (HuCCT-FGFR4), and cells expressing amino acids 391-802 of FGFR4 (R4-ICD; **Figure 3B**). HuCCT-FGFR4 cells had both full length FGFR4 and R4-ICD that migrated similarly to endogenous FGFR4 and R4-ICD in KMCH cells. Plasmid-generated R4-ICD migrates slower than endogenous R4-ICD, likely due to the N-terminal epitope (Hemagglutinin, Flag tags) (data not shown). Clones of HuCCT expressing R4-ICD were named PB1, C3, and C6, and each demonstrated increased phosphorylation of AKT compared to empty vector cells (**Figure 12A, B**). Thus, R4-ICD appears to retain the ability to increase AKT phosphorylation even in the absence of ligand-binding capacity (constitutive activity).

AKT promotes cholangiocarcinoma cell survival [134], so we tested apoptosis resistance in cells expressing R4-ICD. HuCCT cells with empty vector (or parental, not shown) were susceptible to apoptosis upon treatment with the death receptor ligand TRAIL. Several independent empty vector HuCCT cells (EV-9, EV-G3, and EV2 shown) showed similar sensitivity to apoptosis. PB1 cells were the first clone generated and were highly resistant to TRAIL-induced apoptosis (**Figure 12C**). Subsequently, we generated C3 and C6 clones that also showed resistance to TRAIL-induced apoptosis (**Figure 12D**). Thus, expression of the intracellular kinase domain of FGFR4, similar to R4-ICD, is sufficient to activate downstream AKT signaling and to protect cells from apoptosis, similar to full length FGFR4.

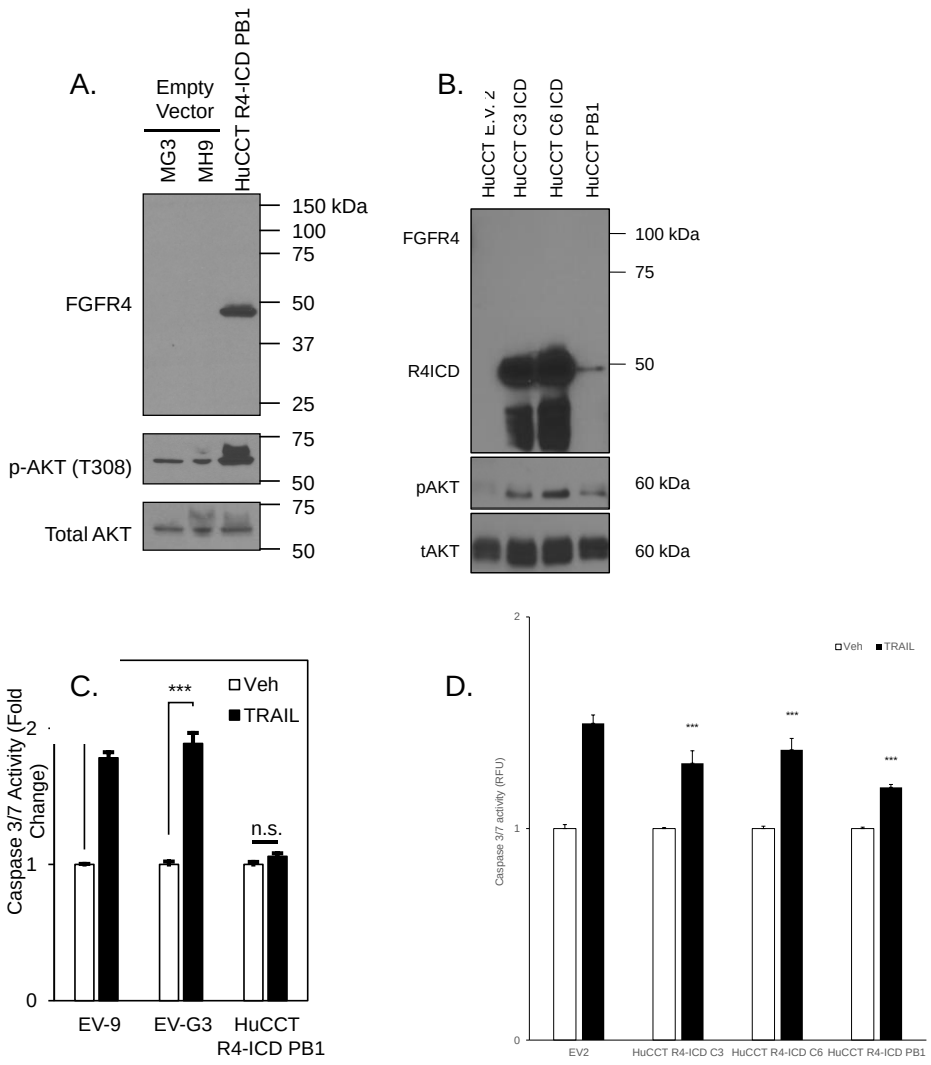

Figure 12. Stable expression of R4-ICD in HuCCT cells.

HuCCT cells lacking endogenous expression of FGFR4 were stably transfected to express amino acids 391-802 of FGFR4 in order to mimic the FGFR4 intracellular domain. Stable HuCCT clones expressing R4-ICD were generated and named PB-1 or R4-ICD C3 and C6. Expression of this domain was observed as a single band at about 49kDa (PB-1, panel A) or as a single 49 kDa band with additional faster migrating fragments (C3 and C6 clones, panel B). Phosphorylated AKT (Thr-308) is abbreviated p-AKT. (C) Apoptosis was assayed by caspase 3/7 activity in HuCCT cells (empty vector or R4-ICD PB-1). Empty-vector cells (EV-9 and EV-G3) were susceptible to apoptosis upon TRAIL treatment (50 ng/mL, 6 hours). *** indicates $p<0.001$ versus vehicle-treated (Veh) cells; n.s. = not significant. (D) Apoptosis was similarly assessed in C3 and C6 clones expressing R4-ICD in HuCCT cells and empty-vector cells (EV2) were more sensitive than any of the three R4-ICD-expressing cells. This experiment was performed one time. *** indicates $p<0.001$ versus TRAIL-treated EV2 cells. For all panels, statistics were performed by ANOVA with *post hoc* Bonferroni correction.

With evidence for R4-ICD function in cholangiocarcinoma cells, and high amounts of R4-ICD in human tumor samples (Phillips et al., 2021, in review; see **Figure 3C**), we next sought to determine the stability of R4-ICD. Cycloheximide, an inhibitor of protein synthesis, was employed here for testing the stability of FGFR4 and R4-ICD. By terminating new protein synthesis, the stability of existing protein could be approximated in terms of half-life. Specifically, the 110 kDa form of FGFR4 was examined, because this form of the protein has been previously demonstrated to be the mature complex-type glycoform (Phillips et al., 2021, in review; see **Figures 4A, 5A**) and involved in signaling [62]. **Figure 13** shows an immunoblot from KMCH cells treated with cycloheximide for up to 6 hours. This experiment was performed four independent times and each time showed that 110 kDa FGFR4 had the shortest half-life, followed by R4-ICD. The calculated half-lives are included in the figure and show that R4-ICD is more stable than full-length FGFR4.

In characterizing R4-ICD, we next used differential centrifugation to determine its localization within cells. Cells were lysed in hypotonic buffer, and the nuclear pellet was collected. The post-nuclear supernatant was then separated into soluble and membrane fractions by centrifugation. Fractions (nuclei, cytoplasm, and membranes) were then analyzed by immunoblot (**Figure 14**). The membrane fraction contained the majority of FGFR4 and R4-ICD. (Note that we did not endeavor to distinguish the plasma membrane from intracellular organelle membranes). In addition to membrane localization, detectable amounts of both full length FGFR4 and R4-ICD were present in both the cytoplasmic and nuclear fractions. Closer examination shows that the 45 kDa R4-ICD band in the membrane fraction appears to consist of at least three bands (see cytoplasmic and nuclear fractions). We have routinely observed multiple bands in the range of 45-50 kDa as well as additional faster-migrating forms (see Fig. 1B, 2C, 3A, 5A,

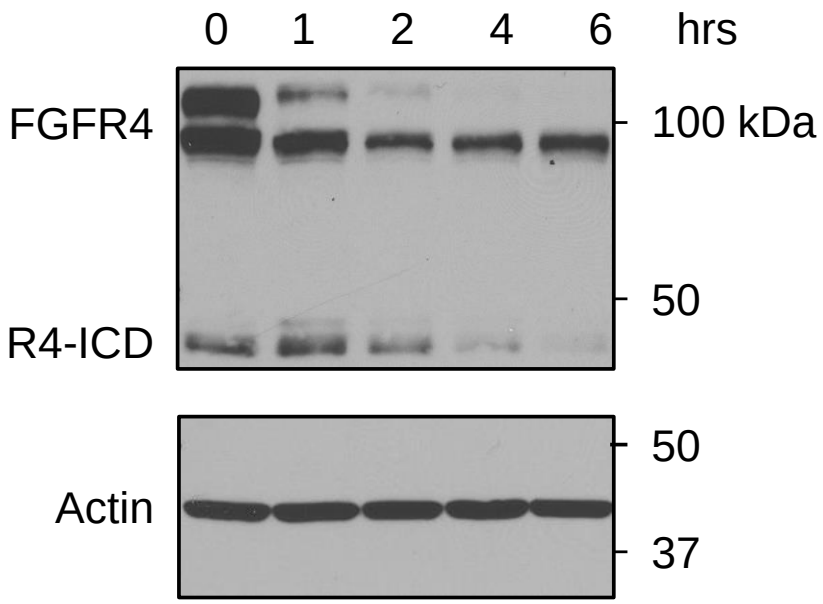

Half-life

FGFR4, 110 kDa	1.24 hours +/- 0.11 hours
R4-ICD	3.20 hours +/- 0.50 hours

Figure 13. Half-life of full length FGFR4 and R4-ICD.

KMCH cells were treated with cycloheximide, 20 µg/mL, for zero to six hours (time indicated above each lane). Analysis by immunoblot showed that full length FGFR4 levels were decreased markedly at 1 hour and beyond, especially the mature 110 kDa glycoform. The 90 kDa full length form was more stable. R4-ICD showed loss of signal by 4-6 hours. R4-ICD half-life is more than double the half-life of FGFR4 110 kDa. This experiment was performed four times, and half-life calculated from the decay constant, modeling exponential decay. From these four experiments, the average half-life was determined for 110 kDa and for R4-ICD forms. Actin did not show decreased protein levels over this 6-hour experiment, consistent with its long half-life in cells.

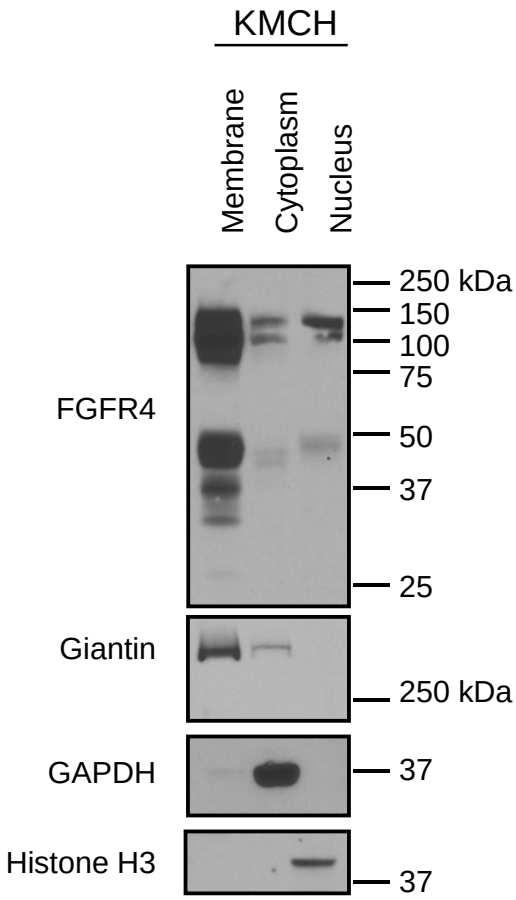

Figure 14. Cellular localization of FGFR4 and R4-ICD.

Differential centrifugation of lysate from KMCH cells was performed to identify the cellular localization of FGFR4. Full length FGFR4 and R4-ICD were primarily localized to the membrane fraction; however, detectable amounts of both were observed in the cytoplasm and nuclear fractions. R4-ICD in the cytoplasmic and nuclear fractions demonstrate three different bands corresponding to the highest molecular weight band in lane 1. Experiment repeated three times.

Markers were used to confirm separation of cellular fractions: membrane (giantin), cytoplasm (GAPDH) and nuclear (Histone H3).

5C-H, 9, and 11). This complexity will partially be discussed and resolved in figures to come.

Next, we sought the protease(s) responsible for R4-ICD formation. First, an initial screening was performed using several protease inhibitors. Inhibitors that were initially included targeted γ-secretase, granzyme B, or MMPs. These inhibitors and targets were specifically chosen based on previous studies of RTK cleavage. FGFR1 and FGFR3 have been shown to undergo receptor cleavage events where full-length receptor is processed to a smaller intracellular domain. FGFR1 was cleaved by MMP2 [39] and granzyme B [40]. FGFR3 underwent RIP with sequential cleavage by an unidentified sheddase followed by cleavage by γ-secretase [22]. Thus, we tested if one or more of these proteases may be involved in FGFR4 processing. Data showed increased rather than a decrease in R4-ICD levels, especially the largest form, following treatment with γ-secretase inhibitor IX (GSI IX) and no dramatic change with granzyme B inhibitor (GBI) treatment. No apparent changes to R4-ICD were seen in OPA (ortho-phenanthroline, MMP inhibitor) treatment (**Figure 15**). An explanation for this data could be that γ-secretase is involved in processing of high molecular weight R4-ICD to lower molecular weight R4-ICD. Because our goal was to determine how R4-ICD is produced and the function it serves, we further pursued γ-secretase. In our experiments to determine regulation, we found that the amount of R4-ICD in cell lysates was variable based on cell confluency (more confluent, generally more R4-ICD up to about 85% cell density, data not shown). However, we also noted that the amount of R4-ICD was variable even when confluency was controlled. To avoid difficulty interpreting the amount of R4-ICD, we developed an assay that allowed us to control the time of R4-ICD production. Active cell lysates, or whole-cell lysates collected through mechanical sheering under non-denaturing conditions in hypotonic buffer, were incubated at 37 degrees C to allow

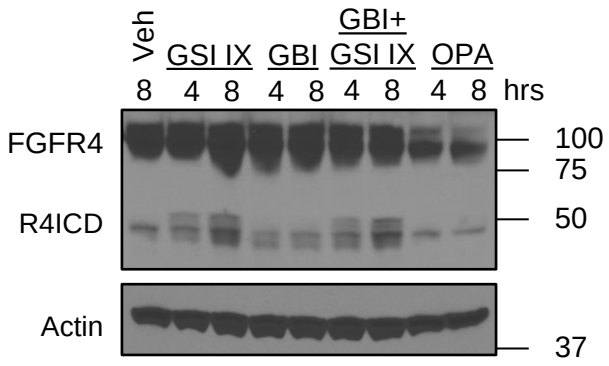

Figure 15. Effects of protease inhibitors on FGFR4 processing to R4-ICD.

KMCH cells were treated for 4 or 8 hours with vehicle (Veh), γ-secretase inhibitor IX, (GSI IX,10 μM), granzyme B inhibitor (GBI, 10 μM), or ortho-phenanthroline (OPA, 100 μM) as a screening to identify proteases involved in cleaving FGFR4 to R4-ICD. In GSI IX-treated samples, there was increased R4-ICD. In samples treated with both GBI and GSI IX, low molecular weight R4-ICD increased in signal. This experiment was performed more than three times.

endogenous proteases to process FGFR4 to R4-ICD. This allowed a comparison of R4-ICD signal from time zero (samples frozen immediately after lysis) to the amount of R4-ICD produced after 20-60 minutes of processing. Incubation of this active cell lysate at 37°C allowed for endogenous protease activity to generate R4-ICD in the absence of new protein synthesis or regulated proteolysis. R4-ICD levels were noticeably increased in the sample incubated for 60 minutes (**Figure 7A** and **Figure 16**), demonstrating production of R4-ICD. The same results were seen in KMCH cells that endogenously express FGFR4 and in HuCCT cells transfected to express FGFR4. For subsequent experiments we routinely employed HuCCT-FGFR4 cells. We reasoned that the lysate contained active proteases and that FGFR4 was a viable substrate. If production of R4-ICD was due to a protease, then heat inactivation of the lysate should prevent processing to R4-ICD. Indeed, heating active lysate to 95°C for 1 or 5 minutes prior to incubation at 37°C nearly completely prevented processing to R4-ICD (**Figure 16**). Thus, FGFR4 retains the capacity for processing after hypotonic cell lysis and a heat-sensitive cellular component is necessary for R4-ICD production, consistent with proteolysis. Next, we used the active lysate assay above to identify protease inhibitors that reduced R4-ICD amounts. Treating the active lysate with a dual ADAM10/ADAM17 inhibitor (GW280264x), or an ADAM10 inhibitor (GI254023x) during incubation markedly reduced R4-ICD production. Treatment with an inhibitor that targets multiple matrix metalloproteases (MMP's), ilomastat, did not significantly reduce R4-ICD formation (**Figure 16**). In KMCH cells especially, we observed a decrease in the 110 kDa signal whenever R4-ICD signal increased, suggesting that the mature functional receptor is the main substrate that generated R4-ICD. The reduction of R4-ICD production with GI254023X, a selective ADAM10 inhibitor, was at least as good as the reduction seen with the dual ADAM10/ADAM17 inhibitor, GW280264X. This led us to further pursue ADAM10 as a protease capable of cleaving FGFR4.

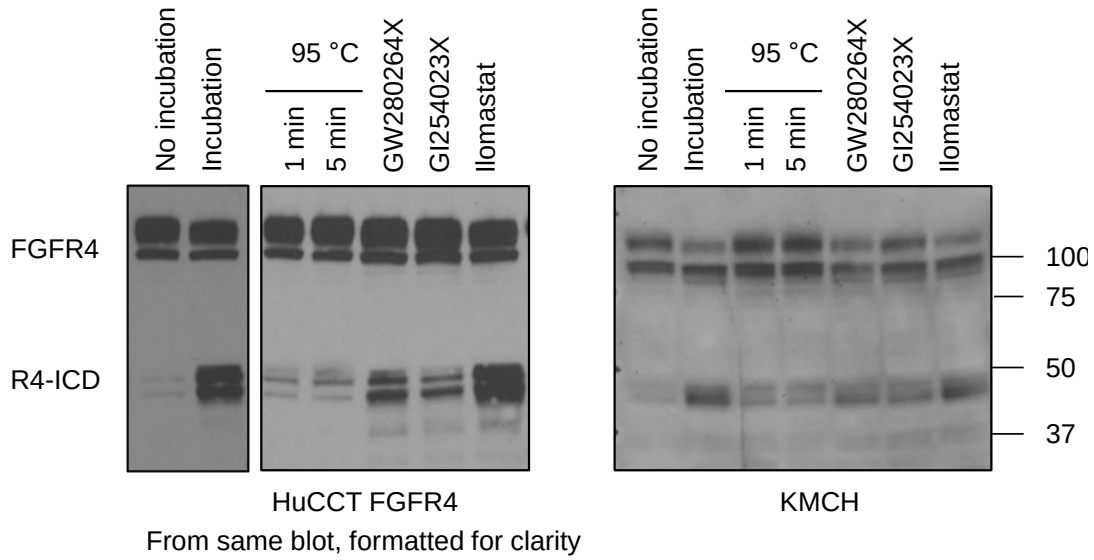

Figure 16. Screening for inhibitors of FGFR4 processing to R4-ICD.

Active lysates were collected from HuCCT1-FGFR4 and KMCH cells. Lysates were either prepared for electrophoresis immediately (No incubation) or were immediately incubated for an hour at 37°C (all other lanes). Prior to incubation at 37 degrees, samples were heated to 95°C or treated with protease inhibitors, as indicated in the figure. Reduced formation of R4-ICD was observed in lysates that were heated to 95°C and lysates treated with GW280264X (ADAM10 and ADAM17 inhibitor) or GI254023X (ADAM10 inhibitor). Ilomastat, an MMP inhibitor, did not alter R4-ICD. The panels on the left are from the same gel and same film exposure and are presented with a gap between the “Incubation” and “1 min 95 degrees” samples because the first two lanes were inadvertently reversed on loading the gel. To keep the image symmetric with the right panel, the first two lanes are mirror-reversed horizontally. This experiment was performed one time in each cell line shown above.

RIP relies on γ-secretase mediated proteolysis following the initial extracellular cleavage (sheddase) event. We reasoned that ADAM10 was the extracellular sheddase. When cells expressing FGFR4 were treated with the γ-secretase inhibitor, GSI IX, we observed an increase in band intensity of the slowest migrating R4-ICD band via immunoblot (shown above, **Figure 15**). This is consistent with the pattern found with receptor tyrosine kinases that undergo γ-secretase cleavage [80].

In support of our data seen with small molecule inhibitors of ADAM10 or γ-secretase, we next genetically depleted the proteases from cells using siRNA to ADAM10 or presenilin 2 (a catalytic subunit of γ-secretase). We demonstrated a 70% depletion of *PSEN2* mRNA with siRNA treatment (**Figure 17**). Experiments to demonstrate depletion of *ADAM10* mRNA are underway. Active cell lysates of cells transfected with negative control, siRNA against PSEN2 or siRNA against ADAM10 were then tested for R4-ICD production. R4-ICD signal at 45-50 kDa was reduced when *PSEN2* or *ADAM10* was knocked down (**Figure 17**). In this experiment, we included both 20 and 60 minute incubations to observe time-dependent processing. Thus, independent data from small molecule inhibition and genetic depletion showed that ADAM10 and γ-secretase contribute to R4-ICD formation.

To further test ADAM10's ability to process FGFR4, recombinant human ADAM10 (rhADAM10) was added to FGFR4, enriched by antibody pulldown (**Figure 18**). HuCCT-FGFR4 cells were lysed in buffer containing 1% NP-40 and pulldown of FGFR4 was performed using protein G beads and mouse primary anti-FGFR4 antibody that recognizes the FGFR4 C-terminus (Invitrogen). After pulldown, enriched FGFR4 was treated with rhADAM10 for one hour at 37°C and blotted with rabbit anti-FGFR4 primary antibody (Cell Signaling) to avoid detection of antibody heavy chain. In rhADAM10-treated groups, R4-ICD levels increased with increasing rhADAM10. We

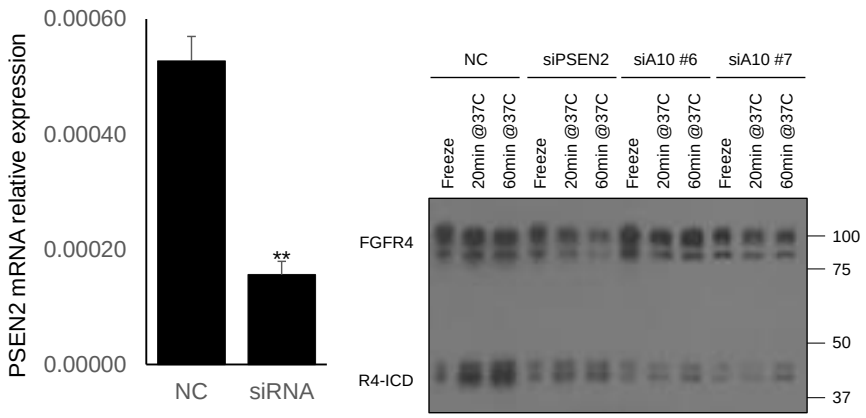

PSEN2 knockdown 70.4% reduction

Figure 17. ADAM10 and PSEN2 knockdown via siRNA affect FGFR4 processing to R4-ICD.

HuCCT-FGFR4 cells were transfected with siRNA targeting Presenilin 2 or ADAM10. Left panel: RT-PCR for *PSEN2* was normalized to 18S rRNA and plotted as relative expression. NC = non-targeting negative control siRNA. siRNA = *PSEN2* siRNA. Data for knockdown of ADAM10 are pending. Right panel: Lysates were acquired through non-denaturing means and frozen immediately, or incubated for 20 or 60 minutes to allow for processing of FGFR4 to R4-ICD. When PSEN2 was knocked down, R4-ICD did not increase as much as seen in NC-transfected cells. When ADAM10 (abbreviated A10 above the blot) was knocked down either with siRNA #6 or #7, processing to R4-ICD was reduced. Knockdown of PSEN2 for mRNA quantification was performed in triplicate, and qPCR was performed in duplicate. Knockdown of PSEN2 or ADAM10 mRNA for immunoblot was performed at least three times.

** indicates $p<0.01$ by Student's t-test versus NC.

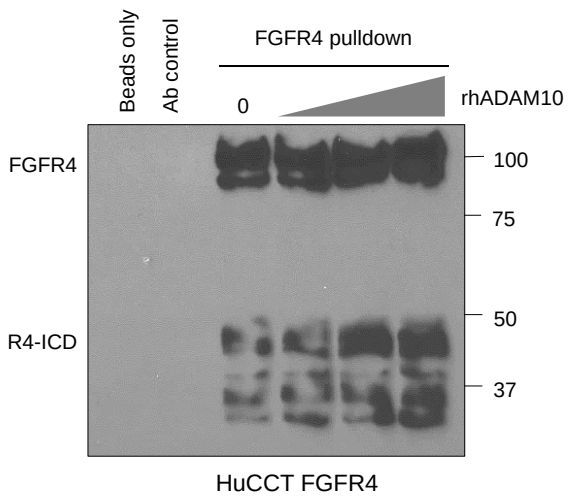

Figure 18. Enriched FGFR4 was cleaved by recombinant human ADAM10 to R4-ICD.

HuCCT-FGFR4 cell lysate were used to enrich for FGFR4 protein by antibody-mediated pulldown (affinity enrichment). Enrichment for FGFR4 was performed using Protein G-coated beads and mouse anti-FGFR4 antibody compared to beads only (no primary), or to beads plus an unrelated antibody (ab control). Beads were washed six times and then incubated for one hour at 37°C with increasing amounts of recombinant human ADAM10 (rhADAM10), 22 ng/μL, 44 ng/μL, or 66 ng/μL (indicated by the shaded triangle above the lanes). Increasing concentrations of ADAM10 were associated with increasing levels of R4-ICD. Samples were blotted with rabbit anti-FGFR4 anti-serum for the immunoblot, allowing R4-ICD to be visualized without interference from the mouse antibody heavy chain. This experiment was performed three times.

employed an ADAM10 substrate containing the cleavable peptide sequence Lys-Pro-Leu-Gly-Leu, a fluorescent 7-methoxycoumarin group, and a 2,4-dinitrophenyl quenching group. Upon proteolysis, the fluorophore is released from the quencher, and the degree of proteolysis is indicated by relative fluorescence units. Cell lysates showed endogenous protease activity that was efficiently ablated by 95°C incubation for one minute. Partially restored proteolytic activity was demonstrated upon addition of 45 pg of rhADAM10 (**Figure 19**). Our data demonstrated that FGFR4 in cell lysates or enriched by antibody-mediated pulldown is a substrate for cleavage by ADAM10 and the proteolytic fragment comigrates with R4-ICD. Inhibition of γ-secretase or siRNA knockdown of ADAM10 impaired processing.

Next, we looked at the effects of receptor activity on processing to R4-ICD. KMCH cells were treated with pan-FGFR inhibitors PD173074 or BGJ398, or FGFR4-selective inhibitor BLU9931 for one to two hours. All inhibitors were able to reduce the levels of R4-ICD, but BGJ398 and BLU9931 reduced it the most, with only modest reduction observed in the PD173074-treated groups (**Figure 20**). Thus, inhibiting FGFR4 kinase activity reduced R4-ICD production. These data are reminiscent of FGFR3 processing, where receptor activation was necessary for RIP to occur [22] and suggest that FGFR4 activity promotes proteolysis.

As our experiments here showed that R4-ICD activated AKT and reduced apoptosis sensitivity, we tested if preventing R4-ICD formation could sensitize cells to apoptosis. Inhibition of ADAM10 alone did not enhance TRAIL-induced apoptosis in HuCCT-FGFR4 cells. Additionally, combined ADAM10 inhibition and FGFR4 kinase inhibition did not sensitize HuCCT-FGFR4 cells to TRAIL-induced apoptosis better than kinase inhibition alone (**Figure 21**). Thus, while R4-ICD can mimic the functions of the full-length receptor, preventing processing of FGFR4 to R4-ICD did not reduce apoptosis

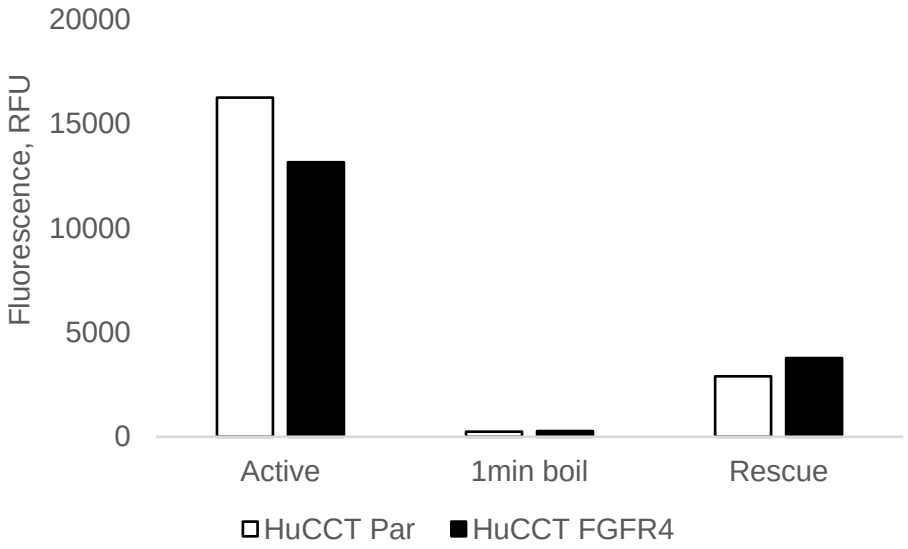

Figure 19. Protease activity of active lysate is reduced through heat and recovered with recombinant protease.

Active cell lysates from HuCCT parental and HuCCT-FGFR4 cells were collected and incubated with pentapeptide ADAM10 substrate (Lys-Pro-Leu-Gly-Leu) containing a fluorescent 7-methoxycoumarin group at one end and a 2,4-dinitrophenyl quenching group at the other. Upon cleavage, fluorescence is increased by separation of the fluorophore and quencher. Endogenous protease activity of active cell lysate from HuCCT parental (HuCCT Par) or HuCCT-FGFR4 cells (bars 1 and 2, respectively) is compared to protease activity after boiling the lysate for one minute prior to adding substrate (bars 3-6), without or with addition of 45 pg of recombinant human ADAM10 (Rescue). Boiling reduced endogenous protease activity by 98.5% (HuCCT) or 97.8% (HuCCT-FGFR4), and rhADAM10 restored protease activity 11.8 fold (HuCCT) or 13.0 fold (HuCCT-FGFR4) when compared to boiled samples. Experiment performed a single time for each cell line, shown.

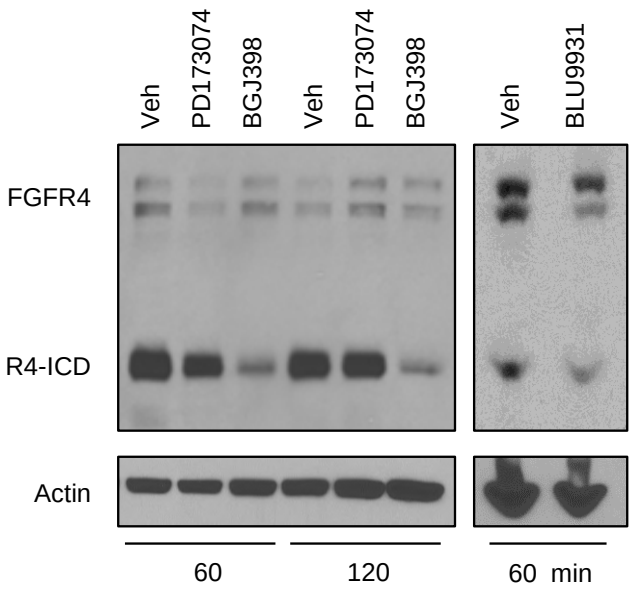

Figure 20. FGFR kinase inhibition reduced processing of FGFR4 to R4-ICD.

KMCH cells were treated with pan-FGFR or FGFR4-selective inhibitors for 60 or 120 minutes prior to protein isolation. Control indicates the zero time point for each condition (Veh, vehicle, PD173074, or BGJ398) just before inhibitor addition. The first three control lanes were run on the same gel and imaged on the same film and exposure as the middle panel, with shorter time points removed for clarity. The right-hand blots are from a different experiment and different gel. Treatment with PD173074 or BGJ398 for 60-120 minutes reduced R4-ICD amounts in the cells. Treatment with BLU9931 for 60 minutes also reduced R4-ICD amounts. Images representative of three experiments.

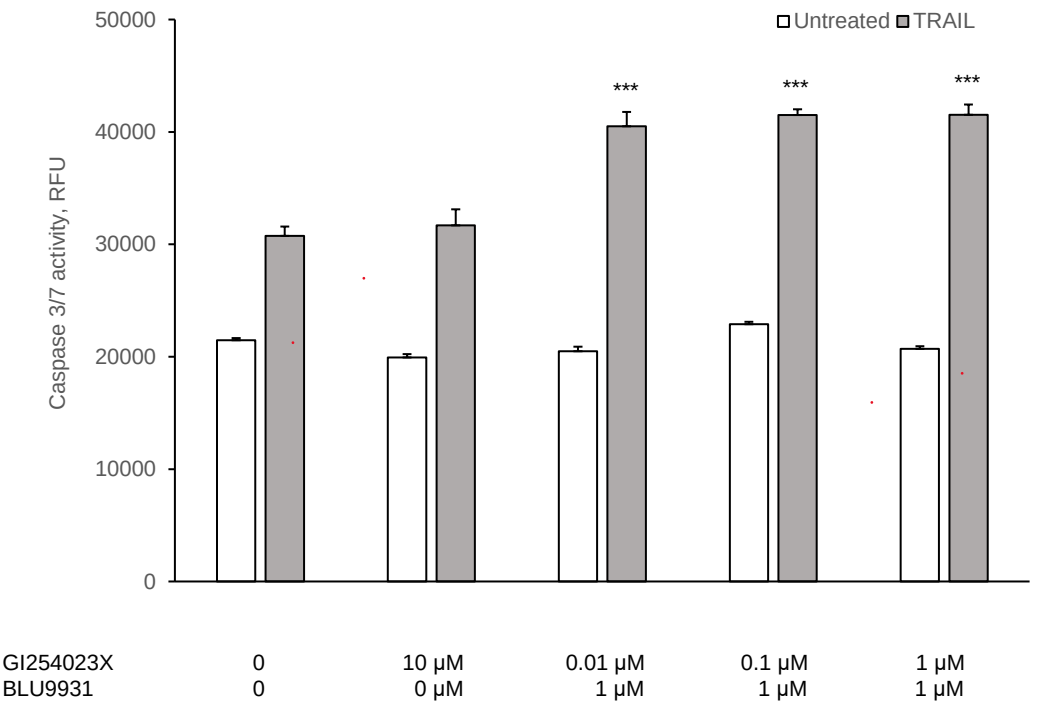

Figure 21. HuCCT-FGFR4 cells show increased sensitization to apoptosis with FGFR4 inhibition, but not ADAM10 inhibition.

HuCCT-FGFR4 cells were treated with the ADAM10 inhibitor, GI254023X and the FGFR4 inhibitor, BLU993 to sensitize cells to TRAIL-induced apoptosis. Apoptosis was measured by Caspase 3/7 activity, plotted on the vertical axis. Untreated HuCCT-FGFR4 cells were relatively resistant to TRAIL-induced apoptosis. Addition of GI254023X did not increase sensitivity. Previous experiments showed that 1 µM BLU9931 was at the low-end of the concentrations that could sensitize to apoptosis (tested 0.03 – 30 µM, not shown), and the sensitization from BLU9931 was detectable, though small. ADAM10 inhibitor (0,01 – 1 µM) was unable to increase sensitization to TRAIL. Treatment groups (ADAM10 inhibitor and FGFR4 inhibitor) were compared to TRAIL-induced caspase activity of untreated group. *** indicates $p<0.001$. Statistics done by ANOVA.

protection by FGFR4. We interpret these findings to indicate that either full length FGFR4 or R4-ICD is sufficient to promote downstream tumor signaling.

Discussion

The overall findings of this study relate to the proteolytic processing of FGFR4 in cholangiocarcinoma cells. Here, we demonstrate that R4-ICD is a proteolytic product from full length FGFR4, R4-ICD has constitutive signaling activity, and R4-ICD is produced by the action of ADAM10 and γ-secretase. Each of these findings will be discussed here.

FGFR4 protein expression was assayed in human cholangiocarcinoma tumor samples. Fourteen tumor samples were collected and probed for FGFR4 by immunoblot. FGFR4 was observed in a majority of samples; however, most striking to us were the robust levels of R4-ICD in all 14 samples. R4-ICD was the dominant form of FGFR4 in these samples (Phillips et al., 2021, in review; see chapter 3, **Figure 3B**). Multiple lines of evidence supported R4-ICD being a proteolytic product derived from FGFR4, rather than a splice form or nonspecific band. We validated the signal as FGFR4 through several experiments, including shRNA knockdown of FGFR4 (which also resulted in R4-ICD knockdown) and transfection of cells with cDNA coding for full length FGFR4 (which produced R4-ICD signal on immunoblot). Both of these findings were consistent with the hypothesis that a single or series of proteolysis events produced R4-ICD.

To test the function of R4-ICD in the absence of full-length receptor, we generated a tagged form of R4-ICD. This R4-ICD mimic was expressed in HuCCT cells that lacked endogenous FGFR4. R4-ICD behaved similarly to full length FGFR4, consistent with the kinase domain retaining constitutive activity. Others have shown that FGFR4 signaling (and receptor tyrosine kinase signaling, in general) is dependent upon

ligand binding, which has been shown to reduce the effects of the autoinhibitory region, producing a conformational change in the protein and allowing phosphorylation events at the kinase domain to occur. R4-ICD, however, lacks a ligand binding domain. Commercial vendors, including Millipore Sigma, Abcam, and Thermo Fisher Scientific, sell recombinant human FGFR4. This recombinant FGFR4 consists of the kinase domain, with molecular weights ranging from 36 kDa to 65 kDa. Data sheets from vendors confirm activity of recombinant FGFR4 under standard assay conditions and in the absence of ligand or any other means of activation. These data strongly suggest that R4-ICD, which is structurally quite similar to these commercial forms, is active independent of ligand. We anticipate that R4-ICD is constitutively active, though we cannot rule out an intracellular event that activates R4-ICD in our cell lines without our intervention. An N-terminally truncated form of FGFR4 has previously been observed in pituitary tumors that includes the kinase domain on a shortened intracellular protein lacking the ligand-binding domain [73, 135]. This form resulted from the expression of FGFR4 via a pituitary-specific cryptic promoter. When this form of FGFR4, termed PTD-FGFR4 (pituitary-tumor-derived FGFR4), was transfected into non-malignant GH4 pituitary cells, the cells showed malignant features (large tumor formation, invasion in mouse models). In contrast, when the same GH4 cells were transfected with empty vector or full length FGFR4, well-delineated tumor nodules formed and no invasion was observed, suggesting benign behavior [135]. We interpret these published findings to demonstrate that an intracellular active FGFR4 kinase, like R4-ICD, promoted tumor features and lacked regulation seen in the full-length receptor. This further supports the findings shown here and helps to expand the importance of FGFR4 processing to R4-ICD to multiple types of cancer.

In our experiments looking at R4-ICD levels in human cholangiocarcinoma cell lines and tumor samples, we were able to consistently observe R4-ICD without the need to block protein degradation through the 26S proteasome or to inhibit γ-secretase to trap a proteolytic intermediate. Thus, in our experiments, we were able to demonstrate that R4-ICD is both stable and functional in cholangiocarcinoma.

As discussed previously, amplification of the *FGF19* genetic locus is observed in over 3% of cholangiocarcinomas [77, 124-126]. Additional data has shown that FGF19 overexpression can promote tumorigenesis [82]. However, our findings suggest that FGF19 amplification is not necessary in all cholangiocarcinomas, as there is processing of the receptor to an active, ligand-independent form. It should be noted that ligand activation of FGFR4 appears to enhance receptor processing to R4-ICD, so increased ligand may further exacerbate R4-ICD tumor signaling.

Regarding processing of FGFR4 to R4-ICD, current data suggest that activation promotes the proteolytic events that result in R4-ICD. However, additional studies could increase the confidence in this finding. Currently, we have only employed small molecule inhibitors to generate evidence that receptor activity promotes R4-ICD production. Past studies on FGFR3 have demonstrated that constitutively active receptor was cleaved, while kinase dead FGFR3 was not, even in the presence of ligand [22]. These data strongly suggest that it is receptor activation and not ligand binding which promoted receptor cleavage. Future studies can employ mutationally-active FGFR4 versus kinase-dead FGFR4 to test activation-dependent cleavage. We have shown that enriched FGFR4 is a direct substrate of the extracellular protease, ADAM10, and that proteolysis leads to increased R4-ICD. We did not attempt to determine the cleavage site or whether ADAM10 or γ-secretase activity is first in FGFR4 processing. Findings from

Merilahti *et al.* and studies on Notch signaling suggest that ADAM10 may be the initial sheddase that allows for subsequent γ-secretase-mediated intramembrane proteolysis.

While the data in this study are consistent with a role for both ADAM10 and γ-secretase in FGFR4 cleavage to R4-ICD, some limitations exist. HuCCT cells lack expression of FGFR4. When we stably expressed just R4-ICD in these cells, they behaved similarly to our stable HuCCT-FGFR4 cell line regarding increased AKT phosphorylation and increased resistance to apoptosis. In comparing the HuCCT R4-ICD and HuCCT-FGFR4 cell lines, one important factor has been the presence of R4-ICD in both cell lines. Because R4-ICD is a proteolytic product of FGFR4, cells expressing FGFR4 and the proper proteases will also have R4-ICD present. As such, producing an FGFR4-positive and R4-ICD-negative cell line (e.g., only full length receptor present) is not currently a reasonable goal. Rather, our HuCCT R4-ICD cell line can be used to understand the role of R4-ICD alone in promoting malignant phenotypes and comparing them to our HuCCT-FGFR4 and HuCCT parental cells. Using these three cell lines, we can reasonably determine the role of FGFR4 and R4-ICD in cholangiocarcinoma tumorigenesis and progression. In order to understand the role of just full length FGFR4 in our cell lines, we would need to produce an uncleavable form of FGFR4. Knowing the exact cleavage sites on FGFR4 would be useful prior to attempting to produce an uncleavable FGFR4. However, this information is not entirely necessary, as long as we have narrowed down a range of amino acids in which cleavage occurs. Domain swapping with the juxtamembrane portion of receptors that are not protease substrates could generate an uncleavable FGFR4. This brings us to our next limitation. We do not know the exact cleavage sites on FGFR4, and data suggest that the R4-ICD neo-N-terminus may not be uniform (multiple R4-ICD bands). We suspect this is because of presenilin's ability to cleave proteins in a sequence-independent manner and

anticipate a range in size of R4-ICD products. In our HuCCT R4-ICD PB-1 cells, R4-ICD is represented by a single band at approximately 50 kDa and is not a product of proteolysis. In our HuCCT R4-ICD C3 and C6 cell lines, R4-ICD is represented by several bands between 30 and 50 kDa, of which the slowest migrating band matched the band seen in the PB1 cell lines. HuCCT R4-ICD cells are stably transfected with cDNA coding for a tag followed by amino acids 391-802 of FGFR4. This is in contrast to the multiple R4-ICD bands observed in KMCH and HuCCT-FGFR4 cells, ranging in molecular weight from 45-50 kDa.

Proteolytic cleavage of FGFR4 in some circumstances could act to reduce growth factor signaling rather than increase it as we have observed. Indeed, for some receptors, intramembrane proteolysis leads to receptor degradation. For example, the antibody datasheet for the Cell Signaling rabbit monoclonal anti-FGFR4 (#8562) shows FGFR4 in two liver and one colorectal cancer cell line. In both liver cell lines, R4-ICD forms are obvious. However, the colorectal cancer cell line, Colo-205 lacked R4-ICD. We speculate these cells (and others like MCF-7 cells) may preferentially degrade cleaved FGFR4, so the R4-ICD kinase is not stable and active. Thus, in different cancer types, increased FGFR4 cleavage could result in increased R4-ICD and increased malignant signaling or in decreased receptor and decreased signaling, dependent on R4-ICD stability.

Some nuances exist in the processing of FGFR4 in the presence of GSI IX when compared to processing when PSEN2 is knocked down. In the case of GSI IX, we observe an increase in R4-ICD. However, siRNA knockdown of PSEN2 caused reduced levels of R4-ICD. A possible explanation is that GSI IX can inhibit both PSEN1 and PSEN2 activity. In our siPSEN2 knockdowns, PSEN1 is not inhibited or knocked down. Under this explanation, γ-secretase containing PSEN1 as the active protease would take

on a protein degradation phenotype, reducing R4-ICD levels via breakdown, while γ-secretase containing PSEN2 as the active protease would have more of a processing function.

When we attempted to eliminate the production of R4-ICD through chemical or genetic inhibitors of ADAM10 and γ-secretase, we were unsuccessful. Cycloheximide treatment of cells suggested the half-life of R4-ICD to be roughly 3.2 hours, and our inhibition was maintained for up to 4 hours (chemical, GSI IX) or several days (genetic knockdown of ADAM10, PSEN 2 or both), so it is likely that there was imperfect inhibition or that other minor proteases were able to compensate.

Overall, this finding of a functional proteolytically released intracellular domain of FGFR4 is exciting. R4-ICD is characterized here as a new form of FGFR4 that exhibits constitutive tumor signaling activity.

CHAPTER 5: DISCUSSION

Phosphorylation of FGFR4 regulates protein function and cancer signaling

On the topic of post-translational modifications (PTMs), glycosylation may be second only to phosphorylation in importance for regulating signaling. This dissertation just touched on phosphorylation of FGFR4 (i.e., Chapter 3, treatment of cell lysate with lambda phosphatase), but did not add a large amount of data or new interpretations of receptor phosphorylation. Still, phosphorylation of FGFR4 and the subsequent downstream pathways are important; numerous studies have been performed to better understand this key aspect of the receptor tyrosine kinase, and mutations have been discovered that impact FGFR4 phosphorylation states or phosphorylation of downstream signaling molecules. FGFR4, like other FGFRs, contains a “split” tyrosine kinase domain, two domains separated by up to 100 mostly hydrophilic amino acids, known as the kinase insertion sequence [7, 10]. This kinase insertion sequence for a specific protein is highly conserved between species. However, this insertion sequence varies significantly from protein to protein, suggesting that the insert has a functional role that is receptor-specific. The kinase insertion sequence is believed to play important roles in RTK interactions with substrates and effector proteins [7]. Regarding phosphorylation sites, FGFR4 contains multiple potential sites within its kinase domain, including tyrosine and serine residues. The FGFR4 kinase transphosphorylates the homodimeric FGFR4 binding partner. This FGFR4 phosphorylation is initially catalyzed by Asp-612 (invariant aspartate) within the conserved histidine-arginine-aspartate motif [136], leading to phosphorylation of Tyr-642 and Tyr-643 (of the YYKK motif in the activation loop). Phosphorylation of these two tyrosine residues is necessary for kinase activity and significantly increases RTK catalytic activity. This YYKK motif and its function is conserved across FGFRs [137]. The remaining phosphotyrosine residues allow for

docking of SH2 domain-containing proteins, leading to activation of downstream pathways [138, 139].

One commonly seen polymorphism that impacts phosphorylation and receptor signaling is FGFR4 G388R. This form of the protein has been shown to be degraded less quickly and has increased phosphorylation following ligand binding when compared to the Gly-388 form of FGFR4 [140]. Residue 388 is located at the C-terminal end of the transmembrane domain (residues 370-390 span the membrane). In the context of a G388R, the arginine residue is hypothesized to modify the structure of the transmembrane region, leading to an additional intracellular STAT3 binding site and promoting STAT3 phosphorylation [141].

In rhabdomyosarcoma, FGFR4 overexpression or activating mutations (N535K, V550E, V550L) are frequently observed, with approximately 10% of embryonal rhabdomyosarcoma patients having an FGFR4 activating mutation [74, 142, 143]. In wild type FGFR4, residues Asn-535, His-530 and Ile-533 form hydrogen bonds and stabilize the inactivated form of FGFR4. In N535K, this hydrogen bonding is disrupted, and the inactive form is destabilized. Val-550 site mutations (V550E and V550L) alter the gatekeeper site where ATP binding occurs. Mutation from valine to a larger glutamate or leucine residue results in a larger gatekeeper residue and stabilization of the active FGFR4 structure [144].

Glycosylation of FGFR4 regulates protein function and cancer signaling

In chapter 3, N-linked glycosylation of FGFR4 and its implications in protein localization, processing, cell migration, and apoptosis susceptibility were examined in depth. Based on the location of putative N-linked glycosylation sites in the ligand-binding and juxtamembrane regions, we tested the role of N-linked glycosylation on FGFR4 function through enzymatic and genetic manipulations.

The recognition that glycosylation of proteins regulates features of cancer goes as far back as 1948 when Winzler and Smyth published on the increased levels of glycoproteins in cancer patients compared to individuals without cancer [145]. Since then, countless studies looking at glycoproteins in cancer have been published. They show altered glycosylation patterns in various cancers including prostate, colorectal, and breast cancers [146-149]. Data showing altered glycosylation of proteins in cancer cells has translated to the use of certain glycoproteins as cancer biomarkers, or indicators of disease status. Some examples include cancer antigen 19-9 (CA 19-9) in gastrointestinal cancers, HER2/neu in breast cancer, haptoglobin in hepatocellular carcinoma [150, 151] and prostate-specific antigen (PSA) in prostate cancer [146, 152, 153]. Typically, biomarker levels are measured over time; however, their use has been expanded. For some biomarkers, like PSA or haptoglobin, glycosylation patterns can help distinguish between the presence or progression of tumor and normal tissue [146, 150, 151].

Notch protein is being investigated as a prognostic biomarker for non-small cell lung cancer and acute myeloid leukemia [154, 155]. Notch activation has been shown to drive cell proliferation and transformation to malignancy. In cancer, variations in Fringe glycosyltransferases also affect Notch signaling [63, 85, 86, 130].

It is nearly impossible to discuss the field of glycoproteins in cancer without mentioning mucins. Mucins are large, heavily glycosylated (O-linked and N-linked) secreted or membrane-bound proteins that make up mucus. Physiologically, they are produced by epithelial cells at areas exposed to harsher conditions and serve as lubricants and molecular barriers, allowing tissues to maintain homeostasis. In cancers, mucins have been hypothesized to play a role in protecting tumor cells from the rather harsh acidic, hypoxic and protease-rich environment associated with solid tumors, in addition to acting as a potential barrier against the immune system and chemotherapeutic agents [156]. Data has shown that glycosylation patterns of mucins produced by tumor cells differ significantly from the glycosylation patterns of mucins produced by healthy cells [157-162].

While glycosylation plays a role in the signaling of cancer molecules (Notch) and the detection and progression of cancer (biomarkers), it can also be used as a target for cancer treatment. NGI-1 (N-linked glycosylation inhibitor 1) is an inhibitor of oligosaccharyltransferase (OST), and has been shown to reduce receptor tyrosine kinase activity in gliomas while sensitizing them to radiation. Because NGI-1 does not completely inhibit OST, drug toxicities are fairly low [163]. Additional studies showed that tumor cells are dependent on receptor tyrosine kinase activity (EGFR or FGFR), and exhibited cell cycle arrest and changes in morphology when they were treated with NGI-1 [164, 165]. It was with these data in mind that the N-linked glycosylation of FGFR4 was targeted as a way to modify receptor signaling and cholangiocarcinoma cell line phenotypes.

Kifunensine is a natural alkaloid that inhibits mannosidase I in cells, trapping N-linked glycoproteins in their high-mannose form and preventing trimming and subsequent modification to complex-type N-glycans. Thus, while NGI-1 blocked the

addition of N-glycans, kifunensine blocked their maturation. We observed that both NGI-1 and kifunensine reduced the amount of complex N-glycosylated FGFR4. When complex-type glycosylation of FGFR4 was completely prevented (100 μM NGI-1 or 16 hours with kifunensine), this prevented processing of FGFR4 to R4-ICD. However, when complex-type glycosylation was partially prevented (10 μM NGI-1 or 8 hours of kifunensine), there was an increase in R4-ICD. These results could be due to direct or indirect effects of altered glycosylation on FGFR4. If direct, then FGFR4 that has fully complex-type N-glycosylation is partially resistant to proteolysis. Put another way, partial removal of complex glycans from FGFR4 increased proteolysis. However, we speculate that R4-ICD is not produced from high-mannose and hybrid-type N-glycans, so complete prevention of mature complex-type glycosylation forms of FGFR4 removes the substrate from which R4-ICD is generated. Because R4-ICD has a longer half-life than complex-type glycosylated FGFR4, it was still observed in some experiments when complex glycosylated FGFR4 was absent. If the effect is indirect, then we hypothesize that either ADAM10 or γ-secretase function is increased by partial loss of complex-type glycans but almost completely inhibited by full loss of complex-type glycans.

Proteolysis of FGFR4 regulates protein function and cancer signaling

While alternative splicing of the extracellular immunoglobulin III loop has been clearly observed and demonstrated in FGFRs 1-3, FGFR4 lacks an alternative exon at this location, and thus, does not undergo alternative splicing. In FGFRs 1-3, alternative splicing results in an immunoglobulin III loop that has varying compatible ligands depending upon which exon is expressed. Alternative splicing of FGFRs is observed in other parts of the protein structure including at the autoinhibitory domain (FGFR1 and 2)

[166, 167], Alternatively splicing at the autoinhibitory domain of FGF1 and 2 mRNA produces a more active receptor and alternative splicing in the transmembrane domain (FGFR3 and 4) [168, 169] produces a soluble, secreted receptor. While FGFR4 has been shown to undergo alternative splicing, it is far more commonly observed among the other FGFRs.

Polyacrylamide gel electrophoresis demonstrated multiple forms of FGFR4. We were able to explain these by post-translational modifications rather than alternative splicing. Here, we demonstrate that FGFR4 is a direct substrate of ADAM10 and proteolysis produced R4-ICD. R4-ICD is stable in cholangiocarcinoma cells and has signaling function. Merilahti *et al.* used PMA and γ-secretase inhibitor IX (GSI IX) to show RIP among receptor tyrosine kinases [80]. In the case of FGFR4 (and other receptor tyrosine kinases), the cleaved product was only observed when γ-secretase was inhibited, even when the receptor was being expressed under a strong promoter. This suggests that γ-secretase-mediated proteolysis may be involved in protein degradation for FGFR4 in some cells. In our cholangiocarcinoma cells, we observed an increase in the slowest migrating R4-ICD band when γ-secretase was inhibited, consistent with Merilahti *et al.* findings.

Our finding that R4-ICD was stable in cholangiocarcinoma suggests that γ-secretase-mediated proteolysis promotes degradation in some cells (e.g., MCF7 cells used by Merilahti) and not in other cells (e.g., cholangiocarcinoma cells). The R4-ICD form of the receptor (endogenous N-terminus undetermined or plasmid-driven R4-ICD, amino acids 391-802) is structurally similar to recombinant human FGFR4 sold for kinase assays (Millipore Sigma # 14-583, amino acids 442-755 or Thermo Fisher #P3054, amino acids 460-802). These commercially-available recombinant R4-ICD mimics have constitutive activity and do not require activation for catalytic activity. Thus,

we reasoned that intracellular R4-ICD would also have constitutive activity. Data we currently have show HuCCT R4-ICD cells behaving similarly to HuCCT-FGFR4 cells with regard to AKT phosphorylation and apoptosis resistance. R4-ICD has been shown to access different cellular compartments (**Figure 14**) and promotes cell survival in a ligand-independent manner (**Figure 12**). However additional experiments need to be done to define additional potential biologic functions of R4-ICD.

FGFR proteins undergo dimerization and transphosphorylation in order to become active. In the case of R4-ICD, we speculate that two R4-ICD molecules can dimerize and undergo transphosphorylation. It is also reasonable to suspect that R4-ICD can also dimerize with full length FGFR4. When cells expressing FGFR4 were fractionated by differential centrifugation, data showed that FGFR4 and R4-ICD primarily localized with the membrane fraction, with small amounts of the upper R4-ICD band in the nuclear fraction and small amounts of the lower R4-ICD bands in the cytosol (**Figure 14**). This leads us to hypothesize that FGFR4 shedding (S1 cleavage event) is not always followed by γ-secretase cleavage (S2). If this interpretation holds, that the cytoplasmic R4-ICD form is the product of both sheddase and γ-secretase cleavage and the nuclear R4-ICD form is the transmembrane-associated product of sheddase activity, it may be possible for the membrane-bound intracellular domain of FGFR4 to be internalized and translocated to the nucleus. Finally, the membrane fraction contained the majority of R4-ICD, including both the upper and lower bands. If R4-ICD dimerizes with FGFR4 or interacts with other membrane-bound proteins, it would be present in this fraction as a peripheral membrane protein. This is reasonable to hypothesize, because R4-ICD contains domains known to bind other proteins. Additionally, it contains a new N-terminus, which may also contribute to binding potential. As such, additional experiments

must be done before we can determine which, if any, R4-ICD forms act in new cellular compartments.

Another characteristic of R4-ICD is its prolonged half-life. In cells treated with an inhibitor of new protein synthesis, we showed that R4-ICD was more stable than the 110 kDa FGFR4 form. The half-life of R4-ICD was approximately two hours longer than that of 110 kDa FGFR4 (3.20 hours vs 1.24 hours). Since R4-ICD is suspected to no longer be a transmembrane protein, it is reasonable to hypothesize that it no longer undergoes the same receptor recycling that FGFR4 and other FGFRs do.

Implications of findings shown here on different fields

Data and findings shown in this dissertation primarily relate to two types of post translational modifications (glycosylation and proteolysis) on FGFR4 protein signaling in cholangiocarcinoma. The implications of regulated intramembrane proteolysis on FGFR4 signaling have been discussed here; however, 11 additional RTKs were reported to undergo RIP [80]. Future studies could lead to the discovery of new proteolytic products (like R4-ICD) that have the potential to promote malignant phenotypes or play a role in cancer. Should additional studies show that these cleaved forms of RTKs are involved in disease states, there may be an additional push to develop drugs targeting γ-secretase (or presenilin-1 or -2) while minimizing the toxicities associated with past attempts. Alternatively, researchers may look into targeting the specific sheddases involved in priming RTKs for RIP. This approach is more targeted and thus, may be associated with fewer adverse outcomes. Additional studies in other cancers are needed to identify if R4-ICD regulates cancer signaling. Observations of immunoblots from pancreatic cancer cells suggest R4-ICD is present beyond biliary tract cancers.

Implications of findings shown here on the field of cholangiocarcinoma

Findings shown here may directly impact the field of cholangiocarcinoma and cholangiocarcinoma treatments moving forward. First, elevated amounts of FGFR4 and R4-ICD proteins were common and observed in the majority of cholangiocarcinomas. Thus, relying on RNA or DNA sequencing data will miss altered FGFR signaling in many cholangiocarcinoma patients. Further, inhibitors that are selective to FGFR1-3 may not provide patients with the full benefit. FGFR kinase inhibitors have been used to treat cholangiocarcinomas positive for FGFR2 fusion proteins. However, these fusion proteins are seen in only 10-15% of cholangiocarcinomas.

Data here showed that FGFR4 and R4-ICD are observed at abundant levels in >80% of cholangiocarcinomas. Despite the small sample size (n=14), these findings and other data shown here support the use of FGFR4 inhibitors in cholangiocarcinoma patients. While knowing the FGFR2 fusion protein status is certainly important and can provide a rationale for kinase inhibitor use in 10-15% of patients with cholangiocarcinoma, our data suggests that knowing the FGFR4 status and treating FGFR4-positive cholangiocarcinomas with kinase inhibitors may be beneficial for a majority of cholangiocarcinoma patients. We note the caveat that the current studies do not show that the majority of cholangiocarcinoma tumors are *dependent* on FGFR4, simply that this receptor is commonly increased. With FGFR4-selective inhibitors currently in clinical trials, we may soon see significantly improved outcomes for patients with cholangiocarcinoma.

Evidence suggests that while the individual glycosylation sites on FGFR4 may not significantly modify its signaling ability or cell phenotypes, reducing the ability of cells to perform N-linked glycosylation, as a whole, may hold potential to increase apoptosis sensitivity in cholangiocarcinoma cells. These data are supported by other published

findings that showed inhibition of N-linked glycosylation sensitized to radiotherapies while maintaining minimal toxicities. Overall, FGFR4 in cholangiocarcinoma is expressed at high levels, is processed via glycosylation and proteolysis, and mediates cancer signaling.

REFERENCES

1. Razumilava, N. and G.J. Gores, *Cholangiocarcinoma.* Lancet, 2014. **383**(9935): p. 2168-79.
2. Robles, R., et al., *Liver transplantation for hilar cholangiocarcinoma.* World J Gastroenterol, 2013. **19**(48): p. 9209-15.
3. Prueksapanich, P., et al., *Liver Fluke-Associated Biliary Tract Cancer.* Gut Liver, 2018. **12**(3): p. 236-245.
4. Shaib, Y. and H.B. El-Serag, *The epidemiology of cholangiocarcinoma.* Semin Liver Dis, 2004. **24**(2): p. 115-25.
5. West, J., et al., *Trends in the incidence of primary liver and biliary tract cancers in England and Wales 1971-2001.* Br J Cancer, 2006. **94**(11): p. 1751-8.
6. Valle, J., et al., *Cisplatin plus gemcitabine versus gemcitabine for biliary tract cancer.* N Engl J Med, 2010. **362**(14): p. 1273-81.
7. Ullrich, A. and J. Schlessinger, *Signal transduction by receptors with tyrosine kinase activity.* Cell, 1990. **61**(2): p. 203-12.
8. Lemmon, M.A. and J. Schlessinger, *Cell signaling by receptor tyrosine kinases.* Cell, 2010. **141**(7): p. 1117-34.
9. Zwick, E., J. Bange, and A. Ullrich, *Receptor tyrosine kinase signalling as a target for cancer intervention strategies.* Endocr Relat Cancer, 2001. **8**(3): p. 161-73.
10. Heldin, C.H., *Dimerization of cell surface receptors in signal transduction.* Cell, 1995. **80**(2): p. 213-23.
11. Mohammadi, M., J. Schlessinger, and S.R. Hubbard, *Structure of the FGF receptor tyrosine kinase domain reveals a novel autoinhibitory mechanism.* Cell, 1996. **86**(4): p. 577-87.
12. Hubbard, S.R., *Juxtamembrane autoinhibition in receptor tyrosine kinases.* Nat Rev Mol Cell Biol, 2004. **5**(6): p. 464-71.
13. Schlessinger, J., et al., *Crystal structure of a ternary FGF-FGFR-heparin complex reveals a dual role for heparin in FGFR binding and dimerization.* Mol Cell, 2000. **6**(3): p. 743-50.
14. Pellegrini, L., et al., *Crystal structure of fibroblast growth factor receptor ectodomain bound to ligand and heparin.* Nature, 2000. **407**(6807): p. 1029-34.
15. Schlessinger, J., *Cell signaling by receptor tyrosine kinases.* Cell, 2000. **103**(2): p. 211-25.
16. Pawson, T., *Specificity in signal transduction: from phosphotyrosine-SH2 domain interactions to complex cellular systems.* Cell, 2004. **116**(2): p. 191-203.
17. Schlessinger, J. and M.A. Lemmon, *SH2 and PTB domains in tyrosine kinase signaling.* Sci STKE, 2003. **2003**(191): p. RE12.
18. Kirkin, V. and I. Dikic, *Role of ubiquitin- and Ubl-binding proteins in cell signaling.* Curr Opin Cell Biol, 2007. **19**(2): p. 199-205.
19. Haugsten, E.M., et al., *Different intracellular trafficking of FGF1 endocytosed by the four homologous FGF receptors.* J Cell Sci, 2005. **118**(Pt 17): p. 3869-81.
20. Funamoto, S., et al., *Substrate ectodomain is critical for substrate preference and inhibition of gamma-secretase.* Nat Commun, 2013. **4**: p. 2529.
21. Ni, C.Y., et al., *gamma -Secretase cleavage and nuclear localization of ErbB-4 receptor tyrosine kinase.* Science, 2001. **294**(5549): p. 2179-81.
22. Degnin, C.R., M.B. Laederich, and W.A. Horton, *Ligand activation leads to regulated intramembrane proteolysis of fibroblast growth factor receptor 3.* Mol Biol Cell, 2011. **22**(20): p. 3861-73.

23. Na, H.W., et al., *The cytosolic domain of protein-tyrosine kinase 7 (PTK7), generated from sequential cleavage by a disintegrin and metalloprotease 17 (ADAM17) and gamma-secretase, enhances cell proliferation and migration in colon cancer cells.* J Biol Chem, 2012. **287**(30): p. 25001-9.
24. Lyu, J., V. Yamamoto, and W. Lu, *Cleavage of the Wnt receptor Ryk regulates neuronal differentiation during cortical neurogenesis.* Dev Cell, 2008. **15**(5): p. 773-80.
25. Naresh, A., et al., *The ERBB4/HER4 intracellular domain 4ICD is a BH3-only protein promoting apoptosis of breast cancer cells.* Cancer Res, 2006. **66**(12): p. 6412-20.
26. Vidal, G.A., et al., *A constitutively active ERBB4/HER4 allele with enhanced transcriptional coactivation and cell-killing activities.* Oncogene, 2007. **26**(3): p. 462-6.
27. Xu, J., et al., *Peptide EphB2/CTF2 generated by the gamma-secretase processing of EphB2 receptor promotes tyrosine phosphorylation and cell surface localization of N-methyl-D-aspartate receptors.* J Biol Chem, 2009. **284**(40): p. 27220-8.
28. Lin, K.T., et al., *Ephrin-B2-induced cleavage of EphB2 receptor is mediated by matrix metalloproteinases to trigger cell repulsion.* J Biol Chem, 2008. **283**(43): p. 28969-79.
29. Lu, Y., et al., *Regulated intramembrane proteolysis of the AXL receptor kinase generates an intracellular domain that localizes in the nucleus of cancer cells.* FASEB J, 2017. **31**(4): p. 1382-1397.
30. Foveau, B., et al., *Down-regulation of the met receptor tyrosine kinase by presenilin-dependent regulated intramembrane proteolysis.* Mol Biol Cell, 2009. **20**(9): p. 2495-507.
31. Du, Z. and C.M. Lovly, *Mechanisms of receptor tyrosine kinase activation in cancer.* Mol Cancer, 2018. **17**(1): p. 58.
32. Klaeger, S., et al., *The target landscape of clinical kinase drugs.* Science, 2017. **358**(6367).
33. Kim, R.D., et al., *First-in-Human Phase I Study of Fisogatinib (BLU-554) Validates Aberrant FGF19 Signaling as a Driver Event in Hepatocellular Carcinoma.* Cancer Discov, 2019. **9**(12): p. 1696-1707.
34. Tiong, K.H., L.Y. Mah, and C.O. Leong, *Functional roles of fibroblast growth factor receptors (FGFRs) signaling in human cancers.* Apoptosis, 2013. **18**(12): p. 1447-68.
35. Sarrazin, S., W.C. Lamanna, and J.D. Esko, *Heparan sulfate proteoglycans.* Cold Spring Harb Perspect Biol, 2011. **3**(7).
36. Wang, Y. and Z. Sun, *Current understanding of klotho.* Ageing Res Rev, 2009. **8**(1): p. 43-51.
37. Ornitz, D.M. and N. Itoh, *The Fibroblast Growth Factor signaling pathway.* Wiley Interdiscip Rev Dev Biol, 2015. **4**(3): p. 215-66.
38. Dolegowska, K., et al., *FGF19 subfamily members: FGF19 and FGF21.* J Physiol Biochem, 2019. **75**(2): p. 229-240.
39. Levi, E., et al., *Matrix metalloproteinase 2 releases active soluble ectodomain of fibroblast growth factor receptor 1.* Proc Natl Acad Sci U S A, 1996. **93**(14): p. 7069-74.
40. Loeb, C.R., J.L. Harris, and C.S. Craik, *Granzyme B proteolyzes receptors important to proliferation and survival, tipping the balance toward apoptosis.* J Biol Chem, 2006. **281**(38): p. 28326-35.
41. Chioni, A.M. and R. Grose, *FGFR1 cleavage and nuclear translocation regulates breast cancer cell behavior.* J Cell Biol, 2012. **197**(6): p. 801-17.
42. Chen, M.K. and M.C. Hung, *Proteolytic cleavage, trafficking, and functions of nuclear receptor tyrosine kinases.* FEBS J, 2015. **282**(19): p. 3693-721.
43. Jezela-Stanek, A. and M. Krajewska-Walasek, *Genetic causes of syndromic craniosynostoses.* Eur J Paediatr Neurol, 2013. **17**(3): p. 221-4.

44. Rousseau, F., et al., *Mutations in the gene encoding fibroblast growth factor receptor-3 in achondroplasia.* Nature, 1994. **371**(6494): p. 252-4.
45. Shiang, R., et al., *Mutations in the transmembrane domain of FGFR3 cause the most common genetic form of dwarfism, achondroplasia.* Cell, 1994. **78**(2): p. 335-42.
46. Helsten, T., et al., *The FGFR Landscape in Cancer: Analysis of 4,853 Tumors by Next-Generation Sequencing.* Clin Cancer Res, 2016. **22**(1): p. 259-67.
47. Acevedo, V.D., et al., *Inducible FGFR-1 activation leads to irreversible prostate adenocarcinoma and an epithelial-to-mesenchymal transition.* Cancer Cell, 2007. **12**(6): p. 559-71.
48. Nguyen, P.T., et al., *The FGFR1 inhibitor PD173074 induces mesenchymal-epithelial transition through the transcription factor AP-1.* Br J Cancer, 2013. **109**(8): p. 2248-58.
49. Drago, J.Z., et al., *FGFR1 Amplification Mediates Endocrine Resistance but Retains TORC Sensitivity in Metastatic Hormone Receptor-Positive (HR(+)) Breast Cancer.* Clin Cancer Res, 2019. **25**(21): p. 6443-6451.
50. De Luca, A., et al., *FGFR Fusions in Cancer: From Diagnostic Approaches to Therapeutic Intervention.* Int J Mol Sci, 2020. **21**(18).
51. Kim, H.R., et al., *Fibroblast growth factor receptor 1 gene amplification is associated with poor survival and cigarette smoking dosage in patients with resected squamous cell lung cancer.* J Clin Oncol, 2013. **31**(6): p. 731-7.
52. Weiss, J., et al., *Frequent and focal FGFR1 amplification associates with therapeutically tractable FGFR1 dependency in squamous cell lung cancer.* Sci Transl Med, 2010. **2**(62): p. 62ra93.
53. Borad, M.J., G.J. Gores, and L.R. Roberts, *Fibroblast growth factor receptor 2 fusions as a target for treating cholangiocarcinoma.* Curr Opin Gastroenterol, 2015. **31**(3): p. 264-8.
54. Knowles, M.A., *Role of FGFR3 in urothelial cell carcinoma: biomarker and potential therapeutic target.* World J Urol, 2007. **25**(6): p. 581-93.
55. Singh, D., et al., *Transforming fusions of FGFR and TACC genes in human glioblastoma.* Science, 2012. **337**(6099): p. 1231-5.
56. Nelson, K.N., et al., *Oncogenic Gene Fusion FGFR3-TACC3 Is Regulated by Tyrosine Phosphorylation.* Mol Cancer Res, 2016. **14**(5): p. 458-69.
57. Facchinetti, F., et al., *Facts and New Hopes on Selective FGFR Inhibitors in Solid Tumors.* Clin Cancer Res, 2020. **26**(4): p. 764-774.
58. Ornitz, D.M., et al., *Receptor specificity of the fibroblast growth factor family.* J Biol Chem, 1996. **271**(25): p. 15292-7.
59. Zhang, X., et al., *Receptor specificity of the fibroblast growth factor family. The complete mammalian FGF family.* J Biol Chem, 2006. **281**(23): p. 15694-700.
60. Citores, L., et al., *Fibroblast growth factor receptor-induced phosphorylation of STAT1 at the Golgi apparatus without translocation to the nucleus.* J Cell Physiol, 2007. **212**(1): p. 148-56.
61. Tuominen, H., et al., *Expression and glycosylation studies of human FGF receptor 4.* Protein Expr Purif, 2001. **21**(2): p. 275-85.
62. Triantis, V., et al., *Glycosylation of fibroblast growth factor receptor 4 is a key regulator of fibroblast growth factor 19-mediated down-regulation of cytochrome P450 7A1.* Hepatology, 2010. **52**(2): p. 656-66.
63. Bruckner, K., et al., *Glycosyltransferase activity of Fringe modulates Notch-Delta interactions.* Nature, 2000. **406**(6794): p. 411-5.

64. Lundasen, T., et al., *Circulating intestinal fibroblast growth factor 19 has a pronounced diurnal variation and modulates hepatic bile acid synthesis in man.* J Intern Med, 2006. **260**(6): p. 530-6.
65. Ye, Y.W., et al., *Combination of the FGFR4 inhibitor PD173074 and 5-fluorouracil reduces proliferation and promotes apoptosis in gastric cancer.* Oncol Rep, 2013. **30**(6): p. 2777-84.
66. Ye, Y., et al., *Silencing of FGFR4 could influence the biological features of gastric cancer cells and its therapeutic value in gastric cancer.* Tumour Biol, 2016. **37**(3): p. 3185-95.
67. Tiong, K.H., et al., *Fibroblast growth factor receptor 4 (FGFR4) and fibroblast growth factor 19 (FGF19) autocrine enhance breast cancer cells survival.* Oncotarget, 2016. **7**(36): p. 57633-57650.
68. Xu, Y.F., et al., *Fibroblast growth factor receptor 4 promotes progression and correlates to poor prognosis in cholangiocarcinoma.* Biochem Biophys Res Commun, 2014. **446**(1): p. 54-60.
69. Shi, S., et al., *High Expression of FGFR4 Enhances Tumor Growth and Metastasis in Nasopharyngeal Carcinoma.* J Cancer, 2015. **6**(12): p. 1245-54.
70. Inokuchi, M., et al., *Different clinical significance of FGFR1-4 expression between diffuse-type and intestinal-type gastric cancer.* World J Surg Oncol, 2017. **15**(1): p. 2.
71. Meijer, D., et al., *Fibroblast growth factor receptor 4 predicts failure on tamoxifen therapy in patients with recurrent breast cancer.* Endocr Relat Cancer, 2008. **15**(1): p. 101-11.
72. Priedigkeit, N., et al., *Intrinsic Subtype Switching and Acquired ERBB2/HER2 Amplifications and Mutations in Breast Cancer Brain Metastases.* JAMA Oncol, 2017. **3**(5): p. 666-671.
73. Ezzat, S., et al., *Targeted expression of a human pituitary tumor-derived isoform of FGF receptor-4 recapitulates pituitary tumorigenesis.* J Clin Invest, 2002. **109**(1): p. 69-78.
74. Taylor, J.G.t., et al., *Identification of FGFR4-activating mutations in human rhabdomyosarcomas that promote metastasis in xenotransplanted models.* J Clin Invest, 2009. **119**(11): p. 3395-407.
75. Desnoyers, L.R., et al., *Targeting FGF19 inhibits tumor growth in colon cancer xenograft and FGF19 transgenic hepatocellular carcinoma models.* Oncogene, 2008. **27**(1): p. 85-97.
76. Lee, K.J., et al., *Expression of Fibroblast Growth Factor 21 and beta-Klotho Regulates Hepatic Fibrosis through the Nuclear Factor-kappaB and c-Jun N-Terminal Kinase Pathways.* Gut Liver, 2018. **12**(4): p. 449-456.
77. Nakamura, H., et al., *Genomic spectra of biliary tract cancer.* Nat Genet, 2015. **47**(9): p. 1003-10.
78. Hagel, M., et al., *First Selective Small Molecule Inhibitor of FGFR4 for the Treatment of Hepatocellular Carcinomas with an Activated FGFR4 Signaling Pathway.* Cancer Discov, 2015. **5**(4): p. 424-37.
79. Weiss, A., et al., *FGF401, A First-In-Class Highly Selective and Potent FGFR4 Inhibitor for the Treatment of FGF19-Driven Hepatocellular Cancer.* Mol Cancer Ther, 2019. **18**(12): p. 2194-2206.
80. Merilahti, J.A.M., et al., *Genome-wide screen of gamma-secretase-mediated intramembrane cleavage of receptor tyrosine kinases.* Mol Biol Cell, 2017. **28**(22): p. 3123-3131.
81. Kir, S., S.A. Kliewer, and D.J. Mangelsdorf, *Roles of FGF19 in liver metabolism.* Cold Spring Harb Symp Quant Biol, 2011. **76**: p. 139-44.

82. Nicholes, K., et al., *A mouse model of hepatocellular carcinoma: ectopic expression of fibroblast growth factor 19 in skeletal muscle of transgenic mice.* Am J Pathol, 2002. **160**(6): p. 2295-307.
83. Raja, A., et al., *FGF19-FGFR4 Signaling in Hepatocellular Carcinoma.* Cells, 2019. **8**(6).
84. Downward, J., *Targeting RAS signalling pathways in cancer therapy.* Nat Rev Cancer, 2003. **3**(1): p. 11-22.
85. Xu, K., et al., *Lunatic fringe deficiency cooperates with the Met/Caveolin gene amplicon to induce basal-like breast cancer.* Cancer Cell, 2012. **21**(5): p. 626-41.
86. Zhang, S., et al., *Tumor-suppressive activity of Lunatic Fringe in prostate through differential modulation of Notch receptor activation.* Neoplasia, 2014. **16**(2): p. 158-67.
87. Sawey, E.T., et al., *Identification of a therapeutic strategy targeting amplified FGF19 in liver cancer by Oncogenomic screening.* Cancer Cell, 2011. **19**(3): p. 347-58.
88. Ma, L., et al., *Overexpression of protein O-fucosyltransferase 1 accelerates hepatocellular carcinoma progression via the Notch signaling pathway.* Biochem Biophys Res Commun, 2016. **473**(2): p. 503-10.
89. Garg, V., et al., *Mutations in NOTCH1 cause aortic valve disease.* Nature, 2005. **437**(7056): p. 270-4.
90. Gridley, T., *Notch signaling and inherited disease syndromes.* Hum Mol Genet, 2003. **12 Spec No 1**: p. R9-13.
91. Cigliano, A., et al., *Role of the Notch signaling in cholangiocarcinoma.* Expert Opin Ther Targets, 2017. **21**(5): p. 471-483.
92. Sekiya, S. and A. Suzuki, *Intrahepatic cholangiocarcinoma can arise from Notch-mediated conversion of hepatocytes.* J Clin Invest, 2012. **122**(11): p. 3914-8.
93. Weng, A.P., et al., *Activating mutations of NOTCH1 in human T cell acute lymphoblastic leukemia.* Science, 2004. **306**(5694): p. 269-71.
94. Sakamoto, K., et al., *Distinct roles of EGF repeats for the Notch signaling system.* Exp Cell Res, 2005. **302**(2): p. 281-91.
95. Andersson, E.R., R. Sandberg, and U. Lendahl, *Notch signaling: simplicity in design, versatility in function.* Development, 2011. **138**(17): p. 3593-612.
96. Kopan, R. and M.X. Ilagan, *The canonical Notch signaling pathway: unfolding the activation mechanism.* Cell, 2009. **137**(2): p. 216-33.
97. Steinbuck, M.P. and S. Winandy, *A Review of Notch Processing With New Insights Into Ligand-Independent Notch Signaling in T-Cells.* Front Immunol, 2018. **9**: p. 1230.
98. Tagami, S., et al., *Regulation of Notch signaling by dynamic changes in the precision of S3 cleavage of Notch-1.* Mol Cell Biol, 2008. **28**(1): p. 165-76.
99. Guy, C.S., et al., *Distinct TCR signaling pathways drive proliferation and cytokine production in T cells.* Nat Immunol, 2013. **14**(3): p. 262-70.
100. Palaga, T., et al., *TCR-mediated Notch signaling regulates proliferation and IFN-gamma production in peripheral T cells.* J Immunol, 2003. **171**(6): p. 3019-24.
101. Steinbuck, M.P., K. Arakcheeva, and S. Winandy, *Novel TCR-Mediated Mechanisms of Notch Activation and Signaling.* J Immunol, 2018. **200**(3): p. 997-1007.
102. Bozkulak, E.C. and G. Weinmaster, *Selective use of ADAM10 and ADAM17 in activation of Notch1 signaling.* Mol Cell Biol, 2009. **29**(21): p. 5679-95.
103. Takeuchi, H. and R.S. Haltiwanger, *Significance of glycosylation in Notch signaling.* Biochem Biophys Res Commun, 2014. **453**(2): p. 235-42.
104. Kakuda, S. and R.S. Haltiwanger, *Deciphering the Fringe-Mediated Notch Code: Identification of Activating and Inhibiting Sites Allowing Discrimination between Ligands.* Dev Cell, 2017. **40**(2): p. 193-201.

105. LeBon, L., et al., *Fringe proteins modulate Notch-ligand cis and trans interactions to specify signaling states.* Elife, 2014. **3**: p. e02950.
106. Yang, L.T., et al., *Fringe glycosyltransferases differentially modulate Notch1 proteolysis induced by Delta1 and Jagged1.* Mol Biol Cell, 2005. **16**(2): p. 927-42.
107. Pandey, A., N. Niknejad, and H. Jafar-Nejad, *Multifaceted regulation of Notch signaling by glycosylation.* Glycobiology, 2021. **31**(1): p. 8-28.
108. De Strooper, B., *Aph-1, Pen-2, and Nicastrin with Presenilin generate an active gamma-Secretase complex.* Neuron, 2003. **38**(1): p. 9-12.
109. Struhl, G. and A. Adachi, *Requirements for presenilin-dependent cleavage of notch and other transmembrane proteins.* Mol Cell, 2000. **6**(3): p. 625-36.
110. Morohashi, Y., et al., *C-terminal fragment of presenilin is the molecular target of a dipeptidic gamma-secretase-specific inhibitor DAPT (N-[N-(3,5-difluorophenacetyl)-L-alanyl]-S-phenylglycine t-butyl ester).* J Biol Chem, 2006. **281**(21): p. 14670-6.
111. Noel, A., et al., *New and paradoxical roles of matrix metalloproteinases in the tumor microenvironment.* Front Pharmacol, 2012. **3**: p. 140.
112. Cudic, M. and G.B. Fields, *Extracellular proteases as targets for drug development.* Curr Protein Pept Sci, 2009. **10**(4): p. 297-307.
113. Chang, C. and Z. Werb, *The many faces of metalloproteases: cell growth, invasion, angiogenesis and metastasis.* Trends Cell Biol, 2001. **11**(11): p. S37-43.
114. Chow, F.L. and C. Fernandez-Patron, *Many membrane proteins undergo ectodomain shedding by proteolytic cleavage. Does one sheddase do the job on all of these proteins?* IUBMB Life, 2007. **59**(1): p. 44-7.
115. Thathiah, A. and D.D. Carson, *MT1-MMP mediates MUC1 shedding independent of TACE/ADAM17.* Biochem J, 2004. **382**(Pt 1): p. 363-73.
116. Kibbe, W.A., *OligoCalc: an online oligonucleotide properties calculator.* Nucleic Acids Res, 2007. **35**(Web Server issue): p. W43-6.
117. Arauz, E., et al., *Single-Molecule Analysis of Lipid-Protein Interactions in Crude Cell Lysates.* Anal Chem, 2016. **88**(8): p. 4269-76.
118. Rodgers, K.J. and R.T. Dean, *Assessment of proteasome activity in cell lysates and tissue homogenates using peptide substrates.* Int J Biochem Cell Biol, 2003. **35**(5): p. 716-27.
119. Justus, C.R., et al., *In vitro cell migration and invasion assays.* J Vis Exp, 2014(88).
120. Bitler, B.G., A. Goverdhan, and J.A. Schroeder, *MUC1 regulates nuclear localization and function of the epidermal growth factor receptor.* J Cell Sci, 2010. **123**(Pt 10): p. 1716-23.
121. Ramsby, M.L., G.S. Makowski, and E.A. Khairallah, *Differential detergent fractionation of isolated hepatocytes: biochemical, immunochemical and two-dimensional gel electrophoresis characterization of cytoskeletal and noncytoskeletal compartments.* Electrophoresis, 1994. **15**(2): p. 265-77.
122. Massironi, S., et al., *New and Emerging Systemic Therapeutic Options for Advanced Cholangiocarcinoma.* Cells, 2020. **9**(3).
123. Rizvi, S., et al., *Cholangiocarcinoma - evolving concepts and therapeutic strategies.* Nat Rev Clin Oncol, 2018. **15**(2): p. 95-111.
124. Lee, J.Y., et al., *Genetic alterations in intrahepatic cholangiocarcinoma as revealed by degenerate oligonucleotide primed PCR-comparative genomic hybridization.* J Korean Med Sci, 2004. **19**(5): p. 682-7.
125. Sia, D., et al., *Integrative molecular analysis of intrahepatic cholangiocarcinoma reveals 2 classes that have different outcomes.* Gastroenterology, 2013. **144**(4): p. 829-40.
126. Vasilieva, L.E., et al., *An extended fluorescence in situ hybridization approach for the cytogenetic study of cholangiocarcinoma on endoscopic retrograde*

cholangiopancreatography brushing cytology preparations. Hum Pathol, 2013. **44**(10): p. 2173-9.
127. Lin, B.C., et al., *Liver-specific activities of FGF19 require Klotho beta.* J Biol Chem, 2007. **282**(37): p. 27277-84.
128. Wu, X., et al., *Co-receptor requirements for fibroblast growth factor-19 signaling.* J Biol Chem, 2007. **282**(40): p. 29069-72.
129. Taylor, P., et al., *Fringe-mediated extension of O-linked fucose in the ligand-binding region of Notch1 increases binding to mammalian Notch ligands.* Proc Natl Acad Sci U S A, 2014. **111**(20): p. 7290-5.
130. Yi, F., B. Amarasinghe, and T.P. Dang, *Manic fringe inhibits tumor growth by suppressing Notch3 degradation in lung cancer.* Am J Cancer Res, 2013. **3**(5): p. 490-9.
131. Yamashita, K., Y. Tachibana, and A. Kobata, *The structures of the galactose-containing sugar chains of ovalbumin.* J Biol Chem, 1978. **253**(11): p. 3862-9.
132. Tabas, I. and S. Kornfeld, *The synthesis of complex-type oligosaccharides. III. Identification of an alpha-D-mannosidase activity involved in a late stage of processing of complex-type oligosaccharides.* J Biol Chem, 1978. **253**(21): p. 7779-86.
133. Citores, L., et al., *Uptake and intracellular transport of acidic fibroblast growth factor: evidence for free and cytoskeleton-anchored fibroblast growth factor receptors.* Mol Biol Cell, 1999. **10**(11): p. 3835-48.
134. Rizvi, S., et al., *Cholangiocarcinoma: molecular pathways and therapeutic opportunities.* Semin Liver Dis, 2014. **34**(4): p. 456-64.
135. Ezzat, S., L. Zheng, and S.L. Asa, *Pituitary tumor-derived fibroblast growth factor receptor 4 isoform disrupts neural cell-adhesion molecule/N-cadherin signaling to diminish cell adhesiveness: a mechanism underlying pituitary neoplasia.* Mol Endocrinol, 2004. **18**(10): p. 2543-52.
136. Farrell, B. and A.L. Breeze, *Structure, activation and dysregulation of fibroblast growth factor receptor kinases: perspectives for clinical targeting.* Biochem Soc Trans, 2018. **46**(6): p. 1753-1770.
137. Furdui, C.M., et al., *Autophosphorylation of FGFR1 kinase is mediated by a sequential and precisely ordered reaction.* Mol Cell, 2006. **21**(5): p. 711-7.
138. Mohammadi, M., et al., *Point mutation in FGF receptor eliminates phosphatidylinositol hydrolysis without affecting mitogenesis.* Nature, 1992. **358**(6388): p. 681-4.
139. Peters, K.G., et al., *Point mutation of an FGF receptor abolishes phosphatidylinositol turnover and Ca2+ flux but not mitogenesis.* Nature, 1992. **358**(6388): p. 678-81.
140. Wang, J., et al., *Altered fibroblast growth factor receptor 4 stability promotes prostate cancer progression.* Neoplasia, 2008. **10**(8): p. 847-56.
141. Ulaganathan, V.K., et al., *Germline variant FGFR4 p.G388R exposes a membrane-proximal STAT3 binding site.* Nature, 2015. **528**(7583): p. 570-4.
142. Shern, J.F., et al., *Comprehensive genomic analysis of rhabdomyosarcoma reveals a landscape of alterations affecting a common genetic axis in fusion-positive and fusion-negative tumors.* Cancer Discov, 2014. **4**(2): p. 216-31.
143. Seki, M., et al., *Integrated genetic and epigenetic analysis defines novel molecular subgroups in rhabdomyosarcoma.* Nat Commun, 2015. **6**: p. 7557.
144. Tang, S., et al., *Role of fibroblast growth factor receptor 4 in cancer.* Cancer Sci, 2018. **109**(10): p. 3024-3031.
145. Winzler, R.J. and I.M. Smyth, *Studies on the mucoproteins of human plasma; plasma mucoprotein levels in cancer patients.* J Clin Invest, 1948. **27**(5): p. 617-9.

146. Peracaula, R., et al., *Altered glycosylation pattern allows the distinction between prostate-specific antigen (PSA) from normal and tumor origins.* Glycobiology, 2003. **13**(6): p. 457-70.
147. Kasbaoui, L., et al., *Differences in glycosylation state of fibronectin from two rat colon carcinoma cell lines in relation to tumoral progressiveness.* Cancer Res, 1989. **49**(19): p. 5317-22.
148. Kellokumpu, S., R. Sormunen, and I. Kellokumpu, *Abnormal glycosylation and altered Golgi structure in colorectal cancer: dependence on intra-Golgi pH.* FEBS Lett, 2002. **516**(1-3): p. 217-24.
149. Ng, R.C., et al., *Analyses of protein extracts of human breast cancers: changes in glycoprotein content linked to the malignant phenotype.* Br J Cancer, 1987. **55**(3): p. 249-54.
150. Tai, C.S., et al., *Haptoglobin expression correlates with tumor differentiation and five-year overall survival rate in hepatocellular carcinoma.* PLoS One, 2017. **12**(2): p. e0171269.
151. Ang, I.L., et al., *Study of serum haptoglobin and its glycoforms in the diagnosis of hepatocellular carcinoma: a glycoproteomic approach.* J Proteome Res, 2006. **5**(10): p. 2691-700.
152. Duffy, M.J., *CA 19-9 as a marker for gastrointestinal cancers: a review.* Ann Clin Biochem, 1998. **35 (Pt 3)**: p. 364-70.
153. Ferretti, G., et al., *HER2/neu role in breast cancer: from a prognostic foe to a predictive friend.* Curr Opin Obstet Gynecol, 2007. **19**(1): p. 56-62.
154. Jin, M.M., et al., *Notch signaling molecules as prognostic biomarkers for non-small cell lung cancer.* Oncol Lett, 2015. **10**(5): p. 3252-3260.
155. Takam Kamga, P., et al., *Notch Signaling Molecules as Prognostic Biomarkers for Acute Myeloid Leukemia.* Cancers (Basel), 2019. **11**(12).
156. Hollingsworth, M.A. and B.J. Swanson, *Mucins in cancer: protection and control of the cell surface.* Nat Rev Cancer, 2004. **4**(1): p. 45-60.
157. Gendler, S.J., et al., *Molecular cloning and expression of human tumor-associated polymorphic epithelial mucin.* J Biol Chem, 1990. **265**(25): p. 15286-93.
158. Ligtenberg, M.J., et al., *Episialin, a carcinoma-associated mucin, is generated by a polymorphic gene encoding splice variants with alternative amino termini.* J Biol Chem, 1990. **265**(10): p. 5573-8.
159. Lan, M.S., et al., *Cloning and sequencing of a human pancreatic tumor mucin cDNA.* J Biol Chem, 1990. **265**(25): p. 15294-9.
160. Williams, S.J., et al., *Two novel mucin genes down-regulated in colorectal cancer identified by differential display.* Cancer Res, 1999. **59**(16): p. 4083-9.
161. Pallesen, L.T., et al., *Isolation and characterization of MUC15, a novel cell membrane-associated mucin.* Eur J Biochem, 2002. **269**(11): p. 2755-63.
162. Gum, J.R., Jr., et al., *MUC17, a novel membrane-tethered mucin.* Biochem Biophys Res Commun, 2002. **291**(3): p. 466-75.
163. Baro, M., et al., *Oligosaccharyltransferase Inhibition Reduces Receptor Tyrosine Kinase Activation and Enhances Glioma Radiosensitivity.* Clin Cancer Res, 2019. **25**(2): p. 784-795.
164. Lopez-Sambrooks, C., et al., *Oligosaccharyltransferase inhibition induces senescence in RTK-driven tumor cells.* Nat Chem Biol, 2016. **12**(12): p. 1023-1030.
165. Lopez Sambrooks, C., et al., *Oligosaccharyltransferase Inhibition Overcomes Therapeutic Resistance to EGFR Tyrosine Kinase Inhibitors.* Cancer Res, 2018. **78**(17): p. 5094-5106.

166. Jin, W., et al., *Fibroblast growth factor receptor-1 alpha-exon exclusion and polypyrimidine tract-binding protein in glioblastoma multiforme tumors.* Cancer Res, 2000. **60**(5): p. 1221-4.
167. Moffa, A.B., S.L. Tannheimer, and S.P. Ethier, *Transforming potential of alternatively spliced variants of fibroblast growth factor receptor 2 in human mammary epithelial cells.* Mol Cancer Res, 2004. **2**(11): p. 643-52.
168. Sturla, L.M., A.E. Merrick, and S.A. Burchill, *FGFR3IIIS: a novel soluble FGFR3 spliced variant that modulates growth is frequently expressed in tumour cells.* Br J Cancer, 2003. **89**(7): p. 1276-84.
169. Ezzat, S., et al., *A soluble dominant negative fibroblast growth factor receptor 4 isoform in human MCF-7 breast cancer cells.* Biochem Biophys Res Commun, 2001. **287**(1): p. 60-5.